Unbalance and Resonance Elimination on General Rotors with Active Bearings

Unwucht- und Resonanzeliminierung allgemeiner Rotoren mit aktiven Lagern

Zur Erlangung des akademischen Grades Doktor-Ingenieur (Dr.-Ing.)
genehmigte Dissertation von Stefan Heindel aus Hanau

TECHNISCHE
UNIVERSITÄT
DARMSTADT

Unbalance and Resonance Elimination on General Rotors with Active Bearings

Am Fachbereich Maschinenbau
an der Technischen Universität Darmstadt
zur
Erlangung des Grades eines Doktor-Ingenieurs (Dr.-Ing.)
genehmigte

Dissertation

vorgelegt von

Dipl.-Ing. Stefan Heindel

aus Hanau

Berichterstatter:	Prof. Dr.-Ing. Stephan Rinderknecht
Mitberichterstatter:	Prof. Dr.-Ing. Bernhard Schweizer

Tag der Einreichung:	23.1.2017
Tag der mündlichen Prüfung:	19.4.2017

Darmstadt 2017

D 17

Vorwort

Die hier vorliegende Arbeit entstand während meiner Zeit als Promotionsstudent am Institut für Mechatronische Systeme im Maschinenbau im Rahmen des DFG geförderten Graduiertenkollegs 1344. Ich bedanke mich bei Herrn Professor Dr.-Ing. Stephan Rinderknecht, der mir als Institutsleiter die Promotion ermöglichte und mir großes Vertrauen bei der Gestaltung der Arbeit entgegenbrachte. Bedanken möchte ich mich ebenfalls bei Herrn Professor Dr.-Ing. Bernhard Schweizer, der die Zweitkorrektur der Arbeit übernahm.

Ein ganz besonderer Dank geht an Herrn Professor Dr.-Ing. Peter Christian Müller, der durch umfangreiche postalische Korrespondenz ganz erheblich zum Gelingen dieser Arbeit beitrug. Teile des Stabilitätsbeweises und insbesondere der Nachweis asymptotischer Stabilität basieren auf seinen Ausführungen. Sein herausragendes Fachwissen, die wissenschaftliche Präzision seiner Publikationen und sein freundlicher Umgang haben mich tief beeindruckt.

Die Kolleginnen und Kollegen machten das IMS zu einem Ort, an dem fachliche und private Themen immer offen und in freundschaftlicher Atmosphäre diskutiert werden konnten. In guter Erinnerung bleibt mir auch unsere Sekretärin Frau Ursula Willner, welche die kleinen und großen Probleme des wissenschaftlichen Alltags immer unkompliziert und mit einem Lächeln löste. Ganz besonders möchte ich mich bei den Herren Ramakrishnan Ambur, Fabian Becker und Philipp Zech bedanken, die immer ein offenes Ohr für meine Fragen und Probleme hatten.

Diese Arbeit wäre nicht möglich gewesen ohne die Unterstützung von vielen Studenten und Hiwis, denen ich hiermit für Ihren Einsatz danken möchte. Herrn Bastian Pfau danke ich für die Hilfe bei der Versuchsdurchführung. Den Herren Daniel Plöger, Philipp Zech und Frau Barbara Castro Rojas sei an dieser Stelle für das Gegenlesen der Arbeit gedankt.

Meinen Eltern Roswitha und Josef Heindel danke ich von Herzen für ihre bedingungslose Unterstützung auf meinem Lebensweg. Der wichtigste Dank gebührt aber meiner Freundin Laura Cárdenas Contreras, die mich liebevoll und mit viel Verständnis durch die schwierigen Zeiten der Promotion führte.

Kurzfassung

Rotierende Maschinen haben einen tiefgehenden Einfluss auf heutige Gesellschaften. Moderne Errungenschaften wie Elektrizität, Autos, Flugzeuge und auch Raketen wären ohne diese Maschinen undenkbar. Unwuchten am Rotor führen zu Schwingungen, welche sich in einer reduzierten Lebensdauer und Lärmbelästigung niederschlagen. Für Jahrzehnte waren das Auswuchten des Rotors und die Einbringung von Dämpfung die einzigen Möglichkeiten um diese Schwingungen zu reduzieren.

Magnetlager eröffneten neue Möglichkeiten bei der Schwingungsreduktion, und hochentwickelte Regelungsalgorithmen erlauben das vollständige Entfernen von Unwuchtkräften. Leider sind viele dieser Verfahren mit Nachteilen behaftet, beispielsweise das unbestimmte Verhalten in Resonanzen und die schlechten Stabilitätseigenschaften. Die Einführung von aktiven Lagern mit Piezoaktoren verkomplizierte die Situation zusätzlich: Abhängig von der verwendeten Technologie werden verschiedene, sich scheinbar widersprechende Methoden eingesetzt, welche eine vereinheitlichte Betrachtung des Problems verhindern.

Das Ziel dieser Arbeit ist es, die Widersprüche und Nachteile gegenwärtiger Methoden zur Eliminierung von Lagerkräften zu lösen, wodurch eine vereinheitlichte Betrachtung verschiedener aktiver Lagertechnologien ermöglicht wird. Für den LAVAL-Rotor wird ein neuer Regelungsansatz vorgestellt. Dieser eliminiert nicht nur die Unwuchtkräfte, sondern auch dessen Resonanz. Der Ansatz wird schließlich erweitert, um auch Rotoren mit beliebigen Massen, Steifigkeiten, Dämpfungen und gyroskopischen Effekten abzubilden. Die analytische Lösung des geschlossenen Regelkreises zeigt, dass nicht nur alle Lagerkräfte, sondern auch zwei Resonanzen eliminiert werden können. Dies ist sogar für Rotoren in einem flexiblen Gehäuse möglich.

Die theoretischen Betrachtungen erlauben die Ableitung von Regelgesetzen für verschiedene Aktorprinzipien, Technologien und Anordnungen, welche zu einem vereinheitlichten Problemlösung führen. Auslegungsvorschriften für Aktoren vereinfachen eine praktische Realisierung.

Diese Arbeit führt weiterhin ein neues Stabilitätskriterium für mechanische Systeme mit kollokiertem Regler ein. Mit diesem Kriterium werden die außergewöhnlichen Stabilitätseigenschaften des vorgestellten Reglers geschlossen bewiesen.

Abstract

Rotating machinery has a subtle, but profound impact on contemporary societies. Many modern achievements owe their existence to these machines, ranging from electrical power, cars, airplanes, to rockets. In these machines, rotor unbalances cause vibrations and stresses, decreasing their lifetime and leading to noise pollution. For decades, balancing and damping were the only methods to reduce these vibrations.

The introduction of active magnetic bearings enabled new possibilities for rotor vibration reduction. Sophisticated control algorithms do not only allow for a reduction, but for a complete elimination of bearing forces caused by unbalances. Still, the existing methods suffer from drawbacks, including unclear behavior in rotor resonances, and poor stability. The invention of active bearings based on piezoactuators complicated the situation further: depending on the researcher's background, contradicting methods are used for vibration reduction, resulting in an unclear and fragmented problem understanding.

This work strives to resolve the apparent contradictions and drawbacks of the currently available methods to eliminate unbalances, generating a unified problem solution for different active bearing technologies. After a careful revision of the JEFFCOTT rotor, a new control approach is suggested. The latter does not only eliminate the rotor's unbalance forces, but also the rotor's resonance. The approach is extended to cover rotors with arbitrary mass, stiffness, damping and gyroscopic properties. A general, analytic solution indicates that the proposed control algorithm allows for a complete elimination of bearing forces and two rotor resonances. This is possible even when the rotor is attached to an arbitrary, flexible structure.

The theoretical considerations allow for a derivation of control strategies for different actuator principles, technologies and arrangements, resulting in a consistent problem treatment and understanding. Actuator dimensioning guidelines enable an effortless practical realization.

This work introduces a new stability theorem for arbitrary mechanical systems with collocated controllers. The theorem is subsequently applied to proof the

controller's superior stability properties, resulting in unconditional stability for general rotors.

Symbols

a	Actuator displacement
$\mathbf{a}$	Actuator displacement vector
$\tilde{\mathbf{a}}$	Condensed actuator displacement vector
a_B	Negative compensating controller displacement element
a_D	Dissipating controller displacement element
a_F	Positive compensating controller displacement element
a_{FB}	Reduced actuator displacement
$\mathbf{A}$	Controlled rotor system matrix
$\bar{\mathbf{A}}$	Controller transformation matrix
$\mathbf{A}_\delta$	Controller peak avoidance matrix
$\mathbf{A}_R$	Controller system matrix
$\bar{\mathbf{A}}_R$	Transformed controller system matrix
$\mathbf{B}$	Controlled rotor input matrix
$\mathbf{B}_R$	Controller input matrix
$\mathbf{C}$	Controlled rotor output matrix
$c_C, \tilde{c}_C$	Controller adaption speed
c_D	Inverse controller damping
$\mathbf{C}_R$	Controller output matrix
$d_{...}$	External damping coefficients
$\mathbf{D}$	Outer damping matrix
$\mathbf{D}_I$	Inner damping matrix
E_{kin}	Kinetic energy
E_{pot}	Potential energy
E_{dis}	Dissipated energy
f	Frequency
f_{C1}	Resonance frequency of controlled rotor
f_{P1}, f_{P2}, f_{P3}	Resonance frequencies of passive rotor
F	Active bearing force
$\mathbf{F}$	Active bearing force vector

$\tilde{\mathbf{F}}$	Condensed active bearing force vector
$\bar{\mathbf{F}}$	Estimated active bearing force vector
F_A	Actuator force
$\mathbf{F}_D$	Outer damping force vector
$\mathbf{F}_I$	Inner damping force vector
F_P	Passive bearing force
$\mathbf{F}_P$	Passive bearing force vector
$\mathbf{F}_R$	Shaft node vector
F_S	Parasitic force
$\mathbf{F}_S$	Parasitic force vector
$\mathbf{G}$	Gyroscopic matrix
$\mathbf{H}$	HAMILTONian matrix
i	Imaginary unit
$\mathbf{I}$	Identity matrix
j	Individual bearing identifier
$k_{...}$	Stiffness
$\mathbf{K}$	Stiffness matrix
k_D	Controller stiffness element
$\mathbf{K}_R$	Free rotor stiffness matrix
$\mathbf{K}_L$	Bearing stiffness matrix
$\tilde{\mathbf{K}}_L$	Condensed bearing stiffness matrix
k_S	Parasitic stiffness
$\bar{k}_S$	Estimated parasitic stiffness
$\mathbf{K}_S$	Parasitic stiffness matrix
$\bar{\mathbf{K}}_S$	Estimated parasitic stiffness matrix
$m_{...}$	Mass
$\mathbf{M}$	Mass matrix
$\mathbf{n}$	Bearing allocation matrix
$\mathbf{n}_j$	Bearing allocation vector for j-th active bearing
p	Total number of shaft nodes
$\mathbf{Q}$	RALEIGH dissipation matrix
q_W	Shaft center
$\mathbf{q}_W$	Shaft displacement vector
q_S	Center of mass
$\mathbf{q}_S$	Mass displacement vector
q_0	Homogeneous shaft solution

$\mathbf{q}_{...i}$	Displacement eigenvector
$\mathbf{r}$	Distribution vector
$\mathbf{R}$	Distribution matrix
t	Time
$\mathbf{T}$	Coordinate transformation matrix
t_S	Sampling time
$\mathbf{U}$	Eigenvector matrix active solution
$\mathbf{U}_P$	Eigenvector matrix passive solution
$\mathbf{V}$	Diagonal active eigenvalue matrix
$\mathbf{V}_P$	Diagonal passive eigenvalue matrix
$\mathbf{x}$	Controlled rotor state vector
$\mathbf{x}_i$	State eigenvector
$\mathbf{x}_R$	Controller state vector
$\bar{\mathbf{x}}_R$	Transformed controller state vector
z	Total number of active bearings
$\mathbf{Z}$	Dimensionless stiffness ratio matrix
α	Phase shift / Node rotation angle
$\alpha_{0..5}$	Coefficients of characteristic polynomial
β	Node rotation angle
Δa	Actuator stroke
$\Delta_{1..5}$	HURWITZ-Determinants
ε	Eccentricity
$\boldsymbol{\varepsilon}$	Eccentricity vector
Θ_t	Transversal moment of inertia
Θ_p	Polar moment of inertia
φ	Rotor rotational angle
ω	Angular frequency
ω_0	Natural angular frequency of the passive JEFFCOTT rotor
$\omega_{P...}$	Natural angular frequency of the passive, general rotor
$\omega_{C...}$	Natural angular frequency of the free, general rotor
Ω	Rotor rotational speed
$()^+$	Positive rotating coordinate system (rotor-fixed)
$()^-$	Negative rotating coordinate system
$()^T$	Transpose

$()^H$	Complex conjugate transpose
$()_{A,B,..,j}$	First, second, j-th controller
$()_{+1}$	Next time step
$()_i$	Eigenvector
$()_r$	Rotor-casing interaction: Rotor
$()_c$	Rotor-casing interaction: Casing
$()_g$	Rotor-casing interaction: Full system

const.	Constant
diag	Diagonal matrix
e	Exponential function
min	Minimum
rank	Matrix rank
Re( )	Real part
Im( )	Imaginary part
$\|x\|$	Absolute value of x
$\dot{x}$	Derivative of x with respect to time
$\ddot{x}$	Second derivative of x with respect to time
$\mathbf{X} \geq 0$	Positive semidefiniteness of $\mathbf{X}$
$\mathbf{X} > 0$	Positive definiteness of $\mathbf{X}$

Contents

1 Introduction

Rotating machines are the foundation for our modern civilization, invisibly affecting our daily lives in a multitude of ways. They are commonly used for power generation, transport, spaceflight but also for domestic appliances. Their significance is also reflected in the intense research activities for the past 150 years. With real rotors, the center of mass never coincides with the center of rotation, and the resulting eccentricities lead to rotor bending and alternating bearing forces. Both quantities become especially large when the rotor is operated close to its resonance speed, and scientists initially believed that these critical speeds could not be passed. It was not until De Laval demonstrated that a rotor can be operated above its resonance that refuted these beliefs. Still, De Laval was not the first to doubt the latter. Beforehand, Föppl and Jeffcott had contributed the theoretical foundation for De Laval's findings [53].

Rotor vibrations are generally undesired as they cause material stresses, noise and excessive bearing wear. They do not only affect negatively the machine performance, but are also a nuisance for humans in the machine's vicinity [2, 46]. The most common technique to reduce rotor vibrations is balancing, a procedure where the rotor's mass is redistributed to keep the eccentricity reasonably small [20, 85]. Even for well-balanced rotors, operations conducted at a critical speed are generally avoided. Another technique for vibration reduction is damping, which can be achieved either through inherent material properties or dedicated damping elements [11, 80]. Until today, both methods are prevalent for vibration reduction [94].

The introduction of active bearings enables new possibilities for vibration reduction. The development of active magnetic bearings in the 1980s first allowed to cover applications where conventional bearings might not be feasible [66]. One decade later, Palazzolo investigated active bearings based on piezoelectric actuators [77–79]. Both bearing types allow for electronic adjustments of stiffness and damping to maintain favorable operating conditions.

Even with active bearings and sophisticated control algorithms, unbalance still causes speed-dependent harmonic rotor displacements and bearing forces [66]. These unwanted effects are not only a burden for man and machine, but also cause increased actuator activity and amplifier utilization. This results not only

in higher energy requirements, but may also lead to instability when the maximum actuator forces are exceeded.

1.1 Current state of research

The unique possibility to implement arbitrary control algorithms encouraged researchers to specifically focus on the unwanted effects of unbalances. The numerous approaches can be divided in two different categories. The former one reduces the rotor displacements caused by unbalances [1, 55, 57, 100], which is advantageous when a high radial runout precision is required. In terms of disadvantages, forcing the rotor in a defined position requires high actuator forces. However, many applications do not require a perfect radial rotor runout as long as the displacements remain within the given boundaries. In turbomachinery for example, the exact radial movement is irrelevant as long as the rotor does not touch the casing. In this case, a reduction of the unbalance-induced bearing forces results in a smoother machine run and gives a lesser actuator load. Researchers found a large number of algorithms to accomplish this task such as Adaptive Autocentering Control [54], Adaptive Forced Balancing [86], Convergent Control [91], notch filters [42, 98], Periodic Learning Control [45], Automatic Inertial Autocentering [59], Unbalance Compensation [65], Adaptive Feedforward Compensation [87] and Unbalance Force Rejection Control, a method given in an ISO Standard [51]. Two main concepts have stood out from all of these approaches. The notch filter approach eliminates the synchronous bearing forces so that the rotor rotates around its principal axis of inertia. The main disadvantage is that notch filters become unstable at critical rotor speeds [98]. The second concept is known as adaptive feedforward compensation, where a speed-dependent harmonic signal is injected into the control loop to compensate the unbalance forces [10]. This method generally passes critical speeds but its level of stability remains hard to quantify. Moreover, the physical interpretation of the injected harmonic signal remains unclear. LARSONNEUR recognized that all approaches can be seen as generalized notch filters [42]. Even though it is apparent that all unbalance compensation algorithms exploit the same physical effect, each contribution follows its unique line of wording and argumentation. Some operational principles seemingly contradict each other, as it is the case for filtering and feedforward compensation. The uncertainty grows with each new contribution that introduces new assumptions and opens new lines of argumentation. The situation worsens as different active bearing types require distinct compensation algorithms, often developed in individual scientific communities.

To conclude, the main drawbacks of the existing approaches are:

Explanation limited to rigid rotors. Researchers correctly stated that the elimination of unbalance forces causes the rotor to turn around its principal axis of inertia [10, 54]. The changing geometry of flexible rotors inhibits a definition of the fixed principle axis of inertia. Even though some algorithms work also for flexible rotors, the rotordynamic background remains unclear.

Vague statements about principles of operation. The line of argumentation between filtering and adaptive feedforward compensation appears contradictory. While notch filters eliminate the synchronous bearing forces, "harmonic signals are injected into the control loop in such a way as to minimize the harmonic components of force" [10] in case of the adaptive feedforward compensation. The physical background of the injected signal remains unclear, raising questions how both approaches are linked together.

Rotor model required. Some approaches require a mathematical model of the rotor system [45, 65], making a practical application costly and difficult. Even with available models, unmodeled dynamics may cause additional problems [4]. It is generally acknowledged that collocated controllers have advantages regarding performance, stability and modeling [14, 30].

Unclear resonance behavior. The behavior of unbalance compensation algorithms at critical speeds remains unclear. Some experiments show that unbalance compensation does not work at critical speeds, others show that both forces and displacements can be reduced simultaneously. LARSONNEUR stated that unbalance compensation works in rigid body critical speeds, but could not give a mathematical justification [66].

Poorly reflected rotordynamics. Many approaches originate from a signal-theoretic viewpoint, often leading to an oversimplification of the underlying rotordynamics and a lack of physical insight. A general problem treatment is only available for rigid rotors [54], whereas more complicated rotors are generally treated using numeric simulation. However, this only proves that the algorithm in scope works for a particular setup.

Domain-specific problem description. The existing approaches are specifically tailored to one specific technology, namely magnetic bearings [10], piezoelectric actuators [37, 58] or balancing actuators [23]. Depending on the researchers' background, different solution techniques prevent a generalized problem treatment. Possible similarities and links between different technologies are buried in complex algorithms and domain-specific assumptions.

Unproven stability. Most unbalance compensation algorithms have unproven stability properties. When stable, most controllers offer impressive force reductions, however notch filters in particular tend to instability if operated close to the resonance [10]. Algorithms based on “Open loop adaptive control” [15] or “Adaptive feedforward compensation” [87] claim superior stability while their inner control loop remains unaltered, yet ignore the fact that the adaption process is also a potentially instable feedback loop. Moreover, the complex mathematical background prevents a thorough stability analysis. Some contributions perform a stability analysis for rigid rotors, but can only guarantee stability for certain controller parameters [54].

1.2 Objectives, proceeding and structure

The objective of this work is a complete mathematical treatment of the elimination of unbalance-induced bearing forces using active bearings. The anticipated solution should not only avoid the problems of the existing approaches, but also be easily understandable. It should further be compatible with structural dynamics, control engineering and system theory. Additionally, it should establish a link between different active bearing technologies.

It is good scientific practice to establish theories using only as few assumptions as possible. Among all theories, the easiest explanation is not necessarily the right one, but it is the easiest one to *falsify*. Among two competing theories that both explain the same phenomena, the simpler one should always be preferred [83].

The premises of this work are *explicit assumptions* and *consistency*. The first premise recognizes to simplicity and falsification, while the latter premise allows for a consistent reduction from unnecessarily intricate considerations to the simplest.

A generalized problem description requires a *strict separation between system theory and practical realization*. The advantage of a theoretic problem description is its *technology independence*, making the solution relevant for future realization concepts. Another advantage is that different existing technologies can be consistently explained by the same theoretic considerations.

Based on these objectives and premises, the work is structured in the following manner:

Chapter 2 deals with the unbalance force elimination on the JEFFCOTT rotor using active bearings. After a thorough revision of the underlying kinematics, a new control algorithm is introduced. Subsequent analysis reveals that the controller can eliminate both bearing forces and the rotor resonance. Finally, the remarkable stability properties are proven and discussed.

Chapter 3 extends the considerations from the previous chapter to general rotors. A closed analytical solution demonstrates that the previously introduced controller also works for arbitrary isotropic rotors. The influence of damping, gyroscopy and parasitic stiffnesses is thoroughly investigated. In the last step of generalization, the behavior of general rotors in flexible casings is studied.

Chapter 4 demonstrates possible physical realization of the theoretic considerations. The distinction between displacement and force actuators leads to deviating controller derivations, linking different active bearing principles. Furthermore, it demonstrates that the controller allows for a direct measurement of the rotor's eccentricity. This information can be used for a simple machine health monitoring. The considerations also unveil the connection between balancing actuators and active bearings. Finally, the dimensioning of actuators and the effect of parasitic stiffnesses and remaining rotor resonances are discussed.

Chapter 5 investigates the stability of general, controlled rotors. Proving general stability on arbitrary rotors requires sophisticated calculation methods. Therefore, the fundamentals of LYAPUNOV stability are introduced and discussed. A new stability theorem for mechanical systems with collocated control is developed. Using this theorem, the stability of the controlled rotor is finally proven.

Chapter 6 experimentally validates the previous assumptions. Using two test rigs with active piezoelectric bearings in different rotor configurations, it demonstrates that unbalance forces and resonances can not only be eliminated in theory, but also in practice.

2 The Jeffcott rotor with active bearings

The JEFFCOTT rotor describes the first and most basic rotordynamic model. Despite its age, the model - first used by FÖPPL in 1895, and later rediscovered by JEFFCOTT in 1919 [53] - has lost nothing of its popularity because most rotordynamic effects can be studied in a clear and comprehensible manner.

This chapter extends the JEFFCOTT rotor model with active bearings. After a thorough discussion and illustration of the rotor kinematics, a new control algorithm is introduced. With this new controller, an analytical proof that unbalance-induced bearing forces can be eliminated, is performed. Surprisingly, the controller also eliminates the rotor's only resonance. A subsequent analytical stability proof reveals that the controlled rotor is *always* stable. This remarkable stability behavior is meticulously investigated. The ideas of this chapter are the basis for all following chapters.

The chapter bases on the publication "Unbalance and resonance elimination with active bearings on a Jeffcott Rotor" written by HEINDEL et al. [38]. The Figures are taken from the same source.

2.1 Mechanical properties of the passive system

The purpose of this section is twofold. It serves both as a general introduction to rotordynamics and defines variables which will be subsequently used throughout this work. It is assumed that the rotor is *isotropic*, meaning the rotor's mechanical properties are the same in each direction. In this case, the rotor responds similarly in both axes, and both can be gathered using *complex coordinates*. The real part of a complex coordinate represents one axis, while the complex part represents the perpendicular one. The main advantage of complex coordinates is to halve the governing equations, resulting in clearer results and less calculation effort.

Figure 2.1 shows a model of the rotor in the complex coordinate system. A disc with a mass m is attached to a flexible shaft with the stiffness k. The

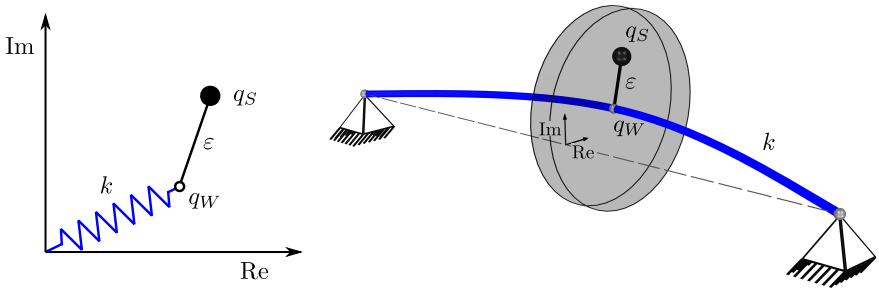

Figure 2.1: Model of the Jeffcott rotor with passive bearings in the complex coordinate plane. The rotor is symmetric with respect to the disc. Left: planar view. Right: three-dimensional view.

intersection between disc and shaft defines the *shaft center* q_W. For reasons of manufacturing, it is generally not possible to perfectly align the disc's *center of mass* q_S with the shaft center q_W. The distance between both coordinates is called *eccentricity* ε.

$$q_S = q_W + \varepsilon \tag{2.1}$$

A displacement of the shaft center q_W leads to an elastic force F_P that returns the shaft to its original, undeflected position.

$$F_P = kq_W \qquad (k > 0) \tag{2.2}$$

The equations of motion can either be given with respect to shaft coordinates q_W or to mass coordinates q_S. In this work, all equations are given in mass coordinates q_S and without loss of generality, as all equations can be easily converted to shaft coordinates q_W using Equation (2.1). With NEWTON's second law of motion, the combination of Equations (2.1) and (2.2) yields:

$$m\ddot{q}_S = -F_P$$

$$m\ddot{q}_S + kq_S = k\varepsilon \tag{2.3}$$

It is further assumed that the rotor turns with the angular *rotational speed* Ω, and that angular rotor accelerations can be neglected.

$$\Omega = \text{const.} \tag{2.4}$$

The eccentricity is a quantity that is bound to the rotor. When the rotor turns, the eccentricity also changes periodically from the viewpoint of the inertial coordinate system. To facilitate its description, a *positive rotating coordinate system* is introduced. It shares the same origin as the inertial coordinate system, but is turned by the angle $\varphi = \Omega t$, with t being the time. All quantities given in the positive rotating coordinate system are identified by the superscript "+". From the viewpoint of the positive rotating coordinate system, the eccentricity is constant.

$$\varepsilon^+ = \text{const.} \tag{2.5}$$

Another advantage of complex coordinates is that coordinate system rotations by φ can be performed by a simple multiplication with $\mathrm{e}^{i\varphi}$ [19], and a coordinate transformation of the eccentricity ε^+ from rotating coordinates to fixed ones, gives:

$$\varepsilon = \varepsilon^+ \mathrm{e}^{i\Omega t} \tag{2.6}$$

Combining Equations (2.3) and (2.6) leads to the differential equation of the passive rotor:

$$m\ddot{q}_S + kq_S = k\varepsilon^+ \mathrm{e}^{i\Omega t} \tag{2.7}$$

Mathematically, this is an ordinary differential equation with constant coefficients that can be solved using the *ansatz* $q_S = q_S^+ \mathrm{e}^{i\Omega t}$. From the theory of linear equations, it is known that q_S^+ is constant, and its second derivative is $\ddot{q}_S = -q_S^+ \Omega^2 \mathrm{e}^{i\Omega t}$. The solutions for the mass center q_S and for the shaft center q_W can be simplified with the introduction of the natural frequency $\omega_0 = \sqrt{m^{-1}k}$. According to Equation (2.2), the passive bearing forces are directly proportional to the displacements of the shaft center q_W.

$$q_S = \left(-\Omega^2 m + k\right)^{-1} k\varepsilon^+ \mathrm{e}^{i\Omega t} \quad = \left(\omega_0^2 - \Omega^2\right)^{-1} \omega_0^2 \varepsilon^+ \mathrm{e}^{i\Omega t} \tag{2.8}$$

$$q_W = \left(-\Omega^2 m + k\right)^{-1} m\Omega^2 \varepsilon^+ \mathrm{e}^{i\Omega t} = \left(\omega_0^2 - \Omega^2\right)^{-1} \Omega^2 \varepsilon^+ \mathrm{e}^{i\Omega t} \tag{2.9}$$

The Equations (2.8) and (2.9) give the solutions for mass and shaft center displacements. For low rotational speeds $\Omega \ll \omega_0$, both shaft displacements and bearing forces remain small, while the center of mass q_S rotates around the bearing centerline and describes a circle with the radius $|\varepsilon|$. When the rotational speed Ω approaches the rotor's natural frequency ω_0, the quantities $|q_S|, |q_W|$ as well as the bearing forces $|F_P|$ become very large. For $\Omega = \omega_0$, the rotor has reached its *critical speed*, and all quantities lean towards infinity with increasing time. Operating a rotor at its critical speed without sufficient damping is generally not recommended. In the late 19th century, engineers believed that the rotor's critical speed could never be passed. It was De Laval who first practically demonstrated that a critical speed could be passed. For rotational speeds $\Omega > \omega_0$, rotor displacements and forces become smaller. Jeffcott described this as "The effect of want of balance" in his pioneering work [53]. For very high rotational speeds $\Omega \gg \omega_0$, the mass center approaches the bearing centerline $q_S \to 0$, while the shaft center q_W circles around it.

Solving a differential equation requires the superposition of a *particular solution* and a *homogeneous solution*. In case of a rotor, the first one describes the unbalance response, while the latter one describes the rotor's natural vibration. The homogeneous solution can be calculated when the right-hand side of Equation (2.7) is set to zero:

$$q_0 = q_O^+ \mathrm{e}^{i\omega_0 t} + q_O^- \mathrm{e}^{-i\omega_0 t} \tag{2.10}$$

The homogeneous solution q_0 is a superposition of two complex quantities defined in different coordinate systems. The quantity q_O^+ is constant in the positive rotating coordinate system, while the solution q_O^- is constant in the *negative rotating coordinate system*, rotating in the opposite direction. Throughout this work, the superscript "$-$" represents quantities defined in the latter coordinate system. Both values depend on the initial conditions and are independent of the unbalance excitation.

2.2 The Jeffcott rotor with active bearings

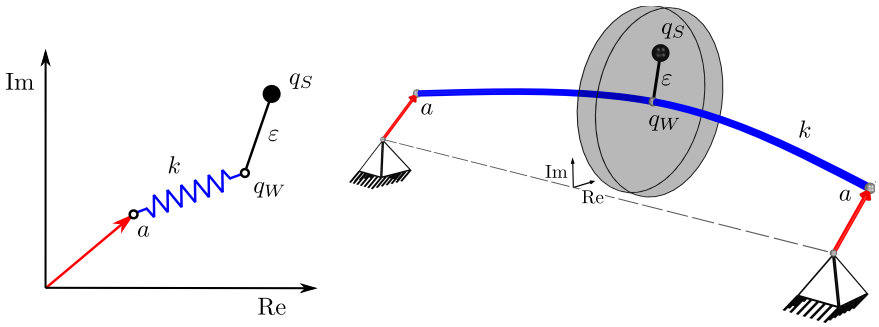

Figure 2.2: Model of the actively supported Jeffcott rotor. The active bearing is represented by an arrow (red) that can move the flexible shaft (blue) in the complex plane. Left: 2D-projection of the extended Jeffcott rotor with active bearings. Right: 3D representation.

As the name already indicates, the purpose of both active and passive bearings is to bear or support the rotor, keeping it in its intended position. The JEFFCOTT rotor is a *statically determinate* system. The forces on a bearing are *reaction forces*, they only depend on shaft loading. Imagine a planar rotor with a constant load F_G on its disc, caused for example by gravity. Under static conditions, the bearing has to develop a reaction force F_L of exactly the same magnitude so that the sum of both vanishes, $F_G + F_L = 0$. Failure to deliver this force leads to *static instability*, regardless of whether the bearing is passive or active, or how sophisticated the underlying control algorithm might be.

Since in statically determinate systems the bearing loads only depend on the shaft forces, active bearings have no opportunity to alter them. In consequence, an active bearing cannot exert arbitrary forces on a rotor, as it leads to static instability. However, what active bearings *can* control is the shaft displacement in the complex plane, as they are able to move the rotor in the complex plane. Figure 2.2 illustrates a model of the JEFFCOTT rotor with active bearings. The red arrow depicts the displacements a of the active bearing in the complex plane. For now, this displacement is thought of as a purely abstract quantity. The goal is a strict separation between system-theoretic considerations and their physical realization, given in Chapter 4. With the actuator displacement a, the active bearing force F is:

$$F = k\,(q_W - a) \tag{2.11}$$

In analogy to Equation (2.7), the equation of motion is:

$$m\ddot{q}_S + kq_S = ka + k\varepsilon \tag{2.12}$$

The equation's right-hand side only differs in the summand ka from its passive counterpart. This summand requires special attention, as it contains products of a stiffness k with the displacement quantities a and ε. In structural mechanics, this product indicates a *footpoint excitation* or *support excitation* [102]. Although the *unit* of the product ka is 'Force', the quantity physically represents a displacement excitation. Although replacing the expression ka with an 'actuator force' f_a is mathematically correct, it leads to ambiguous, if not incorrect interpretations of the physical realities. The only valid definition for the actuator force is the one given in Equation (2.11). This important difference is clarified in an example of a rotor without eccentricity ($\varepsilon = 0$). The equation $m\ddot{q}_S + kq_S = ka$ represents a rotor with active bearings at the shaft ends. In this case, the bearings are able to move the rotor in the complex plane without any forces on the actuator or shaft. In contrast, if just the equation $m\ddot{q}_S + kq_S = f_a$ is given without further explanation, it might as well represent a system with fixed shaft ends and a force f_a directly acting on the disc. Although both equations are almost identical, they represent different physical setups with completely different properties.

Given the findings in Equation (2.12), one can conclude that the evidence is nothing new. Moreover, the authors of standard literature on rotordynamics and active bearings have found similar expressions [26, 29, 66]. The expression a is usually named *reference input* and is either used for a *static* displacement compensation or subsequently omitted. The presented approach differs from the standard one as the actuator displacement a is seen as *dynamic control input*, not a static compensation feature. The controller only uses the displacements a to control the rotor. The advantage of this approach is that the conditions for static stability are automatically satisfied, leading to inherently consistent equations.

2.3 The controlled Jeffcott rotor

This section deals with the properties of the controlled rotor. After the derivation of a new control algorithm, the rotor's controlled unbalance response and its stability are thoroughly investigated.

2.3.1 Controller derivation

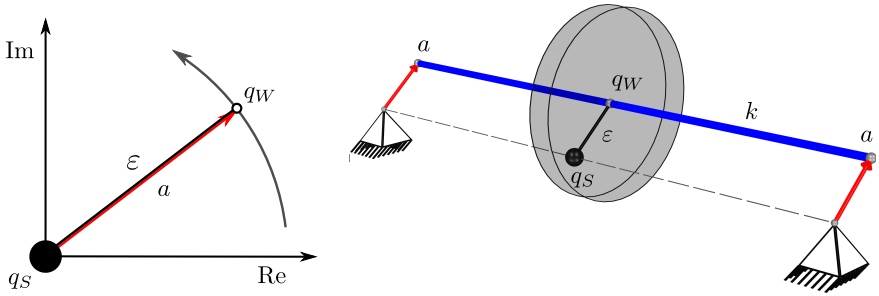

Figure 2.3: Illustration of the force free condition. The mass q_S is kept still in the rotational center without accelerations or forces. The shaft center q_W performs a circular motions, while the bearing displacement a follows this motion, keeping the shaft in an undeflected position.

In this section, a new control algorithm that eliminates unbalance-induced bearing forces is derived. According to NEWTON's second law of motion, the mass is force free when it is kept at the rotational center, $q_S = 0$. In this case, the shaft center q_W performs according to Equation (2.1) and (2.6) circular motions with the radius $|\varepsilon^+|$ around the rotational center, $q_W = -\varepsilon$. However, no forces on the mass also requires an unbent shaft, so according to Equation (2.11), the actuator displacement a and the shaft center q_W must be coincident.

$$a = q_W = -\varepsilon \tag{2.13}$$

Figure 2.3 illustrates the kinematics of this force free condition. The design of an algorithm that meets this condition is challenging due to the following reasons:

- The eccentricity ε changes periodically with the rotational speed Ω from the viewpoint of the inertial coordinate system.
- Although the eccentricity ε^+ is constant in rotating coordinates, it is generally unknown and unavailable for the control algorithm.
- The rotor movement is a combination of the unbalance response and the free rotor vibration, hence a superposition of homogeneous and particular solution. The controller has not only to alter the unbalance response, but also to stop the free vibration.

Considering the findings from Figure 2.3 it is clear that the rotor is in a force free condition when the actuator displacement is exactly opposite to the eccentricity ($a = -\varepsilon$) so that the center of mass remains still in the rotational center ($q_S = 0$). The fact that the eccentricity ε^+ is constant in the positive coordinate system leads to the idea to define a controller with a displacement element a_F^+ in rotating coordinates. In order to reach a force free condition, this displacement control element must be opposite to the eccentricity ($a_F^+ = -\varepsilon^+$). Although it is clear that this steady-state condition must be finally reached, it is unclear *how* to do so. The controller should always be able to *converge* to this force free condition, a demand which is closely linked to the stability of the controlled rotor. A system can be considered stable when its overall energy balance is negative [74]. When this is the case, the free vibration's energy will finally vanish and the movement will stop. As a minimum requirement, the displacement element a_F^+ should not excite the rotor by introducing energy. According to the principle of work, no power will be transferred to the mechanical system when the velocity $\dot{a}_F^+$ is geometrically *perpendicular* to the bearing force F^+. This reasoning was conditionally inspired by conservative *gyroscopic moments*, which are energy-neutral because the involved moments and velocities are also perpendicular to each other. Figure 2.4a illustrates the situation, where the velocity $\dot{a}_F^+$ causes a "spiral dive" of the mass. The control law of the conservative forward compensation element a_F^+ is then:

$$\dot{a}_F^+ = -i\tilde{c}_C F^+ \tag{2.14}$$

Throughout this work, $i = \sqrt{-1}$ represents the imaginary unit, and reflects here the property of perpendicularity. The real parameter $\tilde{c}_C$ represents the adaption speed of the controller element. To express the controller equations

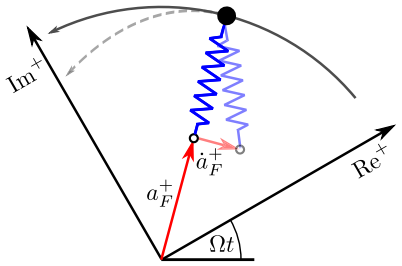

(a) Forward compensating element

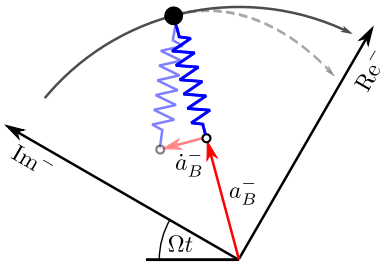

(b) Backward compensating element

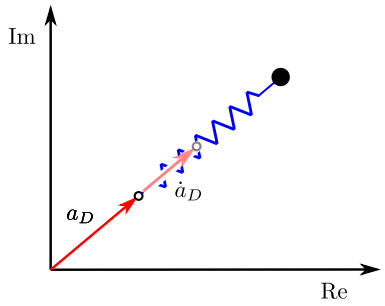

(c) Damping element

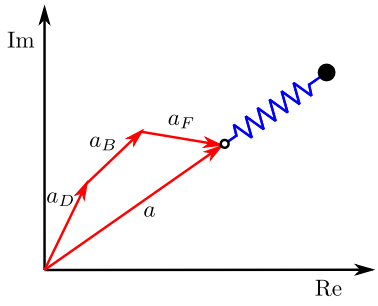

(d) Element superposition

Figure 2.4: The controller's governing elements in their respective coordinate system. The conservative compensating elements (a) and (b) move perpendicular to the bearing force. Only the damping element (c) moves collinear, leading to an energy dissipation. Figure (d) shows the superposition of all controller elements

.

in inertial coordinates, the transformation $a_F^+ = a_F\,\mathrm{e}^{-i\Omega t}$, its derivative $\dot{a}_F^+ = (\dot{a}_F - i\Omega a_F)\,\mathrm{e}^{-i\Omega t}$ as well as the transformed actuator forces $F^+ = F\,\mathrm{e}^{-i\Omega t}$ are required.

$$\dot{a}_F = i\Omega a_F - i\tilde{c}_C F \tag{2.15}$$

Although the controller element will not destabilize the system, it will not stabilize the rotor either – the homogeneous solution will not vanish. This behavior should not surprise as the controller element was specifically designed to be conservative. The stabilization of the controlled system requires a dissipating controller element, depicted in Figure 2.4c. Its differential equation resembles a mechanical spring-damper system.

$$\dot{a}_D = c_D \left(F - k_D a_D\right) \tag{2.16}$$

The parameter c_D represents an inverse damping coefficient, while the factor k_D is the stiffness of a fictitious return spring. A superposition of both controller elements is able to finally stabilize the system. However, this stability is only conditional as it depends on both the rotor properties as well as the exact choice of controller parameters. The problem of conditional stability is present in many unbalance compensation algorithms [10, 55, 60], a unwanted property that inhibits a broad application of these algorithms.

The stability of the controlled system depends on the eigenvalues of the homogeneous differential equation and is independent of the rotor's unbalance response. It is interesting that the rotor's free vibration solution from Equation (2.10) consists of two parts. One is defined in positive rotating coordinates, whereas the other one is defined in the *negative* rotating coordinate system. The superposition of these *counterrotating* pointers leads to a *symmetry* in the homogeneous solution.

A supposition is that the controller's conditional stability is caused by compensation element a_F^+ that is only defined in the positive rotating coordinate system. This asymmetric pointer might disturb the rotor's initial symmetric solution. *The idea is to symmetrize the controller by introducing a second compensating element a_B^- that is defined in the negative rotating coordinate system*.

$$\dot{a}_B^- = +i\tilde{c}_C F^- \tag{2.17}$$

Figure 2.4b depicts the element's governing equation. In analogy to Equation (2.15), a transformation to the inertial coordinate system yields:

$$\dot{a}_B = -i\Omega a_B + i\tilde{c}_C F \tag{2.18}$$

The controller is governed by three superpositioned elements as Figure 2.4d indicates. The forward compensation element a_F^+ from Equation (2.15), the backward compensation element a_B^- from Equation (2.18), and the damping element a_D deduced in Equation (2.16). A state-space representation conveniently gathers all controller elements.

$$\underbrace{\begin{bmatrix} \dot{a}_F \\ \dot{a}_B \\ \dot{a}_D \end{bmatrix}}_{\dot{\mathbf{x}}_R} = \underbrace{\begin{bmatrix} i\Omega & 0 & 0 \\ 0 & -i\Omega & 0 \\ 0 & 0 & -c_D k_D \end{bmatrix}}_{\mathbf{A}_R} \underbrace{\begin{bmatrix} a_F \\ a_B \\ a_D \end{bmatrix}}_{\mathbf{x}_R} + \underbrace{\begin{bmatrix} -i\tilde{c}_C \\ +i\tilde{c}_C \\ c_D \end{bmatrix}}_{\mathbf{B}_R} F$$
$$a = \underbrace{\begin{bmatrix} 1 & 1 & 1 \end{bmatrix}}_{\mathbf{C}_R} \mathbf{x}_R \tag{2.19}$$

The controller uses the bearing or actuator force F as control input while it controls the bearing displacement a. Figure 2.2 indicates that force and displacement are bound to the same degree of freedom. In this case, the sensor / actuator pair is *collocated*, a generally favorable property for controlled systems [30]. Standard controllers have fixed parameters, but in case of Equation (2.19), the system matrix $\mathbf{A}_R$ is *adaptive* as it depends on the rotational speed Ω. The controller's adaptive structure was derived through the coordinate transformations from rotating to inertial coordinates in Equations (2.15) and (2.18), based on the kinematic considerations from Figure 2.3 and Equation (2.13). In contrast to many publications where an adaptive algorithm is an *a-priori* choice [10, 55, 60], the controller's adaptive structure here was the logic result from kinematic considerations. A prerequisite for a successful control is accurate knowledge of the rotational speed Ω.

2.3.2 Unbalance response

Combining the actively supported rotor from Equation (2.12) with the controller from Equation (2.19) using the bearing force Equation (2.11) leads to the state-space description of the controlled rotor:

$$\underbrace{\begin{bmatrix} \dot{q}_S \\ \ddot{q}_S \\ a_F \\ a_B \\ a_D \end{bmatrix}}_{\dot{\mathbf{x}}} = \underbrace{\begin{bmatrix} 0 & 1 & 0 & 0 & 0 \\ -m^{-1}k & 0 & m^{-1}k & m^{-1}k & m^{-1}k \\ -i\tilde{c}_C k & 0 & i\Omega + i\tilde{c}_C k & i\tilde{c}_C k & i\tilde{c}_C k \\ i\tilde{c}_C k & 0 & -i\tilde{c}_C k & -i\Omega - i\tilde{c}_C k & -i\tilde{c}_C k \\ c_D k & 0 & -c_D k & -c_D k & -c_D (k + k_D) \end{bmatrix}}_{\mathbf{A}} \underbrace{\begin{bmatrix} q_S \\ \dot{q}_S \\ a_F \\ a_B \\ a_D \end{bmatrix}}_{\mathbf{x}} + \underbrace{\begin{bmatrix} 0 \\ m^{-1}k \\ i\tilde{c}_C k \\ -i\tilde{c}_C k \\ -c_D k \end{bmatrix}}_{\mathbf{B}} \varepsilon$$

$$\dot{\mathbf{x}} = \mathbf{A}\mathbf{x} + \mathbf{B}\varepsilon^{+}\, \mathrm{e}^{i\Omega t} \tag{2.20}$$

In principle, the derivation of the rotor's controlled unbalance response is similar to the calculation of the rotor's passive response from Equation (2.9), with the difference that the *ansatz* is now a vector and not a constant. With $\mathbf{x} = \mathbf{x}^{+}\, \mathrm{e}^{i\Omega t}$ and its derivative $\dot{\mathbf{x}} = i\Omega \mathbf{x}^{+}\, \mathrm{e}^{i\Omega t}$, the unbalance response is defined as:

$$\mathbf{x}^{+} = (i\Omega \mathbf{I} - \mathbf{A})^{-1}\, \mathbf{B}\varepsilon^{+} \tag{2.21}$$

Throughout this work, $\mathbf{I}$ represents the identity matrix of adequate dimensions. The particular solution exists if $(i\Omega\mathbf{I} - \mathbf{A})$ is invertible, which is the case when:

$$\det(i\Omega \mathbf{I} - \mathbf{A}) = -2\tilde{c}_C k \Omega^3 (i\Omega + c_D k_D) \tag{2.22}$$

A solution exists when the rotor is rotating $\Omega \neq 0$ and all other parameters are real and non-zero. This result differs from the uncontrolled JEFFCOTT rotor from Equation (2.9) which is singular when the rotational frequency matches the rotor's eigenfrequency $\Omega = \omega_0$. It can be concluded that the controlled rotor has no *no resonance* for any rotational speed Ω. The explicit solution of Equation (2.21) requires a symbolic inversion of the (5×5) matrix $(i\Omega\mathbf{I} - \mathbf{A})$. To avoid a tedious symbolic inversion, a particular solution $\mathbf{x}^{+}$ can be *guessed*, followed by a check of whether the preliminary solution solves Equation (2.20). According to Figure 2.3, a force free steady-state solution requires that the mass remains still in the rotational center, so that both q_S and $\dot{q}_S$ must be zero and furthermore according to Equation (2.13) – the negative eccentricity $-\varepsilon$ must match the actuator displacement a. The latter one is a superposition of three

controller elements a_F^+, a_B^- and a_D, but since the eccentricity ε^+ is defined in the positive rotating coordinate system, it is assumed that the controller element a_F^+ compensates the unbalance displacement entirely. Meanwhile, the other elements a_B^- and a_D remain at zero. With these assumptions, the initial hypothetical solution is as follows:

$$\mathbf{x}^+ = \begin{bmatrix} 0 & 0 & -\varepsilon^+ & 0 & 0 \end{bmatrix}^T \tag{2.23}$$

It is now checked if the preliminary solution satisfies the equation:

$$(i\Omega\mathbf{I} - \mathbf{A})\,\mathbf{x}^+ = \mathbf{B}\varepsilon^+$$

$$\underbrace{\begin{bmatrix} \dots & \dots & 0 & \dots & \dots \\ \dots & \dots & -m^{-1}k & \dots & \dots \\ \dots & \dots & -i\tilde{c}_C k & \dots & \dots \\ \dots & \dots & i\tilde{c}_C k & \dots & \dots \\ \dots & \dots & c_D k & \dots & \dots \end{bmatrix}}_{(i\Omega\mathbf{I}-\mathbf{A})} \underbrace{\begin{bmatrix} 0 \\ 0 \\ -\varepsilon^+ \\ 0 \\ 0 \end{bmatrix}}_{\mathbf{x}^+} = \underbrace{\begin{bmatrix} 0 \\ m^{-1}k \\ i\tilde{c}_C k \\ -i\tilde{c}_C k \\ -c_D k \end{bmatrix}}_{\mathbf{B}} \varepsilon^+ \tag{2.24}$$

Equation (2.24) reveals that the guessed solution vector $\mathbf{x}^+$ from Equation (2.23) is indeed the controlled rotor's unbalance response. Since the actuator and shaft displacement are coincident $a = q_W$, the bearing force Equation (2.11) indicates that:

$$F = 0 \tag{2.25}$$

Figure 2.5 compares the rotor's unbalance response in both the uncontrolled passive case and the controlled case. While the passive case has a distinct resonance with large displacements and forces in the vicinity of the rotor's eigenfrequency ω_0, the shaft displacements remain small and the bearing forces completely vanish. Furthermore, there is no resonance for any rotational speed $\Omega > 0$. It is particularly interesting that neither the rotor properties m, k nor the controller parameters $\tilde{c}_C, c_D, k_D$ have an influence on the controlled unbalance response. It is moreover interesting that the force free condition $F = 0$ is *independent* of eccentricity's magnitude. It should be noted that the controller

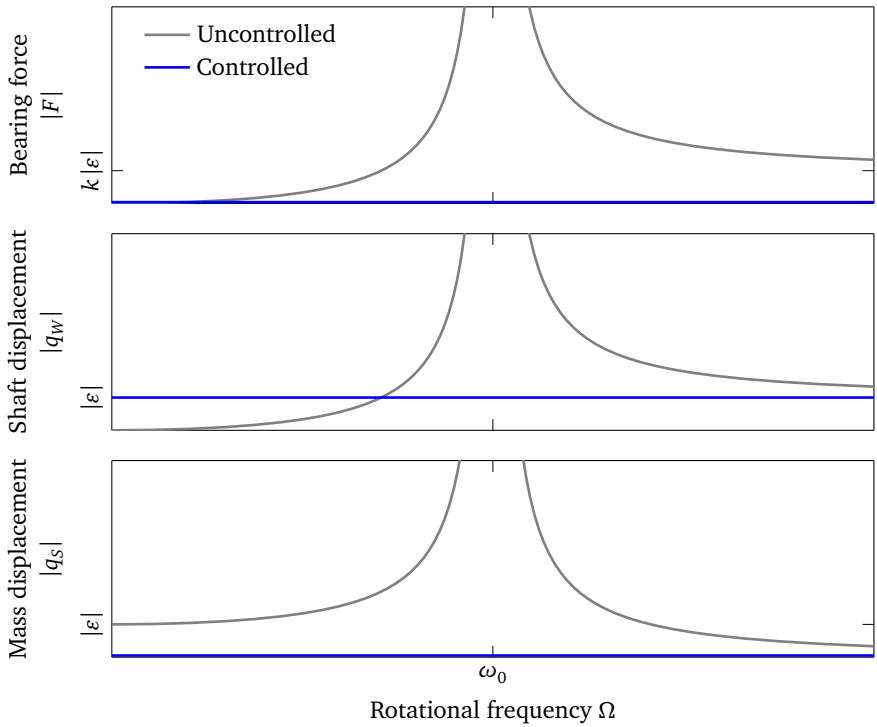

Figure 2.5: Analytical solution of the uncontrolled and controlled Jeffcott rotor. In uncontrolled case, displacements and forces are high in the vicinity of the rotor's critical speed ω_0. In controlled case, the bearing forces $|F|$ as well as mass displacements $|q_S|$ are zero, with no resonance present for any rotational speed Ω.

has no explicit information on the eccentricity ε^+ or the mass center's position q_S. The controller determines both quantities through the bearing forces F only. According to Equation (2.13), the controller displacements equal the negative eccentricities $a_F = -\varepsilon$. The controller state directly represents the rotor's eccentricity, a feature which will be exploited in Section 4.1.1 for balancing or health monitoring.

In summary, the designed controller eliminates both the unbalance-induced bearing force and the resonance at any given rotational speed Ω, even at the rotor's natural frequency ω_0.

2.3.3 Hurwitz stability proof

A system is stable when the homogeneous solution vanishes with proceeding time. According to linear theory, this is the case when the eigenvalues of the homogeneous differential equation $\dot{\mathbf{x}} = \mathbf{A}\mathbf{x}$ have all negative real parts. The dimension of the system matrix $\mathbf{A}$ makes a direct eigenvalue calculation impossible, however the HURWITZ stability criterion [47] allows for a binary decision whether the eigenvalues' real parts are negative or not. A necessary criterion is that all coefficients of the characteristic polynomial are positive:

$$\det(\lambda\mathbf{I}-\mathbf{A}) = \alpha_5\lambda^5 + \alpha_4\lambda^4 + \alpha_3\lambda^3 + \alpha_2\lambda^2 + \alpha_1\lambda + \alpha_0 \tag{2.26}$$

$$\begin{aligned}
\alpha_5 &= 1 \\
\alpha_4 &= c_D\,(k + k_D) \\
\alpha_3 &= \Omega^2 + 2k\tilde{c}_C\Omega + m^{-1}k \\
\alpha_2 &= c_D\,(k + k_D)\,\Omega^2 + 2\tilde{c}_C k k_D\Omega + c_D k_D m^{-1}k \\
\alpha_1 &= m^{-1}k\Omega^2 \\
\alpha_0 &= c_D k_D m^{-1}k\Omega^2
\end{aligned}$$

It is interesting that the coefficients of the characteristic are entirely real, although the matrix $\mathbf{A}$ is complex. Both rotor mass m and stiffness k are positive, and it is assumed that the controller parameters c_D and k_D are chosen positive as well. Some coefficients of the characteristic polynomial have odd exponents for the rotational speed Ω, leading to possible instability for negative rotational speeds. However, this problem has a simple solution. It stands out that the odd exponents of Ω exclusively occur with the parameter $\tilde{c}_C$. In this case, the problem can be circumvented with the introduction of the positive parameter c_C:

$$\tilde{c}_C = \Omega c_C \tag{2.27}$$

Using this definition, all previously odd exponents of Ω are now even. For positive parameters c_C, the necessary condition is satisfied for any rotational speed Ω. A sufficient stability criterion is that all five HURWITZ-determinants Δ are positive.

$$
\begin{aligned}
\Delta_1 &= c_D\,(k + k_D) && > 0\\
\Delta_2 &= c_D k^2 \left(2c_C\Omega^2 + m^{-1}\right) && > 0\\
\Delta_3 &= c_D^2 k^2 \left(\left(2c_C\,(k + k_D) + 4c_C^2 k k_D\right)\Omega^4 + 4c_C k k_D m^{-1}\Omega^2 + k k_D m^{-2}\right) && > 0\\
\Delta_4 &= 2c_C c_D^2 k^4 m^{-1}\Omega^6 && > 0\\
\Delta_5 &= 2c_C c_D^3 k^5 k_D m^{-2}\Omega^8 && > 0
\end{aligned}
$$

The HURWITZ-determinants are all positive for controller parameters $c_C, c_D, k_D > 0$. This is the proof that the controlled system is *always* stable, independent of the rotor or controller parameters. Interestingly, the controlled system is even asymptotically stable at the passive rotor's natural frequency ω_0. Although the property of inherently stable control systems was extensively studied by POPOV and called *hyperstability* or *passivity* [13], the concept primarily focused at standard controllers with mostly damping properties. It is the author's understanding that the unique combination of an unbalance force elimination and hyperstability has not yet been reported or proven.

2.3.4 The secrets of hyperstability

The controller's property of unlimited stability for positive controller parameters is a key finding of this work, and also a feature that sets it apart from other, conditionally stable control approaches. This remarkable stability property shall be further investigated in this section. During the controller derivation in Section 2.3.1, it was revealed that the combination of two counterrotating compensating and a damping element finally led to unlimited stability. Apparently, a controller with one compensating element leads only to conditional stability. In order to better understand the secrets of unconditional stability, a controller with only one compensating element and conditional stability is compared with the hyperstable controller from the previous section.

$$
\begin{bmatrix} \dot{a}_F \\ a_D \end{bmatrix} = \begin{bmatrix} i\Omega & 0 \\ 0 & -c_D k_D \end{bmatrix} \begin{bmatrix} a_F \\ a_D \end{bmatrix} + \begin{bmatrix} -i\tilde{c}_C \\ c_D \end{bmatrix} F
$$

$$
a = \begin{bmatrix} 1 & 1 \end{bmatrix} \begin{bmatrix} a_F & a_D \end{bmatrix}^T \tag{2.28}
$$

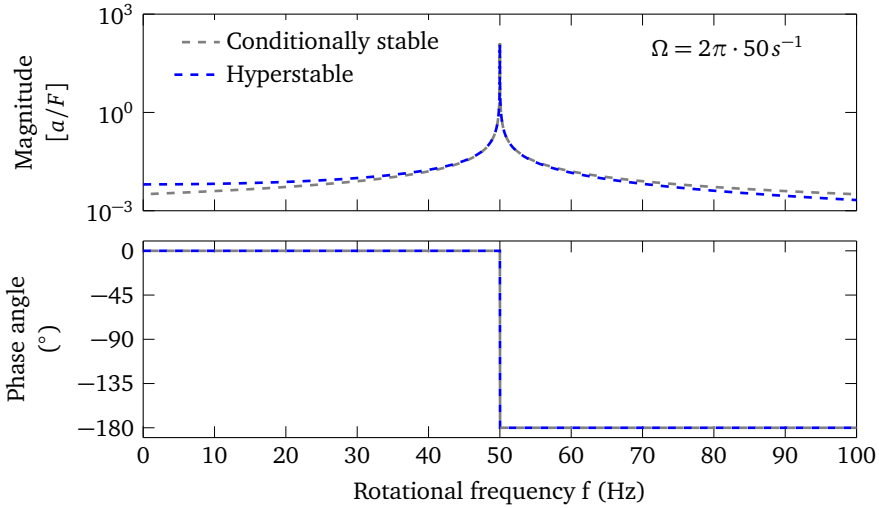

Figure 2.6: Comparison of example frequency response functions for a conditionally stable and a hyperstable controller for a rotational frequency $\Omega = 2\pi 50\,s^{-1}$. The minor magnitude differences give no explanations as to why one controller is hyperstable while the other is not.

Equation (2.28) gives the shortened, conditionally stable controller with only one compensating element defined in the positive rotating coordinate system a_F and a damping element a_D. In a first test, the controller's closed-loop stability is investigated using its characteristic polynomial. Although the dimensions of the system matrix **A** are now (4×4) and therefore smaller than the original (5×5) system from Equation (2.20), its characteristic polynomial is more complicated and also contains complex entries. For stability, all HURWITZ-determinants are regarded as positive. However, the results find out that:

$$\Delta_2 = k^2 m^{-2} \left(-mc_C c_D^2 k_D^2 i + c_D k_D - \Omega i - mc_D \Omega^2\right)$$

Looking at the last summand $-mc_D\Omega^2$, it is clear that the closed-loop system may become unstable, whereas the HURWITZ-determinants of the hyperstable controller (2.19) were always positive. In control engineering, *frequency response functions* or BODE *plots* are used to characterize the controllers [93] in the frequency domain. Figure 2.6 gives the frequency response function for the hyperstable controller from Equation (2.19) and the conditionally stable

controller from Equation (2.28). Magnitude and phase barely differ, and the diagram gives no obvious clues why both controllers have different closed-loop stability properties. The question why controllers with different stability prop-

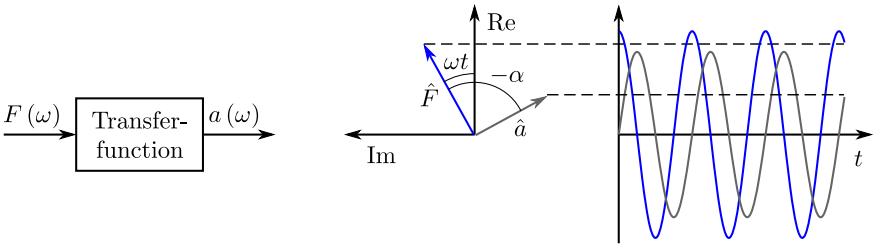

Figure 2.7: Transfer function interpretation in control engineering. A signal F with the angular frequency ω at the input is transferred to the output a. Since control engineers only consider real quantities, the phase shift $-\alpha$ represents the function's time lag.

erties lead to almost identical frequency responses, requires an understanding how frequency response functions are derived. Figure 2.7 shows a transfer function with the input $F(\omega)$ and the output $a(\omega)$. According to linear theory, a harmonic input excitation with the angular frequency ω and the magnitude $\hat{F}$ causes the system to respond at the same angular frequency, but with a different magnitude $\hat{a}$. A transfer function not only affects the output's magnitude, but also causes an offset of $-\alpha$ between the system's response and its corresponding input, a property called *phase shift* in control engineering. According to Figure 2.7, the system's output response is the projection of the rotating output pointer to the real axis. In control engineering, the imaginary axis is insignificant because it is not linked to any physical quantity. A phase angle is therefore interpreted with respect to time, a negative phase shift $-\alpha$ corresponds to a transfer function's time lag.

There is however an important discrepancy in the interpretation of differential equations in control engineering and rotordynamics. Control engineers consider the imaginary axis as calculation quantity with no physical representation. In rotordynamics however, there is a physical interpretation of the complex axis. Going back to the coordinate system definitions of Section 2.1, it can be concluded that the imaginary axis indeed has a physical meaning: it represents the perpendicular axis of the cartesian coordinate system. This revelation leads to a number of important conclusions. In contrast to control theory, where a phase shift $-\alpha$ is considered as a time lag, it represents a *spatial angle* in the rotor-

dynamic complex coordinate system, which also changes the interpretation of the frequency response function. In control engineering, *negative frequencies* represent acausal systems which require knowledge of future events. On the contrary this perspective makes sense from a rotordynamic view. When positive frequencies represent a rotor rotating in the mathematically positive direction of rotation in the complex plane (forward whirling), negative frequencies represent the shaft rotating in the mathematically negative direction of rotation (backward whirling). In this interpretation, negative frequencies do not represent future events, but only a change in the direction of rotation.

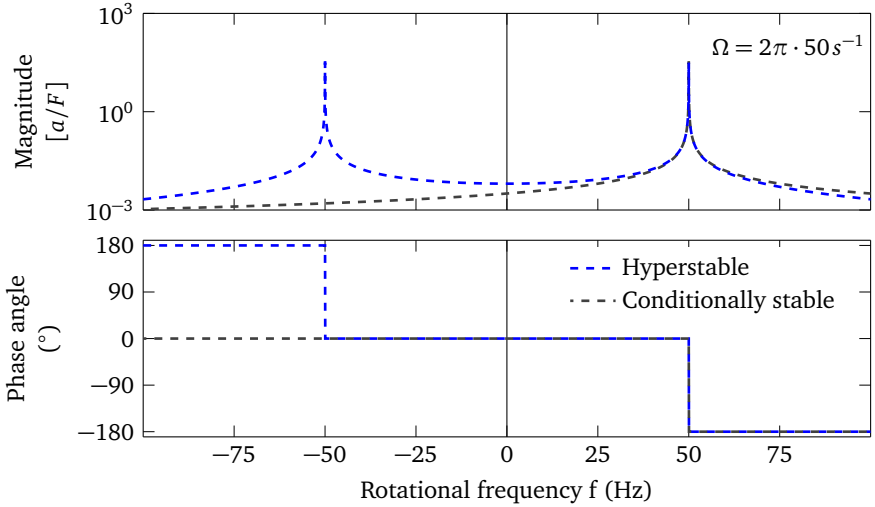

Figure 2.8: Two-sided frequency response functions for both controllers. In rotordynamics, negative frequencies $\omega < 0$ do not represent future events, but rather rotations in mathematically negative direction. In contrast to the conditionally stable controller, its hyperstable counterpart is symmetrical in the complex plane, explaining its unique stability properties.

Figure 2.8 depicts a two-sided frequency response function and extends the one-sided version from Figure 2.6 to negative frequencies. Although both controllers are almost equal for $\omega > 0$, differences become apparent for negative frequencies $\omega < 0$. In contrast to its conditionally stable counterpart, the hyperstable controller has a symmetry in the complex plane. In this case, the phase angle does not represent a time lag, but spatial information about the direction between the inputs and outputs in the complex plane.

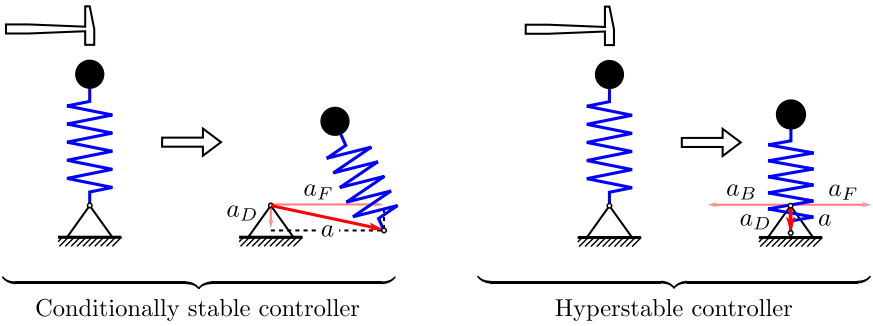

Figure 2.9: Illustration of the controller stability properties. For the conditionally stable controller, a shock excitation in one axis leads to a controller-induced excitation in the perpendicular axis. The symmetry of the hyperstable controller prevents this excitation as both compensation elements a_F and a_B cancel each other out.

A graphic interpretation of the differences between the controllers is depicted in Figure 2.9. It shows a rotor with no eccentricity that is shock-excited in the vertical axis. Immediately after the excitation, the conditionally stable controller responds with two displacement components, the damping displacement a_D and the compensation displacement a_F. The perpendicular compensation displacement a_F leads to system excitation in the horizontal axis, resulting in a controller-induced whirling. In case of the hyperstable controller, the compensators a_F and a_B extend in opposite directions, canceling each other out. This symmetric property keeps the horizontal axis unaffected, avoiding a rotor whirling.

It results that the choice of complex coordinates in Chapter 2.1 did not only result shorter equations, but led to advantages in the stability analysis using the two-sided frequency response function with negative frequencies. Despite the apparent elegance of complex notation, a representation in real coordinates has advantages from the viewpoint of control engineering. An adaption of the controller Equations (2.19) to real coordinates is easy because the imaginary unit i in complex notation translates to a skew-symmetric matrix in real coordinates [22]. In contrast to the complex controller that has one complex input F and one complex output a, the real version requires two inputs F_x, F_y and two outputs a_x, a_y, leading to a total of *four nontrivial controller transfer functions*. Only the interaction of all four transfer functions leads to hyperstability.

It can be concluded that the one-sided transfer function from Figure 2.6 can explain the controlled rotor's unbalance response, but is unable to explain the controller's superior stability properties. In contrast to control engineering where the imaginary axis is physically meaningless, the latter represents a physical dimension in rotordynamics. Under this changed paradigm, negative frequencies as well as phase angles are interpreted not in a time, but in a spatial context. The symmetry of the two-sided frequency response function depicted in Figure 2.8 finally explains the controller's unique stability properties. In real coordinates, the controller requires four non-trivial transfer functions. *The reason of the controller's stability properties lies in the special controller coupling of the rotor axes.*

3 General rotors with active bearings

The ideas of the previous chapter are now extended to general rotor systems. After a revision of the rotor's elastic properties and its passive unbalance response, the research turns to a thorough investigation of the kinematics for rotors with active bearings. Using the controller from the previous section, a closed-loop state-space model is built. The controlled unbalance response is calculated. Two examples demonstrate that the controller allows for a force free operation and an elimination of resonances even for arbitrary rotors. The approach is extended to rotors with gyroscopy and damping, and the influence of parasitic stiffnesses as well as the bearing placement is discussed. In many applications not only the rotor, but also the bearing foundations are flexible. The chapter's last topic gives also a solution for this common problem.

The contents as well as some figures of this chapter are based on the publication "Unbalance and resonance elimination with active bearings on General Rotors" written by HEINDEL et al. [39].

3.1 Mechanical model

This section derives the matrix properties of elastic rotors, discusses the rotor's passive behavior and finally highlights the characteristics of flexible rotors with active bearings.

3.1.1 Elastic properties of free rotors

Throughout this section, the theoretical analysis and the derivation of the rotor's characteristic elastic features are demonstrated on a slender beam, accentuating the connection between physical and mathematical properties. It is stressed that the following considerations are manifested on, but not limited to this particular beam structure. The continued use of complex notation limits the considerations to isotropic rotors only. This limitation is motivated in

the notation's simplicity and is barely a real mathematical or technological burden. The considered beam has a total number of p nodes with the coordinates $\mathbf{q}_W = \left[q_{W1} \dots q_{Wp}\right]^T$. Its elastic stiffness properties are stored in the $(p \times p)$

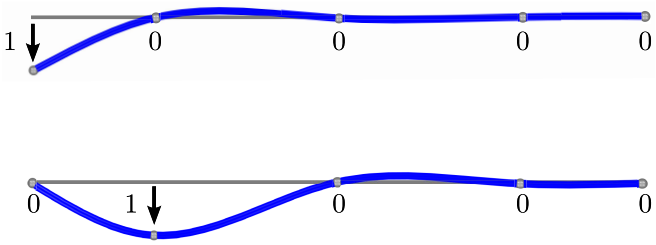

Figure 3.1: The properties of a flexible object are derived with unit displacements.

rotor stiffness matrix $\mathbf{K}_R$. In theory, stiffness matrices can be derived using *unit displacements*. Figure 3.1 demonstrates the derivation process. An arbitrary node is displaced by one unit, while the other nodes are held tight. The deformation causes reaction forces on the nodes. These reactions can be measured and directly represent the stiffness coefficients k of one column. Sequential displacements of the other nodes derive more columns until the stiffness matrix is fully determined.

$$\begin{bmatrix} F_1 \\ F_2 \\ F_3 \end{bmatrix} = \begin{bmatrix} k_{11} & \cdots & \cdots \\ k_{21} & \cdots & \cdots \\ k_{31} & \cdots & \cdots \end{bmatrix} \begin{bmatrix} 1 \\ 0 \\ 0 \end{bmatrix}, \qquad \begin{bmatrix} F_1 \\ F_2 \\ F_3 \end{bmatrix} = \begin{bmatrix} \cdots & k_{12} & \cdots \\ \cdots & k_{22} & \cdots \\ \cdots & k_{32} & \cdots \end{bmatrix} \begin{bmatrix} 0 \\ 1 \\ 0 \end{bmatrix}$$

A lot of work is saved when one builds on the foundational results of Maxwell and Betti's reciprocal theorem [43]. It states that a unit load that acts on an arbitrary node A causes the same deflection of node B as the deflection of A when the unit load is applied to B. In simple terms, the matrix coefficients are symmetric, hence $k_{xy} = k_{yx}$. This symmetry is no coincidence; it is a result of equal *virtual works*. This property is characteristic for conservative systems. This property plays a central role in the stability analysis in Chapter 5. Throughout this work, the elastic properties of the unconstrained beam are stored in the rotor's symmetric stiffness matrix.

$$\mathbf{K}_R = \mathbf{K}_R^T \qquad (p \times p) \qquad (3.1)$$

The relation between displacements $\mathbf{q}_W$ and corresponding node forces $\mathbf{F}_R$ is given by HOOKE's law.

$$\mathbf{F}_R = \mathbf{K}_R \mathbf{q}_W \tag{3.2}$$

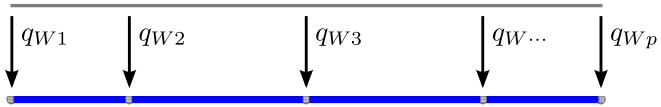

(a) Beam translation

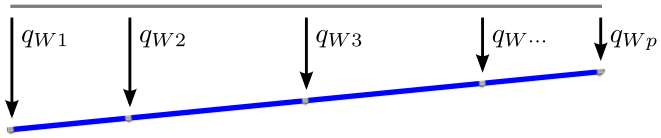

(b) Beam rotation

Figure 3.2: The free beam can be translated and rotated without any node forces.

Symmetry is not the only exploitable property of the stiffness matrix. Objects can be moved or turned as a whole. These movements cause no internal stresses and deformations, leaving the object as it is, and are subsequently called *rigid body motions*. Figure 3.2 shows these cases. Although never explicitly derived, this special property is already included in the stiffness matrix. Both shaft *translations* $\mathbf{q}_{Wt}$ and *rotations* $\mathbf{q}_{Wr}$ leave the shaft unbent and cause no bearing forces [67].

$$\mathbf{0} = \mathbf{K}_R \mathbf{q}_{Wt}, \qquad \mathbf{0} = \mathbf{K}_R \mathbf{q}_{Wr} \tag{3.3}$$

A general three-dimensional body has six rigid body modes, three translations plus the same quantity of rotations. Since rotor movements in axial direction are neglected and the rotor rotates around one axis with the rotational angle Ωt, only four rigid body modes remain. These split up in one translational and rotational mode for each plane. The use of complex notation already accounts for two perpendicular axes, so only two vectors are needed to represent four rigid body motions.

From the mathematical viewpoint, the matrix $\mathbf{K}_R$ is a linear map that relates the displacement vector $\mathbf{q}_W$ to the force vector $\mathbf{F}_R$. A deduction of Equation (3.3)

is that the stiffness matrix $\mathbf{K}_R$ maps any linear combination of $\mathbf{q}_{Wt}$ and $\mathbf{q}_{Wr}$ to the null vector. This property is named *rank deficiency*, and since the $(p \times p)$ matrix $\mathbf{K}_R$ maps two linear independent eigenvectors to the null vector, its rank deficiency is two [3].

$$\operatorname{rank}(\mathbf{K}_R) = p - 2 \tag{3.4}$$

This makes $\mathbf{K}_R$ singular, making it impossible to determine the shaft displacements $\mathbf{q}_W$ when only the node forces $\mathbf{F}_R$ are known. Another implication is that two eigenvalues of $\mathbf{K}_R$ are zero. These two zero eigenvalues correspond to one free translation and rotation. In real coordinates, the shaft's stiffness matrix would have four zero eigenvalues.

Stiffness matrices are normally generated with *finite elemente software*, such as *Nastran* or *Ansys*. Many programs generate stiffness matrices that have not only translational, but also rotational degrees of freedom. For these matrices, a *static condensation* technique eliminates the unnecessary rotational degrees of freedom [67, 103]. Matrices with rotational degrees of freedom will be considered in Section 3.2.6.

3.1.2 The rotor with passive bearings

The distribution of matter on a real rotor is continuous, but for modeling purposes, these distributions are discretized by a finite number of masses. One can imagine this discretization as if the real rotor was cut into slices. Each slice has a different weight and center of gravity, represented by point masses in the model. When the slices get thinner, the model reaches higher fidelity, but also gets more complex and more difficult to handle. In many cases, the rotor's masses are not evenly distributed, but concentrate on specific elements, such as discs, fans, impellers, etc. whereas the interconnecting shaft is thin. Then it is often sufficient to consider each of these features as a total number of p point masses connected to a massless shaft. The coordinates of the centers of gravities $q_{S1}, \ldots, q_{Sp}$ are gathered in the $(1 \times p)$ vector $\mathbf{q}_S$, while the mass points $m_1, \ldots, m_p$ are joined in the mass matrix $\mathbf{M}$. The further considerations do not account for massless nodes, so it is demanded that $\mathbf{M}$ is regular.

It is practically impossible to perfectly align the slices' centers of gravity to the shaft, leading to small residual eccentricities $\varepsilon_1^+, \ldots, \varepsilon_p^+$, which are all gathered in the rotor-fixed eccentricity vector $\boldsymbol{\varepsilon}^+$. Analogous to Equation (2.1), the relation between fixed and rotating coordinate system is:

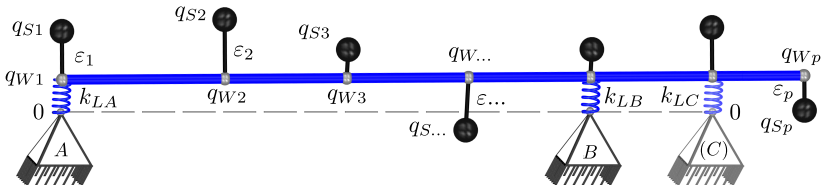

Figure 3.3: Model of the rotor with passive bearings. The bearings $A, B, \ldots$ can be attached to any shaft node q_{Wj} with the bearing allocation matrix $\mathbf{n}$.

$$\boldsymbol{\varepsilon} = \boldsymbol{\varepsilon}^{+}\, \mathrm{e}^{i\Omega t} \tag{3.5}$$

The kinematic relation between the shaft nodes $\mathbf{q}_W$, the eccentricities $\boldsymbol{\varepsilon}$ and the center of mass $\mathbf{q}_S$ is similarly:

$$\mathbf{q}_S = \mathbf{q}_W + \boldsymbol{\varepsilon} \tag{3.6}$$

It is now assumed that the free rotor is supported by a total number of z passive supports. The bearings are named alphabetically $A, B, \ldots, j, \ldots, z$. The index j selects one specific bearing out of this quantity. Any of these passive bearings can be connected to any shaft node. Suitable allocation vectors $\mathbf{n}_A, \ldots, \mathbf{n}_j, \ldots, \mathbf{n}_z$ assign each individual bearing to one shaft node.

$$\mathbf{n}_j = \begin{bmatrix} \ldots & 1 & 0 & \ldots \end{bmatrix}^T \qquad (p \times 1) \tag{3.7}$$

Each allocation vector must be non-zero, and it is demanded that $\mathbf{n}_j^T \mathbf{n}_j = 1$. Another demand is that each rotor node is exclusively attached to one support only. This means that $\mathbf{n}_j^T \mathbf{n}_{\neq j} = 0$ for each bearing. For a more convenient representation, all vectors are horizontally stacked in a single allocation matrix $\mathbf{n}$.

$$\mathbf{n} = \begin{bmatrix} \mathbf{n}_A & \ldots & \mathbf{n}_j & \ldots & \mathbf{n}_z \end{bmatrix} \qquad (p \times z) \tag{3.8}$$

Because of the previous definitions, the matrix $\mathbf{n}$ has the special identity:

$$\mathbf{n}^T \mathbf{n} = \mathbf{I} \qquad (z \times z) \tag{3.9}$$

The bearings are not entirely rigid, but have the stiffnesses $k_{LA}, \ldots, k_{Lj}, \ldots, k_{Lz}$. All stiffnesses are gathered in the condensed bearing stiffness matrix $\tilde{\mathbf{K}}_L$.

$$\tilde{\mathbf{K}}_L = \operatorname{diag}\left(k_{LA}, \ldots, k_{Lj}, \ldots, k_{Lz}\right) \qquad (z \times z) \qquad (3.10)$$

For all following considerations, it is demanded that each stiffness element k_{Lj} is positive, making $\tilde{\mathbf{K}}_L$ regular. Finally, the diagonal and spare bearing stiffness matrix $\mathbf{K}_L$ can be defined.

$$\mathbf{K}_L = \mathbf{n}\tilde{\mathbf{K}}_L\mathbf{n}^T \qquad (p \times p) \qquad (3.11)$$

The careful definition of the matrices $\mathbf{n}$, $\tilde{\mathbf{K}}_L$ and $\mathbf{K}_L$ is important as many future results make extensive use of the defined matrices and their identities. Since the bearings are attached to the shaft, they both share the same coordinate vector $\mathbf{q}_W$. The passive bearing forces $\mathbf{F}_P$ that act on the shaft are then:

$$\mathbf{F}_P = \mathbf{K}_L\mathbf{q}_W \qquad (3.12)$$

For static stability, it is further assumed that the rotor is supported in a *statically (in-)determinate* manner. This condition is satisfied when the rotor is supported at least in two bearing planes. The total system stiffness matrix is then positive definite, which is signalized using the "$>$" symbol:

$$\mathbf{K}_R + \mathbf{K}_L > 0 \qquad (3.13)$$

Two basic forces act on the mass. The rotor's elastic forces $\mathbf{F}_R$ that were defined in Equation (3.2) and the passive bearing forces $\mathbf{F}_P$ defined in Equation (3.12). Applying NEWTON's second law of motion yields:

$$\mathbf{M}\ddot{\mathbf{q}}_S = -\mathbf{F}_P - \mathbf{F}_R \qquad (3.14)$$

As already stated in Section 2.1, the equations of motion can be either expressed in shaft coordinates $\mathbf{q}_W$ or in mass coordinates $\mathbf{q}_S$. Although books on basic rotordynamics introduce both variants [26, 64], shaft coordinates $\mathbf{q}_W$ are commonly used. For the sake of a comprehensive presentation, the following results are presented in mass coordinates $\mathbf{q}_S$. This is without loss of generality, since the coordinates can be transformed from one system to the other. With the eccentricity definition from Equation (3.5) and the kinematic relations from Equation (3.6), the equation of motion is:

$$\mathbf{M}\ddot{\mathbf{q}}_S + (\mathbf{K}_R + \mathbf{K}_L)\,\mathbf{q}_S = (\mathbf{K}_R + \mathbf{K}_L)\,\boldsymbol{\varepsilon}^+ \mathrm{e}^{i\Omega t} \qquad (3.15)$$

In analogy to Section 2.1, the unbalance response is calculated using the *harmonic ansatz* $\mathbf{q}_S = \mathbf{q}_S^+ \, \mathrm{e}^{i\Omega t}$ in vectorized form.

$$\mathbf{q}_S = \left(-\Omega^2 \mathbf{M} + (\mathbf{K}_R + \mathbf{K}_L)\right)^{-1} (\mathbf{K}_R + \mathbf{K}_L)\, \boldsymbol{\varepsilon}^+ \, \mathrm{e}^{i\Omega t} \tag{3.16}$$

A modal transformation helps to understand the solution's properties. The decomposition $\mathbf{M}^{-1}(\mathbf{K}_R+\mathbf{K}_L) = \mathbf{U}_P \mathbf{V}_P \mathbf{U}_P^{-1}$ can be applied where the diagonal matrix $\mathbf{V}_P$ stores the p squared eigenfrequencies of the passive system:

$$\mathbf{V}_P = \mathrm{diag}\left(\omega_{P1}^2, \ldots, \omega_{Pp}^2\right) \tag{3.17}$$

Both $\mathbf{M}$ and the total stiffness matrix $(\mathbf{K}_R + \mathbf{K}_L)$ are positive, real and symmetric [25]. The eigenvectors are then orthogonal and can be normalized in a way that $\mathbf{U}_P^{-1} = \mathbf{U}_P^T$. Through the decomposition Equation (3.16), the system simplifies to p modal oscillators.

$$\begin{aligned} \mathbf{q}_S &= \mathbf{U}_P \left(\mathbf{V}_P - \Omega^2 \mathbf{I}\right)^{-1} \mathbf{V}_P \mathbf{U}_P^T \boldsymbol{\varepsilon}^+ \, \mathrm{e}^{i\Omega t} \\ &= \mathbf{U}_P \, \mathrm{diag}\left(\frac{\omega_{P1}^2}{\omega_{P1}^2 - \Omega^2}, \ldots, \frac{\omega_{Pp}^2}{\omega_{Pp}^2 - \Omega^2} \right) \mathbf{U}_P^T \boldsymbol{\varepsilon}^+ \, \mathrm{e}^{i\Omega t} \end{aligned} \tag{3.18}$$

An analysis of Equation (3.18) indicates that the diagonal entries become very large when the rotational frequency Ω approaches the system's eigenfrequencies ω_p. When the both frequencies match exactly , the solution is no longer valid: the *resonance* requires a different type of *ansatz*. When the rotational speed Ω is raised even further so that it is higher than the system's eigenfrequencies ω_p, the diagonal entries get smaller again and finally approach zero. It is interesting though that the sign shifts as the resonance is passed. Close to the resonance, the mass deflections $\mathbf{q}_S$ become very large. The corresponding shaft displacements $\mathbf{q}_W$ are calculated with Equation (3.6).

$$\begin{aligned} \mathbf{q}_W &= \mathbf{U}_P \left(\left(\mathbf{V}_P - \Omega^2 \mathbf{I}\right)^{-1} \mathbf{V}_P - \mathbf{I} \right) \mathbf{U}_P^T \boldsymbol{\varepsilon}^+ \, \mathrm{e}^{i\Omega t} \\ &= \mathbf{U}_P \, \mathrm{diag}\left(\frac{\Omega^2}{\omega_{P1}^2 - \Omega^2}, \ldots, \frac{\Omega^2}{\omega_{Pp}^2 - \Omega^2} \right) \mathbf{U}_P^T \boldsymbol{\varepsilon}^+ \, \mathrm{e}^{i\Omega t} \end{aligned} \tag{3.19}$$

The shaft deflections $\mathbf{q}_W$ behave similarly to the mass deflections $\mathbf{q}_S$ derived in Equation (3.18). Both have in common that they become very large close to

the rotor's resonance frequency, and that they change their sign from positive to negative. From Equation (3.12) it is clear that the passive bearing forces are directly proportional to the shaft deflections, $\mathbf{F}_P = \mathbf{K}_L \mathbf{q}_W$. The following statements summarize the main results of the rotor with passive bearings.

- For a given rotational speed Ω, the system's force response behaves linearly. Doubling the eccentricity $\boldsymbol{\varepsilon}$ also doubles the bearing forces $\mathbf{F}_P$.
- A rotor system with p degrees of freedom has p resonances.
- In the vicinity of a resonance, both rotor deflections $\mathbf{q}_W$ and passive bearing forces $\mathbf{F}_P$ are very high.
- The p resonance frequencies $\omega_1, \ldots, \omega_p$ depend on the properties of the rotor as well as on the bearings, including their quantity, position and stiffness.

3.1.3 The rotor with active bearings

It is now assumed that the free rotor from Section 3.1.1 is now supported by active bearings. In analogy with the controlled JEFFCOTT rotor, they are also represented by abstract displacement quantities. Generally speaking, both active and passive bearings need to hold a rotor in its designated position. Without bearings, the rotor would just move through space under the influence of external forces, a behavior which is almost never desired. The purpose of a bearing is to oppose these forces to keep the rotor in its desired position.

Similar to their passive counterparts, active bearings are unable to modify the forces on a statically determinate rotor. A rotor displacement *causes* a bearing *reaction force* as an *effect*, not vice versa. This fact raises the question of what active bearings can actually control. Unable to change the rotor forces directly, they can control the rotor displacements. In a *statically determinate* configuration, active bearings are able to *actively translate* and *rotate* the rotor without bearing forces. These force free movements occur in two perpendicular planes, leading to four degrees of freedom. It must be stressed that this property does not depend on the active bearings' physical realization. Whether they are based on piezoelectricity, magnetic effects, or other technological realizations, all forms are able to statically move the rotor without forces. The ability to move the rotor without constraints depends only on the system's topology.

Figure 3.4 illustrates the rotor with active bearings. Each active bearing $A, \ldots, z$ is able to displace the rotor; the displacement vectors $a_A, \ldots, a_z$ are represented

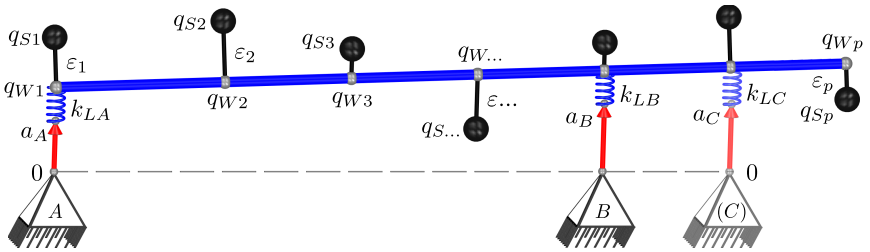

Figure 3.4: Model of the rotor with active bearings. The red arrows denote the controllable active bearing displacements.

by red arrows. All z bearing displacements are gathered in the condensed displacement vector $\tilde{\mathbf{a}}$.

$$\tilde{\mathbf{a}} = \begin{bmatrix} a_A & \dots & a_z \end{bmatrix}^T \qquad (z \times 1) \qquad (3.20)$$

Similar to the passive bearings from the previous section, the active bearings are connected in series with the stiffnesses $k_{LA}, \dots, k_{Lz}$. These can be either seen as stiffnesses of the bearing, the actuator, or a combination of both, depending on the considered case. The sparsely populated vector $\mathbf{a}$ distributes the actuator displacements to the shaft nodes previously defined in the matrix $\mathbf{n}$.

$$\mathbf{a} = \mathbf{n}\tilde{\mathbf{a}} \qquad (p \times 1) \qquad (3.21)$$

In passive case, the bearing forces depended according to Equation (3.12) on the shaft deflections $\mathbf{q}_W$ only. The illustration in Figure 3.4 indicates that the individual bearing forces now depend on the difference between the individual shaft displacements $q_{W...}$ and their assigned active bearing displacements $a_A, \dots, a_z$, which can be stated more elegantly using matrix notation:

$$\mathbf{F} = \mathbf{K}_L \left(\mathbf{q}_W - \mathbf{a} \right) \qquad (3.22)$$

The vector $\mathbf{F}$ represents the *active bearing forces*. The equations of motion are similar to the one of Equation (3.14), with the only difference being that the passive bearing force $\mathbf{F}_P$ is now replaced by its active counterpart $\mathbf{F}$. The modified equation of motion for the system with active bearings is then:

$$\mathbf{M}\ddot{\mathbf{q}}_S + \left(\mathbf{K}_R + \mathbf{K}_L \right) \mathbf{q}_S = \mathbf{K}_L \mathbf{a} + \left(\mathbf{K}_R + \mathbf{K}_L \right) \boldsymbol{\varepsilon}^+ \, \mathrm{e}^{i\Omega t} \qquad (3.23)$$

The only difference between the passive equation of motion (3.14) and the active one is the actuator displacement summand $\mathbf{K}_L\mathbf{a}$ on the equation's right-hand side. In analogy to the JEFFCOTT rotor from Section 2.2, the active bearings stimulate the rotor via a *footpoint excitation* [92]. The right-hand side expression requires special attention: although the *unit* of $\mathbf{K}_L\mathbf{a}$ is 'force', it does not represent an actual force. The right-hand side expression $\mathbf{K}_L\mathbf{a}$ is nonzero and may lead to the tempting but false conclusion that the right-hand side expression actually represents a real physical force excitation. This false conclusion might sneak in gradually: the expression $\mathbf{K}_L\mathbf{a}$ might be renamed as an 'active bearing force'. Although this substitution is mathematically faultless, it paves the way to wrong conclusions about the system's physical realities. A more detailed treatment of this topic is given in Section 4.2.

When the free rotor is supported in more than two bearing planes, it is *statically indeterminate*. In this case, individual actuator displacements cause shaft bending and consequently impose forces on the bearings. This behavior is already covered by Equation (3.23). It is revealed later that a force free operation is guaranteed even when the rotor is supported by active bearings in a statically indeterminate manner.

3.2 The controlled rotor

During the study of the JEFFCOTT rotor in Chapter 2, an inherently stable adaptive controller was introduced. This controller did not only eliminate the bearing forces, but also removed the rotor's resonance. These special properties seemed interesting enough to apply the control algorithm to general, isotropic rotors with an arbitrary number of masses and stiffnesses.

3.2.1 Control approach

In Section 3.1.3, the mechanical model for an arbitrary rotor with a total number of z active bearings was introduced. It is now assumed that each active bearing is equipped with its own, individual controller. The state-space notation for this controller is identical to the one given in Equation (2.19), but since the subindices have changed, it is repeated here for completeness:

$$\underbrace{\begin{bmatrix} \dot{a}_{Fj} \\ \dot{a}_{Bj} \\ \dot{a}_{Dj} \end{bmatrix}}_{\dot{\mathbf{x}}_{Rj}} = \underbrace{\begin{bmatrix} i\Omega & 0 & 0 \\ 0 & -i\Omega & 0 \\ 0 & 0 & -c_{Dj}k_{Dj} \end{bmatrix}}_{\mathbf{A}_{Rj}} \underbrace{\begin{bmatrix} a_{Fj} \\ a_{Bj} \\ a_{Dj} \end{bmatrix}}_{\mathbf{x}_{Rj}} + \underbrace{\begin{bmatrix} -i\tilde{c}_{Cj} \\ +i\tilde{c}_{Cj} \\ c_{Dj} \end{bmatrix}}_{\mathbf{B}_{Rj}} F_j$$

$$a_j = \underbrace{\begin{bmatrix} 1 & 1 & 1 \end{bmatrix}}_{\mathbf{C}_{Rj}} \mathbf{x}_{Rj} \tag{3.24}$$

The force of the j-th active bearing is denoted as F_j, while a_j is the actuator displacement (represented by the red arrow in Figure 3.4) of the same active bearing. Since all controllers are independent from each other, they are all arranged in a block-diagonal matrix structure:

$$\underbrace{\begin{bmatrix} \dot{\mathbf{x}}_{RA} \\ \mathbf{x}_{RB} \\ \vdots \end{bmatrix}}_{\dot{\mathbf{x}}_R} = \underbrace{\begin{bmatrix} \mathbf{A}_{RA} & \mathbf{0} & \mathbf{0} \\ \mathbf{0} & \mathbf{A}_{RB} & \mathbf{0} \\ \mathbf{0} & \mathbf{0} & \ddots \end{bmatrix}}_{\mathbf{A}_R} \underbrace{\begin{bmatrix} \mathbf{x}_{RA} \\ \mathbf{x}_{RB} \\ \vdots \end{bmatrix}}_{\mathbf{x}_R} + \underbrace{\begin{bmatrix} \mathbf{B}_{RA} & \mathbf{0} & \mathbf{0} \\ \mathbf{0} & \mathbf{B}_{RB} & \mathbf{0} \\ \mathbf{0} & \mathbf{0} & \ddots \end{bmatrix}}_{\mathbf{B}_R} \underbrace{\begin{bmatrix} F_A \\ F_B \\ \vdots \end{bmatrix}}_{\tilde{\mathbf{F}}}$$

$$\underbrace{\begin{bmatrix} \mathbf{a}_{RA} & \mathbf{a}_{RB} & \dots \end{bmatrix}^T}_{\tilde{\mathbf{a}}} = \underbrace{\operatorname{diag}(\mathbf{C}_{RA}, \mathbf{C}_{RB}, \dots)}_{\mathbf{C}_R} \mathbf{x}_R \tag{3.25}$$

The state vector $\mathbf{x}_R$ has the dimensions $(3z \times 1)$. Similar to the relation between the condensed actuator displacements $\tilde{\mathbf{a}}$ with the actuator displacements $\mathbf{a}$ in node coordinates from Equation (3.21), the condensed bearing forces $\tilde{\mathbf{F}}$ gather the forces $F_A, \dots, F_z$ of all z bearings and are related to the node bearing forces $\mathbf{F}$ in the following manner:

$$\tilde{\mathbf{F}} = \mathbf{n}^T \mathbf{F} \qquad (z \times 1) \tag{3.26}$$

3.2.2 Unbalance response of the controlled system

Both the mechanical system with active bearings as well as the controller have been defined in Sections 3.1.3 and 3.2.1. Both are now joined in a single state-space system for further analysis of the system's unbalance response. The combined state vector $\mathbf{x}$ together with Equations (3.6), (3.22) and the combination of Equations (3.23)-(3.26) leads to the combined state-space description:

$$\underbrace{\begin{bmatrix}\dot{\mathbf{q}}_S\\ \dot{\mathbf{q}}_S\\ \dot{\mathbf{x}}_R\end{bmatrix}}_{\dot{\mathbf{x}}} = \underbrace{\left[\begin{array}{ccc|c}\mathbf{0} & \mathbf{I} & \mathbf{0} & \\ -\mathbf{M}^{-1}(\mathbf{K}_R+\mathbf{K}_L) & \mathbf{0} & \mathbf{M}^{-1}\mathbf{K}_L\mathbf{n}\mathbf{C}_R & \\ \hline \mathbf{B}_R\mathbf{n}^T\mathbf{K}_L & \mathbf{0} & \mathbf{A}_R-\mathbf{B}_R\mathbf{n}^T\mathbf{K}_L\mathbf{n}\mathbf{C}_R & \end{array}\right]}_{\mathbf{A}} \underbrace{\begin{bmatrix}\mathbf{q}_S\\ \dot{\mathbf{q}}_S\\ \mathbf{x}_R\end{bmatrix}}_{\mathbf{x}} + \underbrace{\left[\begin{array}{c}\mathbf{0}\\ \mathbf{M}^{-1}(\mathbf{K}_R+\mathbf{K}_L)\\ \hline -\mathbf{B}_R\mathbf{n}^T\mathbf{K}_L\end{array}\right]}_{\mathbf{B}} \boldsymbol{\varepsilon}$$

$$\dot{\mathbf{x}} = \mathbf{A}\mathbf{x} + \mathbf{B}\boldsymbol{\varepsilon} \tag{3.27}$$

The state-space representation of Equation (3.27) is composed of many submatrices. However, the large monolithic structure of the system matrix $\mathbf{A}$ can be decomposed into several blocks, where each block has its unique designation. The $(2p \times 2p)$ matrix in the upper-left corner represents the equation of motion for the mechanical system. The controller resides in the $(3z \times 3z)$ matrix in the lower-right corner. The controller influences the mechanical systems through actuators, where the $(2p \times 3z)$ matrix on the upper-right corner connects the controllers states to the mechanical degrees of freedom. In the lower-left corner, the $(3z \times 2p)$ sensor matrix feeds the mechanical displacements back to the controller.

Linear theory states that a harmonic unbalance excitation $\boldsymbol{\varepsilon} = \boldsymbol{\varepsilon}^+ \mathrm{e}^{i\Omega t}$ causes the system to respond at exactly the same frequency. Similar to the passive solution of Equation (3.15), a similar *harmonic ansatz* can be used to calculate the system's unbalance response. The unbalance response is assumed to satisfy the equation $\mathbf{x} = \mathbf{x}^+ \mathrm{e}^{i\Omega t}$, with $\mathbf{x}^+$ being a constant vector for a particular rotational speed Ω. Its derivative yields $\dot{\mathbf{x}} = i\Omega\mathbf{x}^+ \mathrm{e}^{i\Omega t}$. Combining these harmonic responses with the system's state-space notation $\dot{\mathbf{x}} = \mathbf{A}\mathbf{x} + \mathbf{B}\boldsymbol{\varepsilon}$ leads to the wanted solution when $(i\Omega\mathbf{I} - \mathbf{A})$ is invertible:

$$\mathbf{x} = (i\Omega\mathbf{I} - \mathbf{A})^{-1}\mathbf{B}\boldsymbol{\varepsilon} \tag{3.28}$$

Although the solution of Equation (3.28) is theoretically straightforward, one has to remember that the system matrix $\mathbf{A}$ is a block matrix of the dimension $(2p + 3z)$, which has to be inverted. A relatively simple system with $p = 3$ masses and $z = 2$ active bearings already requires the inversion of a matrix with the dimensions (10×10). The comprehensible solution for the controlled JEFFCOTT rotor in Section 2.3.2 encouraged the search for a solution on arbitrary rotors, and finding a general solution is one of the key elements of this work. Due to its length, the detailed calculation is moved to Appendix A.1, but a brief description of the necessary steps is also given here. The system matrix $\mathbf{A}$ is divided into a mechanical, controller, sensor and actuator part. The *matrix inversion lemma* [104] allows for a problem simplification because the partitioned smaller matrix blocks can be calculated separately. Finding a general yet simple solution heavily relies on the structure of the involved matrices. Suitable matrix definitions in the Sections 3.1.1 and 3.2.1 allow for the application of the WOODBURY *Matrix Identity*, finally leading to a comprehensive, yet simple solution.

$$\mathbf{x}(t) = \begin{bmatrix} \left(-\Omega^2\mathbf{M} + \mathbf{K}_R\right)^{-1}\mathbf{K}_R \\ i\Omega\left(-\Omega^2\mathbf{M} + \mathbf{K}_R\right)^{-1}\mathbf{K}_R \\ \mathbf{R}\mathbf{n}^T\left(-\Omega^2\mathbf{M} + \mathbf{K}_R\right)^{-1}\mathbf{K}_R - \mathbf{R}\mathbf{n}^T \end{bmatrix} \boldsymbol{\varepsilon}^+ \, \mathrm{e}^{i\Omega t} \tag{3.29}$$

The steady-state unbalance response given in Equation (3.29) contains the matrix $\mathbf{R}$, which was defined during the solution process in Appendix A.1, but is repeated here for convenience. The diagonal matrix $\mathbf{R} = \mathrm{diag}(\mathbf{r}, \mathbf{r}, \dots)$ contains z column vectors $\mathbf{r} = \begin{bmatrix} 1 & 0 & 0 \end{bmatrix}^T$. The implications of the unbalance response (3.29) are successively reviewed in detail, and starts with the discussion of the mass motion:

$$\mathbf{q}_S = \left(-\Omega^2\mathbf{M} + \mathbf{K}_R\right)^{-1}\mathbf{K}_R\boldsymbol{\varepsilon}^+ \, \mathrm{e}^{i\Omega t}$$

When the rotor motion of the active solution is compared to its passive counterpart from Equation (3.16), remarkable similarities can be observed: the only formal difference between the active solution and the passive one is that it lacks the bearing stiffness matrix $\mathbf{K}_L$, while the rest remains exactly the same. A modal decomposition gives a better understanding of the rotor behavior. Suppose that $\mathbf{U}\mathbf{V}\mathbf{U}^T$ is the modal decomposition of $\mathbf{M}^{-1}\mathbf{K}_R$. With this decomposition, $\mathbf{V}$ is:

$$\mathbf{V} = \operatorname{diag}\left(0, 0, \omega_1^2, \ldots, \omega_{p-2}^2\right) \tag{3.30}$$

Two diagonal entries of $\mathbf{V}$ are zero, leading to two zero matrix rows and colums. The reason for this property can be traced back to the matrix product of $\mathbf{M}^{-1}\mathbf{K}_R$. It was stated earlier that the free rotor has two *rigid body modes*. According to Equation (3.4), these are reflected in a rank deficiency of two in the rotor's stiffness matrix $\mathbf{K}_R$. The inequality states that the rank deficiency of $\mathbf{K}_R$ also affects the matrix product:

$$\operatorname{rank}(\mathbf{M}^{-1}\mathbf{K}_R) \leq \min\left(\operatorname{rank}(\mathbf{M}^{-1}), \operatorname{rank}(\mathbf{K}_R)\right) = p - 2 \tag{3.31}$$

This rank deficiency is the reason why the diagonal eigenvalue matrix (3.30) holds at least two zero diagonal entries. The equations of motion for the masses are then:

$$\begin{aligned}\mathbf{q}_S &= \mathbf{U}\left(\mathbf{V} - \Omega^2\mathbf{I}\right)^{-1}\mathbf{V}\mathbf{U}^T\boldsymbol{\varepsilon}^+ \mathrm{e}^{i\Omega t} \\ &= \mathbf{U}\operatorname{diag}\left(0, 0, \frac{\omega_1^2}{\omega_1^2 - \Omega^2}, \ldots, \frac{\omega_{p-2}^2}{\omega_{p-2}^2 - \Omega^2}\right)\mathbf{U}^T\boldsymbol{\varepsilon}^+ \mathrm{e}^{i\Omega t}\end{aligned} \tag{3.32}$$

The two zero diagonal entries from Equation (3.32) indicate that the system lacks two resonances. The passive system from Equation (3.18) had p resonances, leading to theoretically infinite deflections and forces when the rotational speed Ω matches any of these p resonance frequencies. In the active case, the deflections lean to infinity for only $p-2$ frequencies. Consequently, *the controller enables the elimination of two rotor resonances*. This behavior can be traced back to the rank deficiency of Equations (3.4) and (3.31), which originated in the free shaft's property to rotate and tilt without node forces. The shaft deflections $\mathbf{q}_W$ are then:

$$\begin{aligned}\mathbf{q}_W &= \mathbf{U}\left(\left(\mathbf{V} - \Omega^2\mathbf{I}\right)^{-1}\mathbf{V} - \mathbf{I}\right)\mathbf{U}^T\boldsymbol{\varepsilon}^+ \mathrm{e}^{i\Omega t} \\ &= \mathbf{U}\operatorname{diag}\left(-1, -1, \frac{\Omega^2}{\omega_1^2 - \Omega^2}, \ldots, \frac{\Omega^2}{\omega_{p-2}^2 - \Omega^2}\right)\mathbf{U}^T\boldsymbol{\varepsilon}^+ \mathrm{e}^{i\Omega t}\end{aligned} \tag{3.33}$$

Comparing the passive solution from Equation (3.19) with the active one from Equation (3.33) illustrates how the rotor's motion differs. In the passive case, the rotor displacements $\mathbf{q}_W \to \mathbf{0}$ are negligible for small rotational speeds $\Omega \to 0$. In latter case, the diagonal entries (-1) indicate that the shaft executes circular movements with the magnitude of the eccentricity $\boldsymbol{\varepsilon}$, whereas Equation (3.32) expresses that the mass movements $\mathbf{q}_S$ are approximately zero. As a conclusion, the active control system displaces the rotor in a way that the center of masses always stay in the rotational center. Some more interesting properties can be found when the controller states $\mathbf{x}_R$ from Equation (3.29) are reviewed:

$$\mathbf{x}_R = \left(\mathbf{R}\mathbf{n}^T \left(-\Omega^2\mathbf{M} + \mathbf{K}_R\right)^{-1} \mathbf{K}_R - \mathbf{R}\mathbf{n}^T\right) \boldsymbol{\varepsilon}^+ \, \mathrm{e}^{i\Omega t}$$

Finally, the kinematic relations between the shaft and mass displacements from Equation (3.6) allow the following simplifications:

$$\mathbf{x}_R = \mathbf{R}\mathbf{n}^T \left(\mathbf{q}_S - \boldsymbol{\varepsilon}^+ \, \mathrm{e}^{i\Omega t}\right) = \mathbf{R}\mathbf{n}^T \mathbf{q}_W \tag{3.34}$$

Consequently, the controller states $\mathbf{x}_R$ directly depend on the shaft coordinates $\mathbf{q}_W$. This property gets clearer when it is not the states, but the individual controller outputs which are observed. According to Equation (3.25), the relation between the condensed actuator displacements $\tilde{\mathbf{a}}$ and the controller states $\mathbf{x}_R$ is $\tilde{\mathbf{a}} = \mathbf{C}_R \mathbf{x}_R$. This expression leads to the product of the block-matrices $\mathbf{C}_R$ and $\mathbf{R}$, which results in the identity matrix $\mathbf{I}$. The use of Equation (A.9) leads to the condensed actuator displacements:

$$\tilde{\mathbf{a}} = \mathbf{C}_R \mathbf{R}\mathbf{n}^T \mathbf{q}_W = \mathbf{n}^T \mathbf{q}_W \tag{3.35}$$

It is now clear that the actuator displacement matches the shaft displacement at their respective nodes. In steady-state, the actuator movements follow exactly the shaft movements. This is particularly interesting as it has consequences for the actuator forces. Equation (3.22) demonstrated that the active bearing forces $\mathbf{F}$ are the difference between the actuator displacement and shaft displacement. Using the relation $\mathbf{a} = \mathbf{n}\tilde{\mathbf{a}}$ from Equation (3.21) allows the calculation of the bearing forces:

$$\mathbf{F} = \mathbf{K}_L \left(\mathbf{q}_W - \mathbf{a}\right) = \mathbf{K}_L \mathbf{q}_W - \underbrace{\mathbf{K}_L \mathbf{n}\mathbf{n}^T}_{=\mathbf{K}_L} \mathbf{q}_W = \mathbf{0} \tag{3.36}$$

Equation (3.36) is the *proof that the bearing forces in steady-state are always zero*. This result is considered as one of the key elements in this work. It is particular surprising because of the following reasons: apart from the basic definitions in Section 3.1.1, no further assumptions were made on the stiffness, shape or mass of the rotor. It is further surprising given that the force free condition is independent of the eccentricity vector $\boldsymbol{\varepsilon}$. The control algorithm has no specific knowledge about the mass distribution, yet is able to control the actuators in a way that the bearing forces vanish. The result is valid for all rotational speeds Ω. The control algorithm does not require any information about the rotor or the mechanical setup, i.e. the bearing's position or stiffness, since only the rotational speed Ω must be known.

- For a given rotational speed Ω, the system's active bearing force response remains zero for any unbalance distribution $\boldsymbol{\varepsilon}^+$.
- Two resonances can be eliminated – a passive rotor system with p degrees of freedom has $p-2$ resonances in controlled case.
- In the vicinity of a free rotor resonance, the deflections $\mathbf{q}_W$ become large, but the active bearing forces $\mathbf{F}$ remain zero.
- The $p-2$ resonance frequencies $\omega_1, \ldots, \omega_{p-2}$ depend on the properties of the free rotor *only*. The number of active bearings as well as their position or stiffness have no effect on the rotor's unbalance response.

3.2.3 Example rotor with two discs

An example illustrates the solution derived in the previous section. The considered rotor consists of two discs attached to a flexible shaft. Figure 3.5 shows the mechanical setup, but in contrast to the illustration, it is assumed that the active bearings support the rotor directly at the disc location. The mass matrix $\mathbf{M}$ has then the dimension (2×2), and according to the rank deficiency of the free rotor found in Equation (3.4), it is clear that the rank of the rotor's stiffness matrix is zero. Consequently, the rotor's stiffness matrix $\mathbf{K}_R$ is also zero, representing the fact that both nodes are completely independent from each other as the shaft translates and tilts without constraints. The system with two

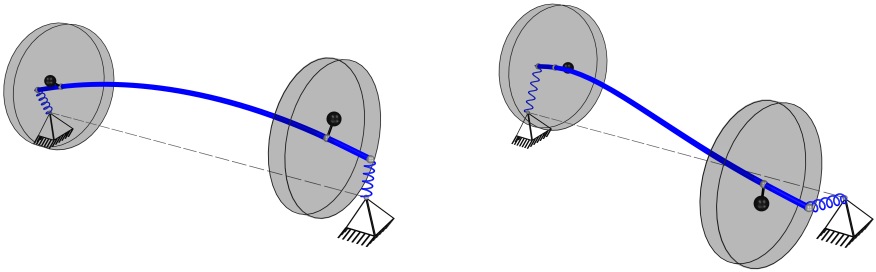

(a) 1st passive resonance at frequency f_{P1}

(b) 2nd passive resonance at frequency f_{P2}

Figure 3.5: Uncontrolled (passive) rotor with two discs. In passive operation, two discs lead to two resonances with distinct eigenmodes.

masses essentially degenerates to two controlled, uncoupled JEFFCOTT rotors. The bearing stiffness matrix $\mathbf{K}_L$ is assumed to be diagonal, but with different stiffnesses for two distinct passive eigenfrequencies. Figure 3.7 compares rotor run-ups in passive and active cases. Two distinct resonances develop at the frequencies f_{P1} and f_{P2} in the passive case. There are no resonances in the active case because the controller is able to always align the center of both masses in the rotational center, as Figure 3.6 indicates. The bearing forces vanish because in steady-state operation, the actuator displacements a_j follow exactly the shaft movement q_{Wj} at the corresponding node. This example pursues two different

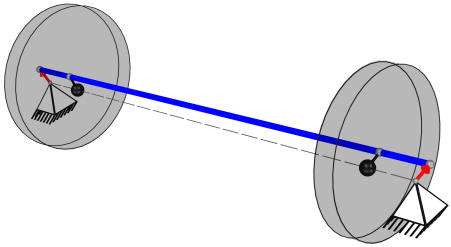

Figure 3.6: Controlled (active) rotor with two discs. The rotor is resonance-free for any rotational speed Ω due to the masses remaining in the center of rotation.

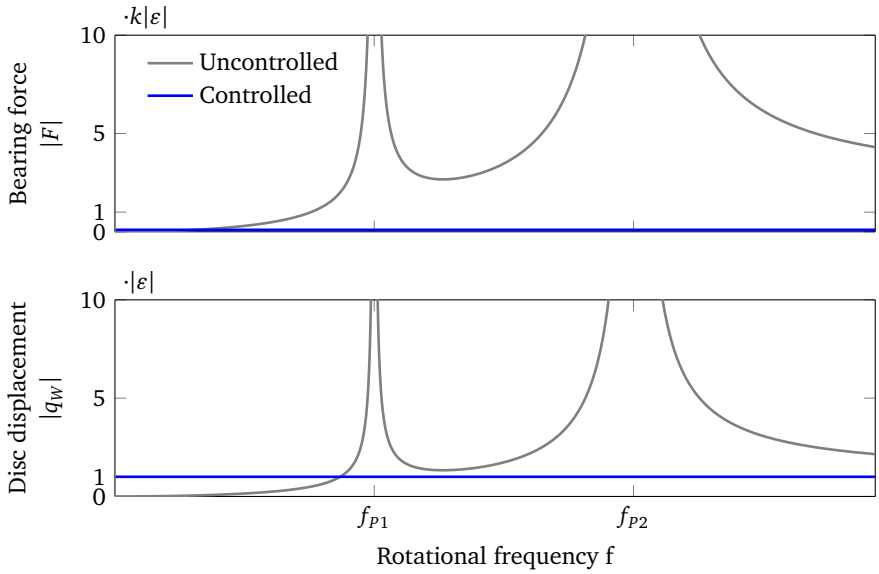

Figure 3.7: Analytical unbalance response for a rotor with two masses. No resonances develop in the controlled case as the controller always keeps the center of mass in the rotational center.

objectives. First, it is the extension of the planar JEFFCOTT rotor to a three-dimensional case with two masses. The system description for general rotors from Equation (3.27) and its solution from Equation (3.29) also contains the JEFFCOTT rotor as a special case: for $\mathbf{K}_R = 0$, $\mathbf{K}_L = k$ and $\mathbf{n} = 1$, the equations degenerate to the ones of the controlled JEFFCOTT rotor from Equations (2.20) and (2.23), leading to a consistent problem description. The second objective of this work was to provide the answer why a maximum of two resonances can be eliminated: only two masses with independent eccentricities can be aligned to the rotational center.

3.2.4 Example rotor with three discs

The following example considers a rotor with three discs, serving as a prototype for more general, arbitrary rotors. Realistic physical assumptions allow the transferability to real-world machinery. Consider a rotor assembly that bases on a round steel shaft with a diameter of 12 mm and an overall length of 200 mm. One finds three discs with negligible gyroscopic effect and an individual mass of 1 kg, which are attached to the middle and the ends of the shaft. Two bearings with given stiffnesses are also attached to the shaft ends. Assuming that both disc and bearing positions are coincident, the allocation vectors are chosen to $\mathbf{n}_A = \begin{bmatrix} 1 & 0 & 0 \end{bmatrix}^T$ and $\mathbf{n}_B = \begin{bmatrix} 0 & 0 & 1 \end{bmatrix}^T$. The other matrices are then:

$$\mathbf{M} = \begin{bmatrix} 1 & 0 & 0 \\ 0 & 1 & 0 \\ 0 & 0 & 1 \end{bmatrix} \text{kg},\ \mathbf{K}_R = \begin{bmatrix} 3 & -6 & 3 \\ -6 & 12 & -6 \\ 3 & -6 & 3 \end{bmatrix} \cdot 10^5\,\text{N m}^{-1},\ \mathbf{K}_L = \begin{bmatrix} 1 & 0 & 0 \\ 0 & 0 & 0 \\ 0 & 0 & 1 \end{bmatrix} \cdot 10^7\,\text{N m}^{-1}$$

The stiffness matrix $\mathbf{K}_R$ of the free shaft has indeed a rank deficiency of two, reflecting two zero eigenvalues. The passive bearings support and stabilize the rotor statically, hence $\mathbf{K}_R + \mathbf{K}_L > 0$. According to the passive unbalance response from Equation (3.16), the rotor has three resonances at $f_{P1} = 116\,\text{Hz}$, $f_{P2} = 159\,\text{Hz}$ and $f_{P3} = 240\,\text{Hz}$. Figure 3.9 plots the unbalance responses for shaft displacements and bearing forces, whereas Figures 3.8(a, c, e) illustrates the corresponding rotor deflections in the vicinity of the critical speeds. The depicted coil springs indicate that the rotor deflections are accompanied by large bearing forces.

With active bearings and the proposed control strategy, the shaft displacements behave according to the controlled solution from Equation (3.29). Since the bearing stiffness matrix $\mathbf{K}_L$ is absent in the solution, only the rank deficient shaft matrix $\mathbf{K}_R$ remains, leading to only one resonance at the frequency $f_{C1} = 214\,\text{Hz}$. This resonance has some surprising properties. First, its frequency is *higher* than the first two passive resonances, extending the effective resonance-free rotor operating range. Second, the shaft deflections depicted in Figure 3.8(b, d, f) completely differ from their passive counterparts. This difference is particularly visible when the passive bearing stiffnesses are high. The third surprising property is the absence of bearing forces, even in the vicinity of the free rotor resonance f_{C1}. Even large rotor displacements cause no bearing forces, a statement which is true for any unbalance distribution $\boldsymbol{\varepsilon}^+$.

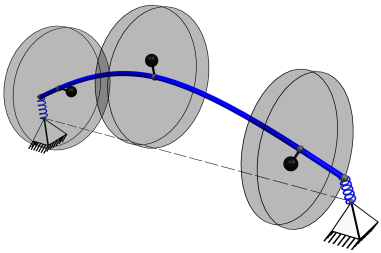

(a) 1st passive resonance at frequency f_{P1}

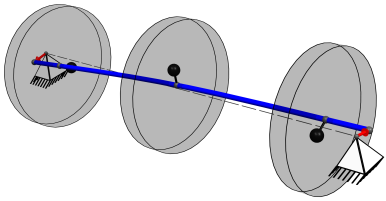

(b) No resonance with control at frequency f_{P1}.

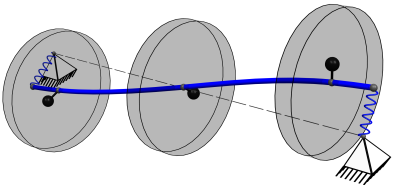

(c) 2nd passive resonance at frequency f_{P2}

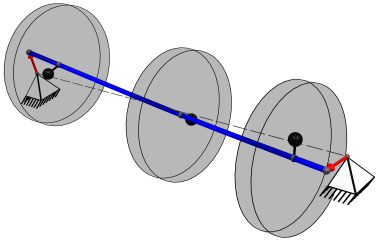

(d) No resonance with control at frequency f_{P2}.

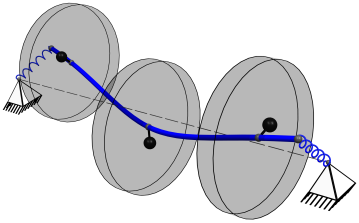

(e) 3rd passive resonance at frequency f_{P3}

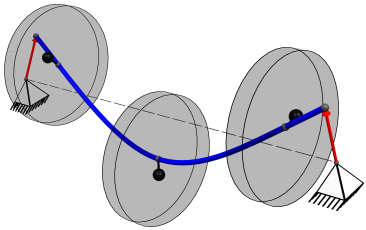

(f) Force-free resonance with control at frequency f_{C1}.

Figure 3.8: Graphical comparison of a rotor with three discs in passive (left column) and active case (right column). Three critical frequencies develop in the passive case, leading to high bearing forces. With active bearings, only one force free resonance develops (Figure f).

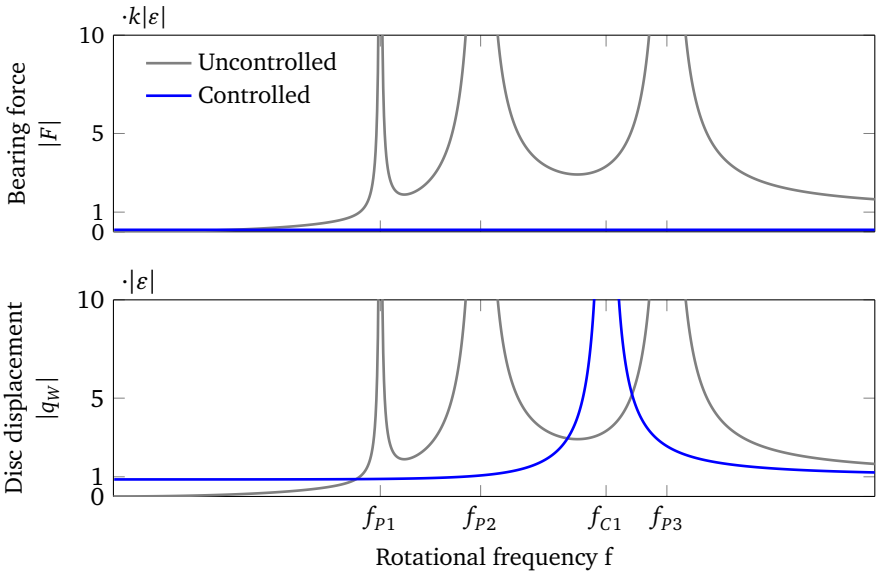

Figure 3.9: Comparison of forces and displacements of a three-mass rotor in passive and active case. The three passive resonances lead to large forces and displacements. In this example, the frequency of the only force free resonance is higher than the first two passive resonances, leading to an extension of the resonance-free rotor operation range.

3.2.5 Outer and inner damping

The introduction of damping is an effective way to reduce the impact of vibration on technical systems. Despite having positive effects on oscillations, it generally also augments a system's stability. Damping may be introduced by dedicated elements, for example as shock absorbers in vehicles [71], or as vibration absorbers in washing machines [16]. However, damping may also occur implicitly. Experience shows that bolted or riveted structures introduce a significant amount of damping, as the microscopic joint friction dissipates energy [5, 81]. On the contrary, welded structures provide only little damping. One of the main sources of damping arises when a structure interacts with viscous fluids such as air, oil, or other gases and liquids. This damping effect may be specifically wanted or not; it is fact that the vast majority of systems are exposed to some kind of medium that provides at least a minimal amount of damping.

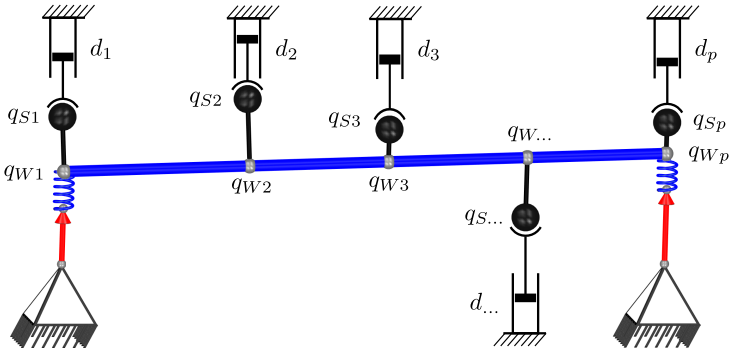

Figure 3.10: Rotor with external damping. Although external damping reduces free rotor deflections, it creates a parallel path to the environment. This parallel path transmits forces to the ambiance, voiding the rotor's force free operation.

Since some amount of damping is generally unavoidable, the implications of its occurrence are studied in this section. Rotordynamic theory distinguishes between two kinds of damping: *outer* or *external damping* and *inner damping*. Outer damping results from the rotor's interaction with the fixed environment and has the effect that a mechanical engineer would expect – it reduces the rotor vibrations and augments the rotor's stability margin. On the other hand, inner damping describes the rotor's intrinsic dissipation. Surprisingly, inner damping has an adverse effect on stability, leading to the paradox effect that augmenting the rotors' inner damping eventually leads to instability. It took decades and many damaged or destroyed rotors until this negative effect could finally been deciphered by Newkirk and Kimball. Statements about the stability of inner damping are generally hard, but will be discussed briefly in Section 5.1.7. It is however possible to study both the effects of outer and inner damping on the unbalance response and their effect on the force free operation.

External damping is defined in the inertial coordinate system. The damping forces act on the rotor, and the most obvious approach is that the damping forces are directly proportional to the shaft velocities $\dot{\mathbf{q}}_W$. For the sake of simplicity and presentation, it is assumed here that the damping forces act directly on the masses. Even though this case allows a detailed discussion about the general effects, as this change only affects the right-hand side of the state-space equation. The damping force vector $\mathbf{F}_D$ is assumed to be directly proportional to the absolute mass velocities $\dot{\mathbf{q}}_S$. Because of energy considerations, the external

damping matrix is symmetric, so $\mathbf{D} = \mathbf{D}^T$. Figure 3.10 illustrates the external damping arrangement.

$$\mathbf{F}_D = \mathbf{D}\dot{\mathbf{q}}_S \tag{3.37}$$

Inner damping is entirely defined in rotating coordinates. The inner damping forces defined in the positive rotating coordinate system $\mathbf{F}_I^+$ are directly proportional to the mass velocities $\dot{\mathbf{q}}_S^+$. The inner damping matrix $\mathbf{D}_I$ must satisfy the same energy considerations and is symmetric also: $\mathbf{D}_I = \mathbf{D}_I^T$. For inner damping, the governing equation is:

$$\mathbf{F}_I^+ = \mathbf{D}_I\dot{\mathbf{q}}_S^+ \tag{3.38}$$

Before Equation (3.38) can be incorporated in the equation of motion, it has to be transferred first to the inertial coordinate system. The transformation for the force vector from fixed to rotating coordinates yields $\mathbf{F}_I^+ = \mathbf{F}_I\,\mathrm{e}^{-i\Omega t}$. The displacement transformation is then: $\mathbf{q}_S^+ = \mathbf{q}_S\,\mathrm{e}^{-i\Omega t}$. Its derivative requires the product rule: $\dot{\mathbf{q}}_S^+ = \dot{\mathbf{q}}_S\,\mathrm{e}^{-i\Omega t} - i\Omega\mathbf{q}_S\,\mathrm{e}^{-i\Omega t}$. With these replacements, the equation for the inner damping can be expressed in inertial coordinates:

$$\mathbf{F}_I = \mathbf{D}_I\dot{\mathbf{q}}_S - i\Omega\mathbf{D}_I\mathbf{q}_S \tag{3.39}$$

The transformation to inertial coordinates creates not only a velocity-dependent quantity, but also one which is proportional to the displacement $\mathbf{q}_S$. Until now, position-dependent forces were only used in conjunction with conservative elastic elements. In Section 3.1.1, the principle of virtual works led to symmetry in the stiffness matrices, see Equation (3.1). However, the product $i\Omega\mathbf{D}_I$ is *skew-hermitian*, (Hermitian matrices are the complex equivalent to symmetric real matrices) and consequently not conservative. The existence of this skew-hermitian matrix identifies systems with *circulatory forces*. Considering all forces, the equation of motion yields:

$$\mathbf{M}\ddot{\mathbf{q}}_S = -\mathbf{F} - \mathbf{F}_R - \mathbf{F}_D - \mathbf{F}_I$$

This leads to an updated state-space description. Compared to the state-space notation in Equation (3.27), only the system matrix $\mathbf{A}$ has changed, while the matrix $\mathbf{B}$ remains the same. If the assumptions were changed in a way that the

damping is proportional to the shaft displacement $\mathbf{q}_W$, the matrix $\mathbf{B}$ also would have changed.

$$\mathbf{A} = \begin{bmatrix} \mathbf{0} & \mathbf{I} & \mathbf{0} \\ -\mathbf{M}^{-1}\left(\mathbf{K}_R + \mathbf{K}_L - i\Omega\mathbf{D}_I\right) & -\mathbf{M}^{-1}\left(\mathbf{D} + \mathbf{D}_I\right) & \mathbf{M}^{-1}\mathbf{K}_L\mathbf{n}\mathbf{C}_R \\ \mathbf{B}_R\mathbf{n}^T\mathbf{K}_L & \mathbf{0} & \mathbf{A}_R - \mathbf{B}_R\mathbf{n}^T\mathbf{K}_L\mathbf{n}\mathbf{C}_R \end{bmatrix} \tag{3.40}$$

A solution for the state-space system of Equation (3.27) with the updated system matrix from Equation (3.40) that involves outer and inner damping has been calculated in Appendix A.2. The result from Equation (A.28) is also presented here:

$$\mathbf{x}(t) = \begin{bmatrix} \left(-\Omega^2\mathbf{M} + i\Omega\mathbf{D} + \mathbf{K}_R\right)^{-1}\mathbf{K}_R \\ i\Omega\left(-\Omega^2\mathbf{M} + i\Omega\mathbf{D} + \mathbf{K}_R\right)^{-1}\mathbf{K}_R \\ \mathbf{R}\mathbf{n}^T\left(-\Omega^2\mathbf{M} + i\Omega\mathbf{D} + \mathbf{K}_R\right)^{-1}\mathbf{K}_R - \mathbf{R}\mathbf{n}^T \end{bmatrix} \boldsymbol{\varepsilon}^+ \, \mathrm{e}^{i\Omega t} \tag{3.41}$$

External damping: Comparing the unbalance response for the undamped system from Equation (3.29) with the solution of the damped case from Equation (3.41), shows that only marginal changes occurred in the *dynamic stiffness matrix* $\left(-\Omega^2\mathbf{M} + i\Omega\mathbf{D} + \mathbf{K}_R\right)$, where only the summand $i\Omega\mathbf{D}$ is new. A modal solution is only indicated when the matrix $\mathbf{D}$ is also *diagonalizable* with the eigenvectors of the undamped system, otherwise the solution gets more complicated [25]. However, some important properties are known even without an explicit modal solution. Damping leaves the number of resonances unaffected, the controlled system has only $p-2$ resonances. Furthermore, the introduction of damping limits the modal displacements from infinite to finite values in the resonance. Repeating the calculation from Equation (3.36) reveals that the bearing forces $\mathbf{F}$ remain zero. Both results are generally appreciated, but imply a severe drawback. Looking again at Figure 3.10, it is apparent that the damping elements give a twofold response. The same damping force $\mathbf{F}_D$ that acts on the rotor also requires a *reaction force* of the same magnitude on the environment. Even though the active bearings are in a force free condition, oscillatory forces may still be transmitted to the environment through a *parallel path*. A necessary requirement for a complete rotor isolation is the absence of any external damping $\mathbf{D} = \mathbf{0}$, but this implies large rotor deflections in the vicinity of a free rotor resonance, as it was demonstrated in Equation (3.18). It

is clear that this property depends on the rotor only and has nothing to do with the controller, as its properties are not part of the unbalance response.

As a corollary, it is generally impossible to operate a rotor at the speed of its free resonance and fully eliminate the bearing forces it at the same time.

Internal damping: Although the inner damping matrix $\mathbf{D}_I$ appeared in the system matrix $\mathbf{A}$ from Equation (3.40), it is not present in the unbalance response from Equation (3.41). This is no mistake; it turns out that the unbalance response remains indeed unaffected by inner damping. This surprising result has a plausible explanation. A closer inspection of the unbalance response from Equation (A.28) indicates that the relation between rotor-fixed, constant eccentricity vector $\boldsymbol{\varepsilon}^+$ and rotor displacements in rotating coordinates $\mathbf{q}_S^+$ is actually constant. When observed from the rotating coordinate system, the rotor deflects statically, and for a given rotational speed Ω no movement can be seen. According to Equation (3.38), inner damping was also defined in rotating coordinates, and the absence of any relative movements $\mathbf{q}_S^+ = \mathbf{0}$ also causes that the inner damping forces on the rotor are zero, $\mathbf{F}_I = \mathbf{0}$. The name inner damping already suggests that these forces do not interact with the environment, consequently inner damping allows for a complete force free rotor operation. Although it has no negative impact on the unbalance response, its occurrence should be avoided whenever possible. Its circulatory parts encourage instability for passive rotors, and it is likely that this negative property also applies for the controlled system. Since the stability theorems of Chapter 5 do not apply for systems with circulatory matrices, a numeric stability test is indicated for rotors with suspected inner damping.

3.2.6 Gyroscopic effect and generalized coordinates

The modeling approach of Section 3.1.1 gives good results for slender rotors, but not so much for short and thick rotor shapes. STODOLA discovered more than a century ago that the cause for the deviation between model and experiment could be attributed to the *gyroscopic effect* [89]. It was assumed previously that the rotor is cut into slices, and that the center of mass is represented as a point with an assigned eccentricity. For thick rotors, this assumption is inaccurate. The continuous mass distribution of one slice is not only reflected in a center of mass, but also in a *transversal moment of inertia* Θ_t and a *polar moment of inertia* Θ_p.

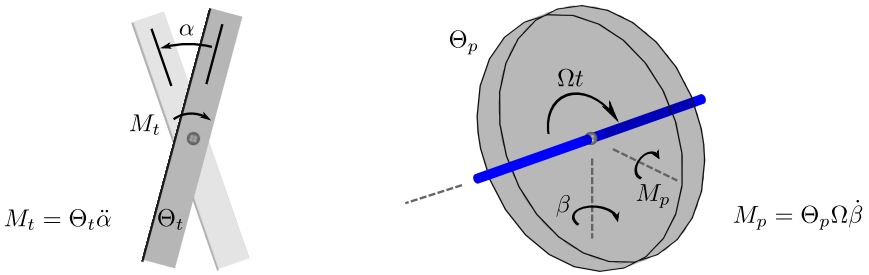

Figure 3.11: Rotor's influence by moments of inertia. Left: the transversal moment of inertia counteracts the rotational acceleration in the same axis. Right: Illustration of the gyroscopic effect. A spinning disc generates a perpendicular gyroscopic moment to a disc rotation.

According to the left drawing of Figure 3.11, an angular acceleration of a disc in one axis causes a counteracting moment around the same axis. The elastic beam responds to these moments with node rotations. In analogy with the previous differential equations that used the mass m as inertia and displacements q as coordinates, the new one uses the transversal moment Θ_t and the rotation α as coordinate. Even the eccentricity has an adequate counterpart in rotating coordinates: a skewed disc assembly exerts oscillating moments on the shaft for a spinning rotor.

The gyroscopic effect is illustrated on the right side of Figure 3.11. It must be stressed that this effect is entirely different from the one explained in the previous paragraph, both physically and mathematically. A disc with the polar moment of inertia Θ_p rotating at the rotational speed Ω responds with a gyroscopic moment $M_\beta = \Theta_p \Omega \dot{\beta}$ when a turning rate of $\dot{\beta}$ is applied to the disc. This statement is valid when the vectors of Ω, $\dot{\beta}$ and M_β are all perpendicular to each other. This perpendicularity leads to a coupling between the axes: a rotational speed in one plane causes a moment in the perpendicular one, and vice versa. When the coordinates are chosen correctly, the use of complex coordinates facilitates also here the problem formulation, as the imaginary unit already accounts for the cross-coupling. Detailed information on gyroscopic modeling can be found in books on rotordynamics [26, 29]. With a number of p discs, the gyroscopic matrix has the general form:

$$\begin{bmatrix} M_{P1} \\ \vdots \\ M_{Pp} \end{bmatrix} = \underbrace{\begin{bmatrix} i\Omega\Theta_{P1} & & \\ & \ddots & \\ & & i\Omega\Theta_{Pp} \end{bmatrix}}_{\mathbf{G}(\Omega)} \begin{bmatrix} \dot{\beta}_1 \\ \vdots \\ \dot{\beta}_p \end{bmatrix} \tag{3.42}$$

The gyroscopic matrix changes with the rotational speed Ω, which means nothing else that the cross-coupling becomes stronger the faster the rotor spins. For the trivial case of that $\Omega = 0$, the matrix vanishes and there is no coupling at all. In complex coordinates, the matrix $\mathbf{G}(\Omega)$ is diagonal but imaginary. The most important property is that the matrix is *skew-hermitian*.

$$\mathbf{G}(\Omega) = -\mathbf{G}^H(\Omega) \tag{3.43}$$

It seems that the introduction of transversal and polar moments of inertia complicate the equations of motions considerably. Previously, it was sufficient to care about masses, displacements and forces. Now a whole new set of variables appears, namely inertia, angles and moments, which are coupled through the gyroscopic effect. This raises the question of whether or not the previously found solutions can be adapted in such a way, that they account for the new effects. When the transversal moment was discussed earlier, it was already implied that the equations of motions for node rotations are in complete analogy to their displacement counterparts. During the derivation of the stiffness matrix in Section 3.1.1, it was already mentioned that a stiffness matrix may also have rotational degrees of freedom, but as they were superfluous, they could be removed using *static condensation*.

Because of the structural analogy between translations and rotations, *generalized coordinates* can be used to facilitate the problem description. The vector $\mathbf{q}_S$ is extended so that it holds not only displacements q_S but also the node rotations β. Then the matrix $\mathbf{M}$ does not only hold masses m, but also transversal moments of inertia Θ_t, and the eccentricity vector $\boldsymbol{\varepsilon}^+$ does not only contain eccentricities ε^+, but also an error for skewed discs. The advantage of generalized coordinates is that the problem's matrix formulation remains exactly the same, and all solutions found in Section 3 are also valid for generalized coordinates. Generalized coordinates allow the problem's abstraction from a specific physical setup to the study of matrix properties. For instance, the rotor's ability to move

freely is expressed in the rank deficiency of $\mathbf{K}_R$, independent if only displacements or displacements and rotations are used as governing coordinates.

Only the speed-dependent, gyroscopic moments have to be updated in the state-space matrix:

$$\mathbf{A} = \begin{bmatrix} \mathbf{0} & \mathbf{I} & \mathbf{0} \\ -\mathbf{M}^{-1}(\mathbf{K}_R + \mathbf{K}_L) & -\mathbf{M}^{-1}(\mathbf{D} + \mathbf{G}(\Omega)) & \mathbf{M}^{-1}\mathbf{K}_L\mathbf{n}\mathbf{C}_R \\ \mathbf{B}_R\mathbf{n}^T\mathbf{K}_L & \mathbf{0} & \mathbf{A}_R - \mathbf{B}_R\mathbf{n}^T\mathbf{K}_L\mathbf{n}\mathbf{C}_R \end{bmatrix} \tag{3.44}$$

The solution has been calculated in Section A.1, but is also given here:

$$\mathbf{x}(t) = \begin{bmatrix} \left(-\Omega^2\mathbf{M} + i\Omega(\mathbf{D} + \mathbf{G}(\Omega)) + \mathbf{K}_R\right)^{-1}\mathbf{K}_R \\ i\Omega\left(-\Omega^2\mathbf{M} + i\Omega(\mathbf{D} + \mathbf{G}(\Omega)) + \mathbf{K}_R\right)^{-1}\mathbf{K}_R \\ \mathbf{R}\mathbf{n}^T\left(-\Omega^2\mathbf{M} + i\Omega(\mathbf{D} + \mathbf{G}(\Omega)) + \mathbf{K}_R\right)^{-1}\mathbf{K}_R - \mathbf{R}\mathbf{n}^T \end{bmatrix} \boldsymbol{\varepsilon}^+ \, \mathrm{e}^{i\Omega t} \tag{3.45}$$

An eigenvalue decomposition for the complete $\mathbf{M}, \mathbf{D}, \mathbf{G}, \mathbf{K}$ system is only possible in special cases. When damping is omitted, the shortened $\mathbf{M}, \mathbf{G}, \mathbf{K}$-system can be decomposed in complex coordinates. This decomposition leads to *complex eigenvectors* and a breakdown of the resonance frequencies into a *forward whirling* frequency and a *backward whirling* frequency. In real coordinates, a diagonalization is still possible when a *bimodal decomposition* that uses different left and right eigenvectors, is applied [25]. More solution techniques, decomposition strategies and interpretations, are found in standard books on rotordynamics [26, 29].

The speed-dependent character of $\mathbf{G}(\Omega)$ leads to a *gyroscopic stiffening*. This effect is not a stiffening in the classical sense as it does not alter the rotor's stiffness matrix, but describes that an augmentation in the rotor's rotational speed Ω also leads to increased forward whirling frequencies ω. At the same time, the backward whirling frequencies diminish. In theory, rotor unbalances $\boldsymbol{\varepsilon}^+ \, \mathrm{e}^{i\Omega t}$ only excite the forward whirling frequencies, whereas the backward whirl does not contribute to the rotor's unbalance response.

Gyroscopic moments are *conservative* and generally have unproblematic stability behavior, as it will be demonstrated in Section 5.2. But since the rotor's eigenvectors change for different rotational speeds, one must check carefully

whether the observability criteria of Section 5.2.4 are always satisfied. Gyroscopic moments do not require any external reaction forces and are entirely bound to the rotor, hence a complete rotor isolation is possible. To simplify presentation, the matrices' $\mathbf{G}(\Omega)$ explicit dependence of the rotational speed Ω will be omitted, and only $\mathbf{G}$ will be used.

3.2.7 Parasitic stiffness

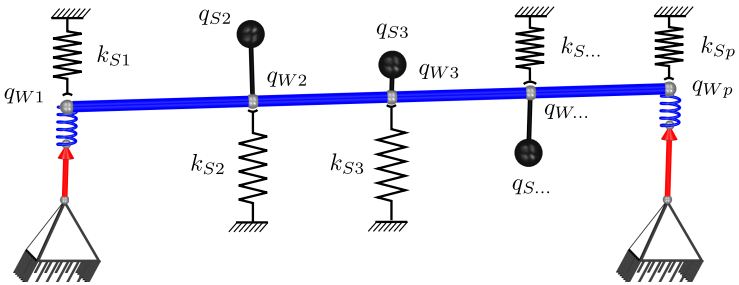

Figure 3.12: Parasitic stiffnesses inhibit a force free rotor operation and create new resonances. However, they can be compensated when they arise in the active bearing planes.

Another effect which has not been considered yet is the presence of parasitic stiffnesses. Until now, it was assumed that active bearings are able to translate and tilt the rotor freely. There are cases where these conditions may not be entirely satisfied. Some machines feature elements that partially hinder a free rotor movement. In some cases, this may be a design feature, for example when the system is equipped with passive bearings. However, sometimes parasitic stiffnesses occur as a secondary effect, this happens for example for a flexible coupling whose primary purpose is the transmission of torque. Finally, even the active bearings may introduce parasitic stiffnesses. In case of displacement actuators, some extra stiffness may create a parallel path which is not measured by the force sensors (see Section 4.1.4).

In this section, the properties of parasitic stiffnesses are investigated. Figure 3.12 shows a sketch of the modified system with the additional spring elements $k_{S1}, \ldots, k_{Sp}$. All are stored in the sparsely populated, diagonal ma-

trix $\mathbf{K}_S$. The forces that are transmitted to the environment via the parasitic stiffnesses are consequently:

$$\mathbf{F}_S = \mathbf{K}_S \mathbf{q}_W \tag{3.46}$$

Parasitic stiffnesses remain unobserved by the active bearings, and the updated state space matrices are then:

$$\mathbf{A} = \begin{bmatrix} \mathbf{0} & \mathbf{I} & \mathbf{0} \\ -\mathbf{M}^{-1}(\mathbf{K}_R + \mathbf{K}_L + \mathbf{K}_S) & \mathbf{0} & \mathbf{M}^{-1}\mathbf{K}_L \mathbf{n} \mathbf{C}_R \\ \mathbf{B}_R \mathbf{n}^T \mathbf{K}_L & \mathbf{0} & \mathbf{A}_R - \mathbf{B}_R \mathbf{n}^T \mathbf{K}_L \mathbf{n} \mathbf{C}_R \end{bmatrix}, \quad \mathbf{B} = \begin{bmatrix} \mathbf{0} \\ \mathbf{M}^{-1}(\mathbf{K}_R + \mathbf{K}_L + \mathbf{K}_S) \\ -\mathbf{B}_R \mathbf{n}^T \mathbf{K}_L \end{bmatrix}$$

Solving the system is straightforward as $\mathbf{K}_R$ is now replaced by $\mathbf{K}_R + \mathbf{K}_S$.

$$\mathbf{x}(t) = \begin{bmatrix} \left(-\Omega^2 \mathbf{M} + \mathbf{K}_R + \mathbf{K}_S\right)^{-1} (\mathbf{K}_R + \mathbf{K}_S) \\ i\Omega \left(-\Omega^2 \mathbf{M} + \mathbf{K}_R + \mathbf{K}_S\right)^{-1} (\mathbf{K}_R + \mathbf{K}_S) \\ \mathbf{R}\mathbf{n}^T \left(-\Omega^2 \mathbf{M} + \mathbf{K}_R + \mathbf{K}_S\right)^{-1} (\mathbf{K}_R + \mathbf{K}_S) - \mathbf{R}\mathbf{n}^T \end{bmatrix} \boldsymbol{\varepsilon}^+ \, \mathrm{e}^{i\Omega t} \tag{3.47}$$

A force free rotor operation always leads to some residual rotor movements. According to Equation (3.46), forces will be transmitted to the environment. The presence of a parasitic stiffness disables the possibility to completely isolate the rotor. In Section 3.2.2, it was stated that two rotor resonances can be eliminated using active bearings. This effect was attributed to the rank deficiency of $\mathbf{K}_R$ in Equation (3.4), a property that reflected the rotor's ability to move freely. In presence of parasitic stiffnesses, not the stiffness matrix $\mathbf{K}_R$ determines the solution properties, but the sum of $\mathbf{K}_R + \mathbf{K}_S$. When the rotor is supported not only by an active bearing, but also by a passive one, only one resonance can be eliminated as the $\operatorname{rank}(\mathbf{K}_R + \mathbf{K}_S) = p - 1$. When the rotor is fully supported by passive bearings, no resonance can be eliminated: the active bearings are useless as they have no influence on the rotor's unbalance response.

These *parasitic resonances* are particularly dangerous as they may occur at rotational frequencies that do neither match the eigenfrequencies of the free, unconstrained rotor nor the ones of the fixed rotor, and may be misidentified as controller instabilities.

Until now, it was assumed that the bearing force and the actuator force are one and the same. For parasitic stiffnesses in the bearing plane, this is no longer the case: the bearing force vector $\mathbf{F}$ differs from the actuator force vector $\mathbf{F}_a$. When the parasitic stiffness k_S at the respective node is known, the control algorithm

may compensate it using the actuator. This enables a complete rotor isolation and resonance elimination even in the presence of these unwanted effects. In Chapter 4, compensating strategies for force and displacement actuators are presented.

In summary, the presence of parasitic stiffnesses counteracts all positive effects that may come from a controlled solution with active bearings: first, they establish a parallel path that transmits unbalance forces to the surrounding, impeding a full rotor isolation. Second, they create new resonances that may occur at unexpected rotational frequencies. Third, they have no positive impact on the resonance magnitudes. External damping in contrast limits the resonance peaks and does not introduce new resonances. As a conclusion, parasitic stiffnesses should be avoided whenever possible or compensated when they occur in a bearing plane.

3.2.8 Bearing invariance

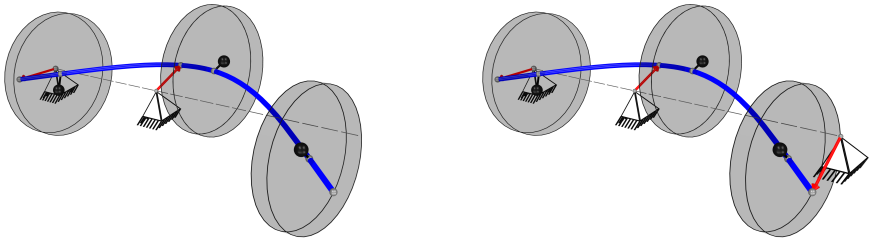

(a) Controlled rotor with two bearings

(b) Controlled rotor with three bearings.

Figure 3.13: Bearing invariance: the rotor's unbalance response is independent of both the number and the placement of the active bearings. This counterintuitive behavior can be explained by the absence of unbalance-induced bearing forces during steady-state operation.

The solution for the controlled shaft from Equation (3.29) does neither depend on the controller parameters nor on the matrix $\mathbf{K}_L$. This matrix contains not only information about the stiffness of each active bearing, but also stores according to Equation (3.11) the position where each individual bearing is attached. Consequently, *the rotor's controlled unbalance response depends neither on the*

position nor the number of the used active bearings. This unintuitive steady-state behavior makes sense, as the force free condition also implies that there is no interaction between the rotor and the bearings. For the unbalance response, the rotor behaves as if there were no bearings. However, the system's homogeneous solution which governs the rotor's natural vibration and damping is certainly affected by active bearing placement, see Chapter 5.

Figure 3.13 depicts two identical rotor systems with the rotational frequency but with different bearing locations. With either two or three bearings, and independent of the the bearing location, the rotor's unbalance response remains the same.

This *bearing invariance* property can be exploited when passing free rotor resonances. Details can be found in Section 4.4.

3.3 Rotor-casing interaction

In real-world machinery, rotor foundations and casings are rarely considered as fixed elements. Weight matters especially when rotating machines are part of transport systems, such as cars, planes, rockets, and so on. To reduce weight, the rotor casings are built as light as possible, leading to softer structures with augmented oscillation tendencies. But even large stationary rotating machines such as generators in power plants or steam turbines do not only excite their thick-walled steel housing, but also the surrounding building. The rotor's casing excitation is not only a nuisance, but also affects the rotor behavior itself, leading to an interaction of both components. Neglecting the casing's effect on the rotor may lead to surprises when they are joined. The aforementioned situation encouraged researchers to study the problem in detail [26] or to develop sophisticated calculation methods [24].

Aircraft engines are particularly susceptible to this problem. The lightweight design of the engine cowling and fuselage encourages the transmissions of unbalance-induced vibrations in the form of audible noises to passengers. Both Borsdorf and Zhao investigated active elements to reduce unbalance-induced engine vibrations with rotor-casing interactions [12, 101]. This section describes the derivation of the unbalance response with a casing. In this section, the rotor coordinates are represented by the subindex "r" (rotor), whereas all casing quantities are represented by the subindex "c" (casing). Both subsystems are joined in the combined system with the subindex "g". The combined displacement vector $\mathbf{q}_{Sg}$ is then:

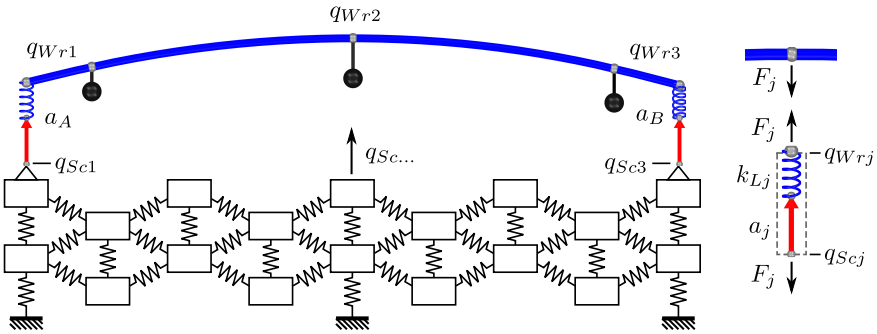

Figure 3.14: Left: illustration of the mechanical model for the rotor-casing interaction. Both subsystems are only connected via the active bearings. Right: Detail for one active bearing with actuator forces.

$$\mathbf{q}_{Sg} = \begin{bmatrix} \mathbf{q}_{Sr} \\ \mathbf{q}_{Sc} \end{bmatrix} \tag{3.48}$$

The mechanical equation of motion for the complete system is consequently:

$$\mathbf{M}_g \ddot{\mathbf{q}}_{Sg} + \left(\mathbf{D}_g + \mathbf{G}_g\right) \dot{\mathbf{q}}_{Sg} + \left(\mathbf{K}_{Rg} + \mathbf{K}_{Lg}\right) \mathbf{q}_{Sg} = \mathbf{K}_{Lg} \mathbf{a}_g + \left(\mathbf{K}_{Rg} + \mathbf{K}_{Lg}\right) \boldsymbol{\varepsilon}_g \tag{3.49}$$

In this system, it is clear that the eccentricity acts on the rotor only:

$$\boldsymbol{\varepsilon}_g = \begin{bmatrix} \boldsymbol{\varepsilon}_r \\ \mathbf{0} \end{bmatrix} \tag{3.50}$$

It is assumed that the rotor is connected to the fixed part only through the active bearings, other coupling mechanisms such as fluid interaction are not considered. In this case, all matrices are strictly block-diagonal, leading to a complete separation of rotor and casing. The only exception is the bearing stiffness matrix $\mathbf{K}_{Lg}$ that couples the rotor with the casing. Figure 3.14 indicates that the bearing forces depend not only on actuator and shaft, but also on the casing displacements.

$$\tilde{\mathbf{F}} = \tilde{\mathbf{K}}_L \left(\tilde{\mathbf{q}}_{Wr} - \tilde{\mathbf{q}}_{Sc} - \tilde{\mathbf{a}} \right) \tag{3.51}$$

Appendix A.4 demonstrates that only small modifications of the previously derived unbalance response are necessary to cover also this problem. Then, the controlled unbalance response for the mechanical system is:

$$\mathbf{q}_{Sg} = \left(-\Omega^2 \mathbf{M}_g + i\Omega \left(\mathbf{D}_g + \mathbf{G}_g \right) + \mathbf{K}_{Rg} \right)^{-1} \mathbf{K}_{Rg} \boldsymbol{\varepsilon}_g \tag{3.52}$$

The solution of Equation (3.52) shows that the bearing stiffness matrix $\mathbf{K}_{Lg}$, which coupled both systems, vanished. Since the remaining matrices are strictly block-diagonal, both systems are completely decoupled. Equation (3.50) revealed that the unbalance only acts on the rotor, consequently there is no excitation of the casing.

To illustrate the findings, the rotor with three masses from example 3.2.4 is now attached to a lightly damped casing with multiple resonances in the rotor's operating range. Since the passive stiffness matrix $\mathbf{K}_{Rg} + \mathbf{K}_{Lg}$ is of full rank, the passive system counts not only with three, but with rank$(\mathbf{K}_{Rg} + \mathbf{K}_{Lg})$ resonances. In these resonances the rotor excites the casing. In controlled case, no forces are transmitted through the bearings, leading to a silent casing. However, the free rotor resonance cannot be eliminated. Figure 3.15 illustrates a rotor run-up in passive and active case.

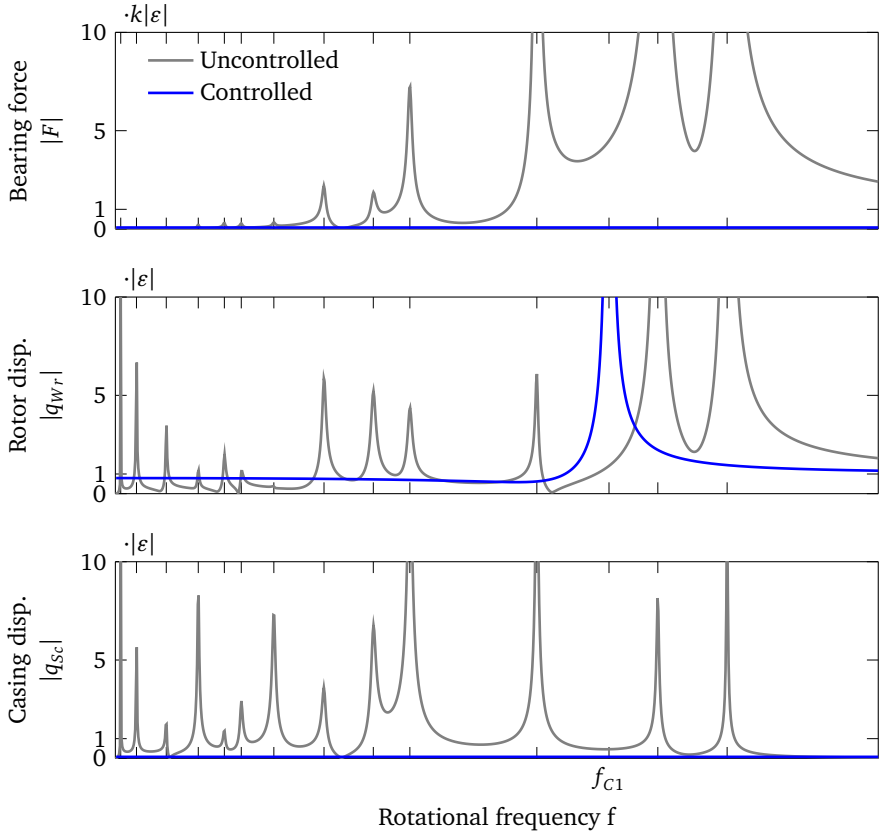

Figure 3.15: Example for a rotor-casing interaction. The run-up of a rotor with three discs excites the multiple resonance frequencies of the flexible casing in the passive case. In active case however, the absence of any bearing forces stops the casing vibration entirely, but a free rotor resonance remains. A complete unbalance decoupling is possible even when the rotor is attached to an arbitrary, flexible casing.

4 Physical realization

Until this point, the problem of a force free rotor operation was only considered from system-theoretic viewpoint. The previous chapters dealt mainly with the question *how to control an ideal actuator so that a complete rotor isolation is possible*. The abstract component focused on ensuring a complete separation between the theoretic foundations and the active bearings' practical implementation. By first establishing the theoretical foundations and discussing their physical properties, two immediate advantages are found: firstly, the system-theoretic considerations are of general nature and *technology independent*, widening the problem's understanding. Second, by deriving control strategies for different technologies emerging from the same theory uncovers connections that would be unnoticed otherwise. For a specific implementation, two major decisions have to be made.

The first decision concerns the actuator type. Independent of the particular technology used, actuators can be categorized into two idealized groups [32]. The first group is formed by *displacement actuators*. These actuators have ideally an infinite *inherent stiffness*. For any given operating point, a change in the actuator force F_a leads to a negligible relative actuator displacement $\Delta a = 0$. Corollary, any small actuator displacement Δa leads to an infinite change in actuator forces $F_a \to \infty$. Latter group is formed by ideal *force actuators* which have no inherent stiffness. Without control, even a small change in the actuator forces F_a leads to infinite displacements $\Delta a \to \infty$, but displacements Δa leave the actuator forces $F_a = 0$ unchanged. The type of actuator naturally affects the required sensor. Collocated controllers require the knowledge of both force and displacement for a respective node. Displacement actuators are invariant to changing forces. Hence only a force sensor may measure the unknown quantity. Force actuators on the other hand require a position measurement as their forces are invariant to displacements. In conclusion, the measured quantity must be *complementary* to the one of the actuator [30].

Figure 4.1 illustrates the behavior of real-world actuators that are only approximations to these idealizations. Displacement actuators have a finite stiffness, whereas force actuators might even have negative stiffnesses. Most actuators are located somewhere in between, and their characterization largely depends

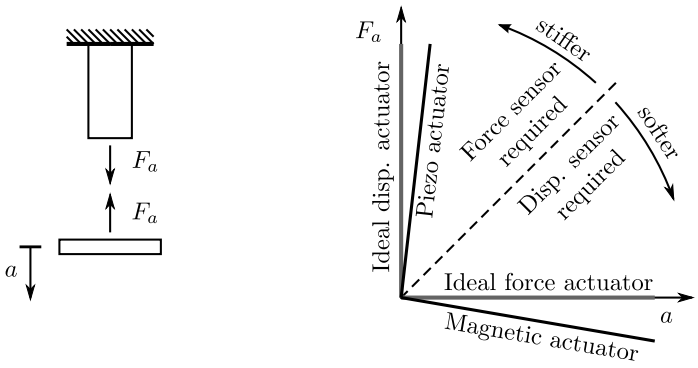

Figure 4.1: Different types of actuators. Ideal displacement actuators have an infinite inherent stiffness, hence the corresponding sensor measures forces. Ideal force actuators have no inherent stiffness, requiring a displacement sensor.

on the context. For instance, a piezoelectric element can generally be considered as displacement actuator because the ceramic layers are stiff, but assembled in a thick-walled steel casing with magnitudes of higher stiffness, it is best to consider it as a force actuator. Through their inherent stiffness, displacement actuators are capable of maintaining a static equilibrium on their own, requiring no additional control. Force actuators on the other hand, are per definition unable to exert returning forces when no feedback loop is present. When a rotor is supported by an actuator without additional control, it is considered as a displacement actuator. In case that the rotor is unstable without control, it can be considered as a force actuator.

The second decision affects the actuator placement. The most common choice for actuator placement is in inertial coordinates, fixed to the frame. Less obvious is the actuator placement in rotating coordinates, hence on the rotor itself. This alternative placement leads to new possibilities and a connection to *balancing actuators* [23]. Each actuator type can be assembled in both rotating and inertial coordinates, leading to four different combinations. Three combinations are discussed in the following sections, with force actuators in rotating coordinates being omitted as there is no immediate technical advantage of this configuration.

This chapter also demonstrates how a practically feasible control algorithm can be derived from the underlying state-space equation. The adaptive controller

structure leads to a different control law for each operating point, making a straightforward implementation difficult. A coordinate transformation technique is presented which allows for an implementation of this controller even on machines with very limited computational power. When the hazardous effects of parasitic stiffnesses from Section 3.2.7 occur in the active bearing plane, they can be compensated. Compensation techniques are presented for both displacement and force actuators. A practical implementation requires dimensioning of the actuators, and it is demonstrated how the closed-loop solution can be used for this purpose. The same solution also revealed that both rotor and actuator displacements may become very large close to the free rotor resonances - a property that is intolerable in real machines. The introduction of an additional controller factor inhibits a perfect force free operation, but also reduces both rotor and actuator displacements to tolerable values. The proposed factor limits the travel of the compensation elements and leads to a blending of rotor isolation and the classical introduction of damping.

The displacement and force formulations in Sections 4.1.1 and 4.2 are based on the publication "Unbalance and resonance elimination with active bearings on a Jeffcott Rotor" by HEINDEL et al. [38].

4.1 Displacement actuators

Displacement actuators with finite stiffness may be realized through different technologies. For slowly turning machines with large eccentricities, the low *bandwidth* of linear electric motors may be negligible. Machines with higher rotational speeds tend to smaller eccentricities, a domain where other actuator principles have their advantages. *Hydraulic actuators* offer very high power densities, large strokes and bandwidths exceeding 100 Hz. For even higher frequencies and smaller strokes, piezoelectric actuators qualify. They offer extremely high bandwidths in the kilohertz range [32], but their small strain of approximately 0.2 % leads to either long actuators or small strokes. Some less common actuator principles include *magnetorestrictive actuators* and *shape memory alloys* [52]. A special role have actuators that are based on *thermal expansion*. They feature large forces, but have the drawbacks of very small strains and only quasi-static operation. However, they may still be suitable for unbalance elimination, as the upcoming sections will show.

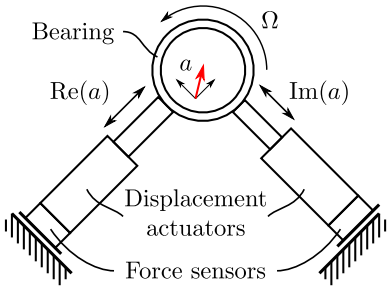

Figure 4.2: Physical realization of an active bearing with displacement actuators. Each actuator displaces the bearing in one plane; the sensors directly measure the shaft forces.

4.1.1 Fixed displacement actuators

Following the previous theoretical derivations, an actuator assembly in inertial coordinates is the most intuitive solution. Figure 4.2 shows such an assembly. A mechanical bearing that allows the shaft's rotation while it prevents the shaft's radial movements is connected in series with two perpendicularly arranged linear displacement actuators. Each actuator is connected to a force sensor; the assembly is then attached to a fixed support. Sample implementations can be found in [6, 82, 88]. The controller outputs the displacement a in complex coordinates, consequently one actuator is fed by the real part $\mathrm{Re}\{a\}$, while its perpendicular counterpart is fed with $\mathrm{Im}\{a\}$. The sensor inputs $\mathrm{Re}\{F\}$ and $\mathrm{Im}\{F\}$ must be converted to complex coordinates using the relation $F = \mathrm{Re}\{F\} + i\,\mathrm{Im}\{F\}$, accordingly. Until now, there was no clear distinction between bearing and actuator stiffness. This was perfectly justified as it made no difference from the system-theoretic viewpoint. If both shall be considered simultaneously, their total stiffness is simply defined by their series connection.

In principle, the implementation of the controller from Equations (2.19) or (3.24) is straightforward. In practice however, many machines do not run at a constant rotational speed Ω, but rather change their rotational frequency to operate at different operating points. In this case, the rotational speed Ω must be measured using a *resolver* or an *encoder*. Thus, in these cases, the controller must be *adaptive* so that it can cover the machine's different operating points. This adaptive structure requires either a parametric model or different

controllers for each operating point. Both variants are rather tedious, making their implementation on systems with little computational power difficult. A more elegant solution takes advantage of the fact that the involved controller elements were defined in different coordinate systems. The controller's forward compensating element a_F^+ was defined in the positive rotating coordinate system, whereas the backward compensating element a_F^- was defined in the negative rotating coordinate system, while the damping element a_D was defined in inertial coordinates. With a modified state vector $\bar{\mathbf{x}}_R$, the controller differential equation can be transformed in a way that its explicit dependence on the rotational speed Ω lapses.

$$\bar{\mathbf{x}}_R = \begin{bmatrix} a_F^+ & a_B^- & a_D \end{bmatrix}^T \tag{4.1}$$

A speed-dependent transformation matrix $\mathbf{T}(\Omega t)$ is introduced which transforms between the two state vectors $\mathbf{x}_R$ and $\bar{\mathbf{x}}_R$. For a shorter representation, its dependency of time and speed it not explicitly annotated, hence only $\mathbf{T}$ will be used. In the same step, their time derivatives are also calculated:

$$\mathbf{x}_R = \underbrace{\begin{bmatrix} \mathrm{e}^{i\Omega t} & 0 & 0 \\ 0 & \mathrm{e}^{-i\Omega t} & 0 \\ 0 & 0 & 1 \end{bmatrix}}_{\mathbf{T}} \bar{\mathbf{x}}_R \qquad \dot{\mathbf{x}}_R = \underbrace{\begin{bmatrix} i\Omega & 0 & 0 \\ 0 & -i\Omega & 0 \\ 0 & 0 & 0 \end{bmatrix}}_{\bar{\mathbf{A}}} \mathbf{T}\bar{\mathbf{x}}_R + \mathbf{T}\dot{\bar{\mathbf{x}}}_R \tag{4.2}$$

Inserting the transformations into the controller Equation (2.19) yields:

$$\begin{aligned} \dot{\bar{\mathbf{x}}}_R &= \mathbf{T}^{-1}\big(\underbrace{\mathbf{A}_R - \bar{\mathbf{A}}}_{\bar{\mathbf{A}}_R}\big)\mathbf{T}\bar{\mathbf{x}}_R + \mathbf{T}^{-1}\mathbf{B}_R F \\ &= \mathbf{T}^{-1}\underbrace{\operatorname{diag}(0, 0, -c_D k_D)}_{\bar{\mathbf{A}}_R}\mathbf{T}\bar{\mathbf{x}}_R + \mathbf{T}^{-1}\mathbf{B}_R F \\ &= \bar{\mathbf{A}}_R\bar{\mathbf{x}}_R + \mathbf{T}^{-1}\mathbf{B}_R F \end{aligned} \tag{4.3}$$

During the process of transformation the transformation matrices $\mathbf{T}^{-1}$ and $\mathbf{T}$ canceled out. It must be stressed that this cancellation is only possible when the including matrix is diagonal. It is now clear that the modified system matrix $\bar{\mathbf{A}}_R$ depends on one constant coefficient only, avoiding an Ω-dependent system matrix. After the measured complex bearing force is multiplied with $\mathbf{B}_R$, each element is transformed to their respective coordinate systems and multiplied with the inverse transformation matrix $\mathbf{T}^{-1}$, which is trivially obtained by swap-

ping the first diagonal matrix elements $e^{i\Omega t}$ and $e^{-i\Omega t}$ of the matrix $\mathbf{T}$. After the calculation of $\bar{\mathbf{x}}_R$, the elements can be transformed to inertial coordinates using the relation of Equation (4.2), and the controller output is then:

$$a = \mathbf{C}_R \mathbf{T} \bar{\mathbf{x}}_R \tag{4.4}$$

When the selected controller architecture prohibits the use of complex coordinates, the use of EULER's identity is indicated, using the relation $e^{i\Omega t} = \cos(i\Omega t) + i\sin(i\Omega t)$. Despite its simplified implementation, another advantage is that the state a_F^+ now directly represents the rotor's eccentricity ε^+ for the JEFFCOTT rotor in physically meaningful units. When not only the relative angle Ωt is known, but an absolute rotor angle φ can be measured with an encoder, *the controller's complex state directly represents magnitude and phase of the eccentricity as constant value*. For stiff rotors which are supported by at least two bearings, the controller states a_F^+ directly represent the rotor's *principal axis of inertia*. As flexible rotors do not have a principal axis of inertia, the controller states a_F^+ represent the magnitude and phase of the shaft center q_W^+ at the respective bearing.

The controller states in rotating coordinates are a direct representation of the rotor's eccentricity in physical meaningful units. When the absolute rotor position φ is known, both magnitude and phase of the eccentricity are stored as constant values in the controller. These values can be used to evaluate the rotor's physical condition, serving as a simple machine health monitoring.

Digital controllers are generally sampled systems, requiring a discretization of the continuous differential controller equations. The forward finite difference method [90] allows for a simple discretization using the approximation $\dot{\bar{\mathbf{x}}}_R \approx (\bar{\mathbf{x}}_{R+1} - \bar{\mathbf{x}}_R)\, t_S^{-1}$, with $\bar{\mathbf{x}}_{R+1}$ defining the state vector at the next time step and t_S being the sample time.

$$\begin{aligned}
(\bar{\mathbf{x}}_{R+1} - \bar{\mathbf{x}}_R)\, t_S^{-1} &\approx \bar{\mathbf{A}}_R \bar{\mathbf{x}}_R + \mathbf{T}^{-1} \mathbf{B}_R F \\
\bar{\mathbf{x}}_{R+1} &\approx \left(\bar{\mathbf{A}}_R t_S + \mathbf{I}\right) \bar{\mathbf{x}}_R + \mathbf{T}^{-1} \mathbf{B}_R t_S F \\
a_{+1} &= \mathbf{C}_R \mathbf{T} \bar{\mathbf{x}}_{R+1}
\end{aligned} \tag{4.5}$$

In contrast to the previous controller representation from Equation (4.3), the discrete time version is only an approximation of the continuous time differential equation. Naturally, the stability considerations of the continuous version do no apply for discrete time controller. However, experience shows that the differences between continuous and discretized controller versions are negligi-

ble when the sampling frequency t_S^{-1} is more than 20 times higher than control loops' cut-off frequency [62]. For lower sampling frequencies, an additional stability analysis that accounts for the discretization effects is required.

In conclusion, the advantages and disadvantages of displacement actuators in inertial coordinates are summarized:

+ Easy accessibility and power supply. The assembly in inertial coordinates simplifies the connection of actuators and sensors.
+ Increased assembly space. Fixed actuators can be integrated into the casing, relaxing the space constraints.
+ No centrifugal forces on the actuators.
+ No rotor modifications necessary.
– Actuator bandwidth depends on the rotational speed Ω. The actuator must follow the rotor's movement, requiring a bandwidth that exceeds the rotational speed Ω of the rotor.
– Power consumption. Even without forces, the oscillatory actuator movements lead to idle energy consumption.

4.1.2 Rotating displacement actuators

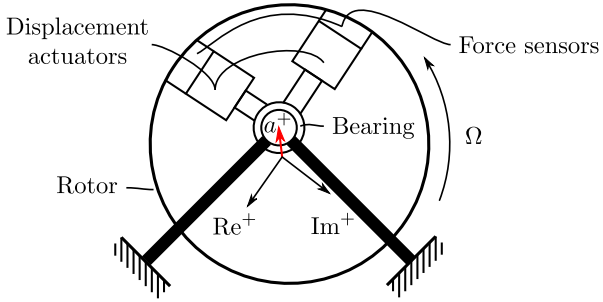

Figure 4.3: Active bearing with rotor-mounted displacement actuators. In rotating coordinates, only static displacements are required for a bearing force elimination.

Less obvious is the actuator placement in rotating coordinates, hence on the rotor itself. Figure 4.3 illustrates such an arrangement. Compared to the technical

realization, the mathematics are simple. Starting with the original state-space description from Equation (2.19), the controller can be converted to rotating coordinates using the relations $\mathbf{x}_R = \mathbf{x}_R^+ \mathrm{e}^{i\Omega t}$ and $F = F^+ \mathrm{e}^{i\Omega t}$, yielding:

$$\underbrace{\begin{bmatrix} \dot{a}_F^+ \\ a_B^+ \\ a_D^+ \end{bmatrix}}_{\dot{\mathbf{x}}_R^+} = \underbrace{\begin{bmatrix} 0 & 0 & 0 \\ 0 & -2i\Omega & 0 \\ 0 & 0 & -i\Omega - c_D k_D \end{bmatrix}}_{(\mathbf{A}_R - i\Omega\mathbf{I})} \underbrace{\begin{bmatrix} a_F^+ \\ a_B^+ \\ a_D^+ \end{bmatrix}}_{\mathbf{x}_R^+} + \underbrace{\begin{bmatrix} -i\tilde{c}_C \\ +i\tilde{c}_C \\ c_{Dj} \end{bmatrix}}_{\mathbf{B}_R} F^+$$

$$a^+ = \underbrace{\begin{bmatrix} 1 & 1 & 1 \end{bmatrix}}_{\mathbf{C}_R} \mathbf{x}_R^+ \tag{4.6}$$

It is assumed that the forces are measured directly on the rotating shaft. If they are measured in inertial coordinates, the transformation $F^+ = F\,\mathrm{e}^{i\Omega t}$ must be applied first. Needless to say, the controller's dependence of the rotational speed Ω can be avoided using the same transformation techniques applied in Equations (4.2) and (4.3).

The advantage of mounting actuators directly on the rotor are visible when the rotor's unbalance responses of Equations (2.23) and (A.23) are studied. They reveal that the state vector $\mathbf{x}^+$ and hence the controller vector $\mathbf{x}_R^+$ depends on the constant eccentricity $\boldsymbol{\varepsilon}^+$, leading to a constant vector $\mathbf{x}_R^+$ for any rotational speed Ω. In steady-state, the actuator displacements a^+ are consequently also constant.

$$a^+ = \text{const.} \qquad (\text{for } \Omega = \text{const.}) \tag{4.7}$$

An actuator assembly in rotating coordinates requires only a *steady actuator displacement* during the operation at one particular rotational speed Ω. This allows not only for a quasistatic and a theoretically powerless operation, but also enables the use of slower actuator principles. It must be stressed that the rotating actuators do neither alter the systems state-space representation from Equation (3.27), nor do they alter the closed-loop solution of Equation (3.29). Considering the latter, it is interesting that the derived theory also covers rotor-fixed actuators which are closely related to *balancing actuators* [23]. The presented arrangement has the drawback that it has a complicated damping mechanism, as the actuator's damping action has to be transferred from rotating to inertial coordinates. From the viewpoint of stability, this process rules out slower actuator principles. However, Section 4.1.3 provides a solution to this problem.

In conclusion, the advantages and disadvantages of this arrangement are:

+ Low actuator bandwidth. The required actuator bandwidth is independent of the rotational speed Ω, allowing slow actuator principles.
+ Low power operation. Quasistatic actuator operation requires almost no power for appropriate actuators.
– Stresses through centrifugal forces.
– Rotor modifications required. Additional actuators might result in increased rotor size, weight or inertia.
– Difficult power and data transmission. The required power can either be directly generated on the rotor or transferred from the stator. The principle's inherent low power requirements make this disadvantage less limiting.

4.1.3 Passive suspension

It was implicitly assumed that rotor damping is provided by the control system. Providing dissipation through the controller has the advantage that the damping coefficients can be dynamically adjusted. Although beneficial in theory, providing damping electronically has many drawbacks in practice. Experience shows that the inherent time delay in the sensor-controller-actuator chain may excite higher structural harmonics for large controller gains. Power or controller failures void rotor damping and make the system inoperable. Moreover, active rotor damping requires some portion of the actuator's stroke - which is subsequently unavailable for the actual unbalance compensation.

A solution for this problem is provided in Figure 4.4. The introduction of a conventional spring-damper system can provide the required rotor damping. For the inertial actuator configuration from Section 4.1.1, passive damping merely requires a serial arrangement between the sensor-actuator pair and the passive spring-damper system. Passive suspension is also advantageous when the actuators are installed on the rotor. In this case, the passive suspension should be arranged on the stator; otherwise the introduced *inner damping* may cause stability problems (see Section 5.1.7).

According to the controller derivation from Section 2.3.1, the control algorithm is based on the superposition of three displacement vectors, the forward compensating element a_F, the backward compensating element a_B and the damp-

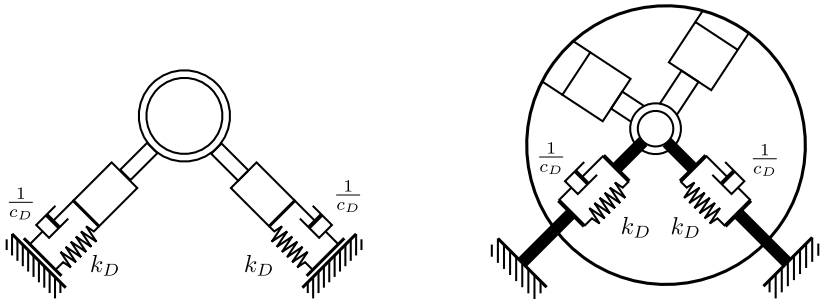

Figure 4.4: Passive actuator suspension has the advantage of being inherently fail-safe and requiring less actuator usage. Left: Suspension for fixed actuators. Right: Suspension for rotating actuators.

ing element a_D. The serial connection of a passive spring-damper element is an exact representation of a_D, and hence yields the same closed loop system behavior. With passive damping, the controller only consists of the compensation elements a_F and a_B, leading to a simplified controller version with the actuator displacements a_{FB} for actuators in inertial coordinates:

$$\begin{bmatrix} \dot{a_F} \\ a_B \end{bmatrix} = \begin{bmatrix} i\Omega & 0 \\ 0 & -i\Omega \end{bmatrix} \begin{bmatrix} a_F \\ a_B \end{bmatrix} + \begin{bmatrix} -i\tilde{c}_C \\ +i\tilde{c}_C \end{bmatrix} F$$

$$a_{FB} = \begin{bmatrix} 1 & 1 \end{bmatrix} \begin{bmatrix} a_F & a_B \end{bmatrix}^T$$

For the rotating actuator assembly, the modified controller equations similarly yield:

$$\begin{bmatrix} \dot{a}_F^+ \\ a_B^+ \end{bmatrix} = \begin{bmatrix} 0 & 0 \\ 0 & -2i\Omega \end{bmatrix} \begin{bmatrix} a_F \\ a_B \end{bmatrix} + \begin{bmatrix} -i\tilde{c}_C \\ +i\tilde{c}_C \end{bmatrix} F^+$$

$$a_{FB}^+ = \begin{bmatrix} 1 & 1 \end{bmatrix} \begin{bmatrix} a_F^+ & a_B^+ \end{bmatrix}^T$$

Since the control algorithm does not have to provide damping, it simplifies the control algorithm, leading to a separation of the unbalance compensation provided by actuators and the vibration damping provided by the passive spring-damper system. In mathematical terms, the actuators exclusively affect the differential's equation *particular solution*, whereas the passive damper part ensures a vanishing *homogeneous solution*, leaving the particular solution unaffected.

Designing the active bearing with a passive suspension provides several advantages. In contrast to damping provided by a control algorithm, passive damping is always stable. This property is especially advantageous for the rotating displacement actuators of Section 4.1.2, where it is difficult to provide damping from rotating coordinates. A further advantage is that the setup is inherently *failsafe*. Any power, controller, sensor or actuator failure disables the possibility to compensate unbalances, however it still allows for a conventional, passive rotor operation. Active bearings with passive suspension qualify for applications where high reliability is mandatory, for example as rotor support in *jet engines*.

Depending on the application, the complexity of the passive suspension design may vary. In simple machines, *O-rings* provide sufficient damping [24], whereas in high-performance applications more sophisticated suspension elements such as *Squeeze-Film-Dampers* are required to provide adequate damping [18].

4.1.4 Stiffness compensation for displacement actuators

During the system-theoretic considerations of the controlled system in Chapter 3, a detailed analysis of possible force mechanisms was performed. It became clear that the gyroscopic effect has no negative impact on the force free rotor operation, and that external damping inhibits a complete rotor isolation, but instead has a positive effect on the rotor deflections in the vicinity of the free rotor resonances. On the other hand, parasitic stiffnesses have an overall negative effect on the unbalance elimination, as it was demonstrated in Section 3.2.7. The parallel path transmits oscillations to the environment and introduces two additional resonances with large rotor deflections. Parasitic stiffnesses may occur for a variety of reasons, one of them lying in the mechanical setup of the active bearing itself, see Figure 4.5. However, they can be compensated when they occur in the active bearing plane.

Until now, both bearing and actuator forces were considered to be identical. For parasitic stiffnesses in the bearing plane, both forces differ. The effective bearing force vector $\mathbf{F}$ denotes the effective forces on the rotor through the bearings (including parasitic stiffness and actuator forces). They must be distinguished from the actuator forces, represented though the vector $\mathbf{F}_a$. Both forces are related through Equation (3.46).

$$\mathbf{F} = \mathbf{F}_a + \mathbf{F}_S = \mathbf{F}_a + \mathbf{K}_S \mathbf{q}_W \tag{4.8}$$

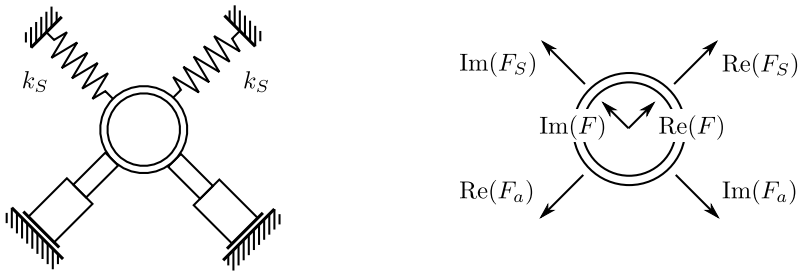

Figure 4.5: Actuator with parasitic stiffnesses. Left: Sketch. Right: Free body diagram.

Figure 4.5 reveals that the sensor can only measure the actuator force vector $\mathbf{F}_a$, not the total bearing forces $\mathbf{F}$. When $\mathbf{F}_a$ is used as controller input, the actuator forces indeed vanish, but the parallel path from the parasitic stiffness remains. It is therefore necessary to build a *virtual sensor* that *estimates* the effective bearing forces. The estimated effective bearing forces $\bar{\mathbf{F}}$ are as follows:

$$\bar{\mathbf{F}} = \mathbf{F}_a + \bar{\mathbf{K}}_S \mathbf{q}_W \tag{4.9}$$

The stiffness compensation matrix $\bar{\mathbf{K}}_S$ is structurally identical to the bearing stiffness matrix $\mathbf{K}_L$ from Equation (3.11). It is a diagonal, sparsely populated matrix with z entries that contain the estimates $\bar{k}_S$ for each parasitic bearing stiffness k_S. The state-space system with uncompensated stiffnesses was already given in Equation (3.2.7). For compensation, the controller of Equation (3.25) uses now the estimated bearing force vector $\bar{\mathbf{F}}$ from Equation (4.9). The matrices of the updated state-space system and the resulting unbalance response can be found in Appendix (A.3), but will be discussed also here.

$$\mathbf{x}^+ = \begin{bmatrix} \left(-\Omega^2\mathbf{M} + \mathbf{K}_R + \mathbf{K}_S - \bar{\mathbf{K}}_S\right)^{-1}\left(\mathbf{K}_R + \mathbf{K}_S - \bar{\mathbf{K}}_S\right) \\ i\Omega\left(-\Omega^2\mathbf{M} + \mathbf{K}_R + \mathbf{K}_S - \bar{\mathbf{K}}_S\right)^{-1}\left(\mathbf{K}_R + \mathbf{K}_S - \bar{\mathbf{K}}_S\right) \\ \mathbf{R}\mathbf{n}^T\mathbf{Z}\left(-\Omega^2\mathbf{M} + \mathbf{K}_R + \mathbf{K}_S - \bar{\mathbf{K}}_S\right)^{-1}\left(\mathbf{K}_R + \mathbf{K}_S - \bar{\mathbf{K}}_S\right) - \mathbf{R}\mathbf{n}^T\mathbf{Z} \end{bmatrix} \boldsymbol{\varepsilon}^+ \tag{4.10}$$

The solution structure differs from the previous ones, mainly because of the dimensionless factor matrix $\mathbf{Z}$, which is defined as:

$$\mathbf{Z} = \mathbf{n}\tilde{\mathbf{K}}_L^{-1}\mathbf{n}^T\left(\mathbf{K}_L + \bar{\mathbf{K}}_S\right) = \mathbf{n}\left(\mathbf{n}^T\mathbf{K}_L\mathbf{n}\right)^{-1}\mathbf{n}^T\left(\mathbf{K}_L + \bar{\mathbf{K}}_S\right) \tag{4.11}$$

Equation (A.28) indicates that a complete force free rotor operation and resonance elimination is possible when the estimated parasitic bearing stiffnesses in the matrix $\bar{\mathbf{K}}_S$ match their real counterparts from $\mathbf{K}_S$, resulting in two conclusions. First, the individual parasitic bearing stiffnesses must be exactly known, so that $k_S = \bar{k}_S$. Second, a complete compensation is only possible when parasitic stiffnesses occur exclusively in the active bearing planes, since the matrix structure must be identical. Imperfect compensation $\bar{\mathbf{K}}_S \approx \mathbf{K}_S$ still leads to resonances; in practical applications these resonance frequencies can be lowered sufficiently to be well below the rotor's operational speeds. It is worth mentioning that the actuator displacements $\mathbf{a}$ are not coincident with the shaft displacements $\mathbf{q}_W$ for the force free condition as it was seen previously.

The controller implementation bases on Equation (3.25), with the difference being that now the estimated forces $\bar{\mathbf{F}}$ from Equation (4.9) are used as control inputs. Estimating the bearing force requires the unavailable shaft position $\mathbf{q}_W$. Since the actuator force vector $\mathbf{F}_a$ is known, the coordinate can be calculated using the actuator force equation $\mathbf{F}_a = \mathbf{K}_L (\mathbf{q}_W - \mathbf{a})$. Using Equations (4.9) and (4.11) leads to a force estimate $\bar{\mathbf{F}}$ that only depends on the actuator forces $\mathbf{F}_a$ and the actuator displacements $\mathbf{a}$.

$$\bar{\mathbf{F}} = \mathbf{Z}\mathbf{F}_a + \bar{\mathbf{K}}_S \mathbf{a} \tag{4.12}$$

In conclusion, the results of this section are summarized:

- Parasitic stiffnesses can be fully compensated when they occur in the active bearing plane.
- An incomplete compensation leads to additional resonances. For practical purposes, these should be below the rotor's operational speed.
- Shaft displacements $\mathbf{q}_W$ and actuator displacements $\mathbf{a}$ are not coincident anymore.
- Any uncompensated stiffness nullifies a complete rotor isolation.
- Parasitic stiffnesses should be avoided wherever possible. When they are unavoidable, they should be chosen as soft as possible to minimize their impact.

4.2 Force actuators

This section demonstrates how the system-theoretic considerations from the previous sections can be used to derive a control algorithm for force actuators. This actuator type has no inherent stiffness. The reason for this is mostly the absence of any solid connection between the active surfaces. These actuator principles are based mainly on field effects, taking advantage of electrostatic [35, 36] or magnetic fields [68]. Actuator principles with fluids as working medium also qualify within this category.

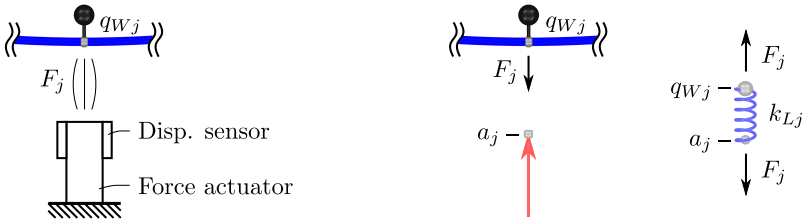

Figure 4.6: Derivation of a controller for force actuators. Left: An actuator exerts a force F_j on a node of the free, unbound rotor. Without control, this system is unstable. Right: Electronic implementation of the virtual stiffnesses k_{Lj}. When the position q_{Wj} is measured, the controller can bind the rotor to the virtual position setpoint a_j, leading to a stable force equilibrium.

Ideal force actuators have no inherent stiffness and cannot support a rotor because of their inability to provide returning forces. This changes when a control loop feeds back the shaft's position in such a way that a returning actuator force is generated. In this case, the combination of sensor, controller and actuator is able to support the rotor, working as a bearing. During the derivation of the JEFFCOTT rotor in Section 2.2, it was stated that bearings determine the rotor's position. To hold this position, a force equilibrium has to be maintained, resulting in bearing *reaction forces*. In other words, neither a passive bearing nor an active one can arbitrarily choose how much force to put on an object. To clarify this statement, consider a simple planar rotor with the weight force F_G that is supported by an active bearing based on force actuators. In static conditions, the active bearing force F opposes the weight force in a way that $F_G + F = 0$. No matter how sophisticated the underlying control algorithm might be, all must satisfy this equilibrium condition. Failure to do so results in static instability.

In statically determined systems, the actuator force depends on the rotor load *only*, raising the question what an active bearing can actually control. Active bearings are able to control the rotor *displacements*.

Active bearings with force actuators measure the shaft displacement q_W and control a force F and thus, from the viewpoint of control engineering, it is tempting to believe that the actuator force F is the *cause*, while the displacement q_W is the *effect*. From the viewpoint of structural engineering, it is clear that the situation is reversed. Holding the rotor in its position (*cause*) results in an actuator reaction force (*effect*). The latter statement is always compatible with the equilibrium conditions, while the former one is not. Although this difference might seem inconsequential, it alters the understanding of the force free condition. Going back to the considerations from Sections 3.1.1 and 3.1.3, the equations of motion for the free, unconstrained rotor are:

$$\mathbf{M}\ddot{\mathbf{q}}_S + \mathbf{K}_R \mathbf{q}_W = -\mathbf{F} \tag{4.13}$$

Naturally, this system is unstable as the stiffness matrix $\mathbf{K}_R$ of the free rotor is rank deficient, but active bearings can stabilize the system. When the shaft position q_{Wj} is known at the j-th active bearing, a simple proportional controller with the gain k_{Lj} can bind the rotor to a *virtual position setpoint* a_j using the actuator force F_j. The variable names are no coincidence: the mechanical properties for displacement actuators are now transferred to their controller counterparts. The bearing/actuator stiffness k_{Lj} is now a controller gain, and what was previously an actuator displacement a_j is now a controller-internal virtual position setpoint. The commanded actuator force is then $F_j = k_{Lj}\left(q_{Wj} - a_j\right)$, and using the assignments from Section 3.1.3 yields:

$$\mathbf{M}\ddot{\mathbf{q}}_S + \left(\mathbf{K}_R + \mathbf{K}_L\right)\mathbf{q}_S = \mathbf{K}_L \mathbf{a} + \left(\mathbf{K}_R + \mathbf{K}_L\right)\boldsymbol{\varepsilon}$$

This is the same equation that was already found in (3.23), describing a mechanical system with force actuators. Now the same equation describes a controlled system that binds a rotor to the virtual position setpoint a. Special care must be taken of the right-hand side of the equation. The unit of the expression $\mathbf{K}_L\mathbf{a}$ is 'force', although it physically describes an actuator displacement or a position setpoint. Some books and publications [26, 29] substitute the expression $\mathbf{K}_L\mathbf{a}$ with a 'generalized force' $\mathbf{f}_a$, the expression $\left(\mathbf{K}_R + \mathbf{K}_L\right)\boldsymbol{\varepsilon}$ with an

'unbalance force' $\mathbf{f}_\varepsilon$, and the stiffness matrix of the supported system $\mathbf{K}_R + \mathbf{K}_L$ with a generalized stiffness matrix $\mathbf{K}$, leading to the simplified representation:

$$\mathbf{M}\ddot{\mathbf{q}}_S + \mathbf{K}\mathbf{q}_S = \mathbf{f}_a + \mathbf{f}_\varepsilon$$

Although these substitutions are mathematically precise, they pave the way for subsequent misinterpretation. A comparison between the equations of the free rotor from Equation (4.13) contrasted with the supported one from Equation (4.2), reveals that they are mathematically almost identical, although they represent systems with completely different properties. The right-hand side of Equation (4.13) represents real, physical forces, but the right-hand side of Equation (4.2) are actually displacements, disguised as forces. It is in fact tempting to draw the *wrong* conclusion that the 'actuator forces' $\mathbf{f}_a$ must *counteract* the 'unbalance forces' $\mathbf{f}_\varepsilon$ so that $\mathbf{f}_a + \mathbf{f}_\varepsilon = \mathbf{0}$. The formula's correct interpretation gets clear when JEFFCOTT rotor's steady state condition from Figure 2.3 is considered: the actuator displacement a must oppose the eccentricity ε so that the center of mass remains in the rotational center, leading to vanishing node forces.

4.2.1 Fixed force actuators

A controller for force actuators performs two different tasks. The first and most important task, is to bind the rotor to the virtual position setpoint a_j so that the rotor is statically stabilized. The second task is the elimination of the unbalance-induced bearing forces. From the previous section it is clear that the stabilizing part of the controller simply resembles the displacement actuator stiffness electronically. Using the relation $F = k_L\,(q_W - a)$ (The subindex j will be omitted for improved clarity), the controller for displacement actuators from Equation (3.24) can be transformed in:

$$\begin{aligned} \dot{\mathbf{x}}_R &= (\mathbf{A}_R - \mathbf{B}_R k_L \mathbf{C}_R)\,\mathbf{x}_R + \mathbf{B}_R k_L q_W \\ F &= k_L\,(q_W - \mathbf{C}_R \mathbf{x}_R) \end{aligned} \tag{4.14}$$

The control input is the measured shaft displacement at the coordinate q_W, while the control output is the actuator force F. Although the controller was derived from the displacement controller, their structure differs. For displacement controllers the system matrix was diagonal, while force controllers feature

a full system matrix. The output equation also has a structural difference. It depends on the sensor input q_W, resulting in a direct feedthrough. Figure 4.7 illustrates an exemplary frequency response function for such a controller. Its characteristic bandstop behavior is adaptive and shifts depending on the rotor's rotational speed Ω. The magnitude can be interpreted as a *dynamic bearing stiffness*. The complete state-space system can be obtained by joining all z

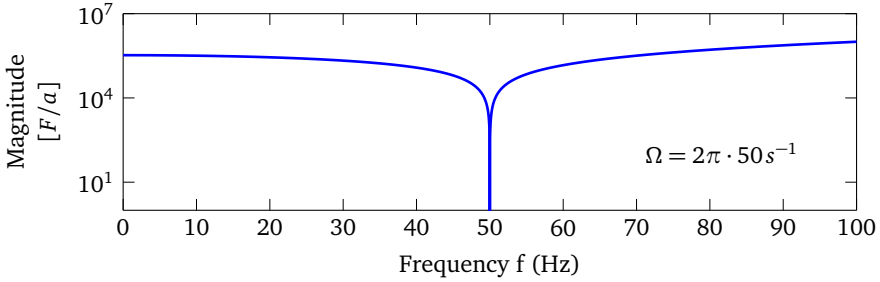

Figure 4.7: Exemplary one-sided force controller frequency response. The characteristic notch is adaptive and depends on the rotational speed Ω. The frequency response can be interpreted as a dynamic controller stiffness.

controllers and attaching them to their respective shaft nodes, using the definitions from Section 3.1.3. It should come as no surprise that it results in the exact same state-space representation that was exhaustively investigated in Chapter 3. There is no difference in the closed-loop description for force and displacement actuators, when the controllers are consistently transformed.

For a convenient controller implementation, a coordinate transformation technique was introduced in Section 4.1.1. The same transformations will also be applied for force controllers. Using the coordinate transformation (4.2) with the force controller Equation (4.14) yields:

$$\begin{aligned} \dot{\tilde{\mathbf{x}}}_R &= \mathbf{T}^{-1}\left(\bar{\mathbf{A}}_R - \mathbf{B}_R k_L \mathbf{C}_R\right)\mathbf{T}\tilde{\mathbf{x}}_R + \mathbf{T}^{-1}\mathbf{B}_R k_L q_W \\ F &= k_L\left(q_W - \mathbf{C}_R \mathbf{T}\mathbf{x}_R\right) \end{aligned} \tag{4.15}$$

The transformation here, also removes the speed-dependency of the system matrix. In contrast to the displacement controller, a cancellation of the transformation matrices $\mathbf{T}^{-1}(...)\mathbf{T}$ is impossible because the matrix elements of

$(\bar{\mathbf{A}}_R - \mathbf{B}_R k_L \mathbf{C}_R)$ are all non-zero. A *forward difference* discretization facilitates a controller implementation:

$$\begin{aligned} \bar{\mathbf{x}}_{R+1} &\approx \mathbf{T}^{-1}\left(\left(\bar{\mathbf{A}}_R - \mathbf{B}_R k_L \mathbf{C}_R\right) t_S + \mathbf{I}\right) \mathbf{T}\bar{\mathbf{x}}_R + \mathbf{T}^{-1}\mathbf{B}_R k_L q_W \\ F_{+1} &= k_L \left(q_W - \mathbf{C}_R \mathbf{T}\bar{\mathbf{x}}_R\right) \end{aligned} \tag{4.16}$$

All relationships that were found for the displacement controller states $\bar{\mathbf{x}}_R$ in Section 4.1.1 are also valid for force controllers. In steady-state, the controller states directly represent the rotor's eccentricity in magnitude and phase.

This section ends with some concluding remarks on controllers for force actuators. Figure 4.7 shows the typical notch-filter behavior for unbalance elimination algorithms [42]. This behavior resulted elegantly from system-theoretic deductions, whereas in most other works it was an a-priori choice. Even though many unbalance compensation algorithms share a similar notch filter behavior, only the one presented in this work guarantees stability, as it was demonstrated in Section 2.3.4. The considerations also help to resolve the apparent contradictions between notch filters and adaptive feedforward compensation algorithms mentioned in the introductory Section 1.2. In case of unconstrained rotors, the controller exhibits a notch filter behavior as it has to support the rotor and eliminate the unbalance forces. When the rotor is statically stabilized, either through the actuators or through an additional control loop, adaptive feedforward compensation can be applied. The injected harmonic signal then represents an actuator displacement which adjusts the rotational axis until all bearing forces vanish.

4.2.2 Stiffness compensation for force actuators

Parasitic stiffnesses are not only limited to displacement actuators, but often may be present when force actuators are used. According to Section 3.2.7, these stiffnesses impede the rotor's force free operation, but may be compensated when they occur in the bearing plane. This is of particular interest for *Active Magnetic Bearings* [76]. Building on that, this section demonstrates how the controller can be adapted in a way that also parasitic stiffnesses for force actuators can be compensated.

The basis for the following considerations is the partitioning of the effective bearing force F into a controllable part F_a and displacement-dependent part

F_S, as it was previously done in Equation (4.9). The modified output for the controller of Equation (4.15) is then:

$$F_A = k_L \left(q_W - \mathbf{C}_R \mathbf{x}_R\right) - \bar{k}_S q_W \tag{4.17}$$

The difference between the force controller from Equation (4.14) and its stiffness compensated counterpart lies only in the presence of the estimated stiffness $\bar{k}_S$. With parasitic bearing stiffnesses, the effective bearing force F and the controllable bearing forces F_a differ, leading to some apparent control action $F_a \neq 0$ even when the effective bearing force F is zero.

4.3 Actuator dimensioning

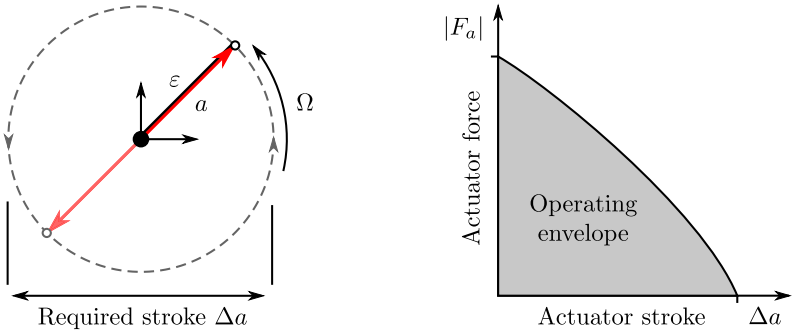

Figure 4.8: Actuator dimensioning. Left: derivation of the minimal required actuator stroke. Right: maximum force and maximum stroke do not occur simultaneously.

The practical design of a rotating machine with active bearings requires the determination of actuator's key parameters, in particular stroke and force. In the design phase, it is generally sufficient to have estimates for these quantities. The analysis of the controlled JEFFCOTT rotor from Section 2.3 revealed that the actuators move the shaft center q_W in a manner through which the mass coordinate q_S always remains in the rotational center during steady-state operation. Figure 4.8 illustrates that the shaft center q_W describes a circle, and it is obvious that the actuator stroke must at least cover the circle's diameter. For the JEFF-

COTT rotor, the circle's radius equals the eccentricity ε^+, resulting in minimal absolute actuator stroke Δa of:

$$\Delta a \geq 2 \left| \varepsilon^+ \right| \tag{4.18}$$

The steady-state actuator stroke directly depends on the rotor's eccentricity. More than 90% of all rotors can be considered rigid [26]; in this case the *International Standard ISO 1940* [85] provides orientation on the expected eccentricities.

In steady-state operation, the actuator forces are zero, consequently the maximum forces during passive rotor operation are the limiting design criterion. According to Equation (2.2), the forces are:

$$|F_P| = k \left| \frac{\Omega^2}{\omega_0^2 - \Omega^2} \varepsilon^+ \mathrm{e}^{i\Omega t} \right| = k \left| \frac{\Omega^2}{\omega_0^2 - \Omega^2} \varepsilon^+ \right| \tag{4.19}$$

When the rotor's eigenfrequency $\omega_0 = \sqrt{m^{-1}k}$ is well above the rotational speed Ω, the rotor can be considered rigid. With $k \to \infty$, the equation simplifies to:

$$|F_P| = m\Omega^2 \left| \varepsilon^+ \right| \qquad \text{(rigid rotor)} \tag{4.20}$$

Equation (4.20) allows the determination of the maximum actuator forces for rigid rotors. Together with the minimal actuator stroke from Equation (4.18), the actuator's basic parameters are completely known. The situation is more complicated for flexible rotors, because according to Equation (4.19), they result in theoretically unlimited forces on the bearing. For a realistic actuator dimensioning, additional assumptions are required. Either the maximum rotor displacements are limited through the rotor casing or *retainer bearings*, or external damping must be assumed to limit the maximal forces and displacements. On the positive side, both forces and strokes do not occur simultaneously, as Figure 4.8 illustrates. For general rotors, the minimal required actuator strokes are a direct result of the steady-state solution (3.44):

$$\left[\Delta a_A, ..., \Delta a_z\right]^T = 2\mathbf{n}^T \left| \left(\left(-\Omega^2 \mathbf{M} + i\Omega(\mathbf{D} + \mathbf{G}) + \mathbf{K}_R \right)^{-1} \mathbf{K}_R - \mathbf{I} \right) \boldsymbol{\varepsilon}^+ \right| \tag{4.21}$$

This solution is the generalization of the rotor with a single mass from Equation (4.18), but in contrast to the previous solution, the required actuator dis-

placements change with the rotational speed Ω. Without damping, the actuator displacements become very large in the vicinity of a free rotor resonance, tending to infinity. Without assuming external damping, no reasonable actuator dimensioning is possible.

Even without external damping, one can exploit the *bearing invariance* property from Section 3.2.8. Because the bearing's position has no effect on the rotor's unbalance response, they can be positioned in the vibration node of a free rotor resonance. In this case, the actuator displacements remain small even if the rotor is in a free bending eigenmode.

The maximum actuator forces occur during passive rotor operation. The combination of Equations (3.6), (3.12), (3.16) and (3.26) results in the passive bearing forces at each bearing. Similar to its single-mass counterpart from Equation (4.19), some damping $\mathbf{D} \neq \mathbf{0}$ is required when the rotor should pass a passive, critical speed.

$$\begin{bmatrix} |F_{PA}| \\ \vdots \\ |F_{Pz}| \end{bmatrix} = \mathbf{n}^T \mathbf{K}_L \left| \left(\left(-\Omega^2 \mathbf{M} + i\Omega(\mathbf{D}+\mathbf{G}) + \mathbf{K}_R + \mathbf{K}_L \right)^{-1} (\mathbf{K}_R + \mathbf{K}_L) - \mathbf{I} \right) \boldsymbol{\varepsilon}^+ \right| \quad (4.22)$$

It is worth mentioning that the dimensioning guidelines only consider the forces and strokes during steady-state operation. Naturally, the actuator requires additional strokes and forces to cover also the rotor's transient behavior. The presented equations consequently establish only lower bounds for actuator strokes and forces.

The section concludes with a summary of the derived dimensioning guidelines:

- Maximum actuator displacements and forces are proportional to the rotor's eccentricity. Without knowledge or reliable assumptions on the rotor's unbalance, a useful actuator dimensioning is impossible.
- For rigid rotors, the required actuator strokes and forces can be evaluated using Equations (4.18) and (4.20).
- When passing a free eigenmode on a flexible rotor, additional assumptions on the external damping are required. Alternatively, the bearings can be placed in the nodes of the rotor's free eigenforms.
- The maximum actuator stroke and force do not occur simultaneously.

4.4 Resonance peak avoidance

The investigated controller allows for a complete isolation of the unbalance-induced bearing forces for arbitrary rotors. In Section 3.2, it was found that a force free rotor operation close to a free resonance leads to large rotor and actuator displacements. Large rotor displacements are generally unwanted and a operation close to a free resonance should be avoided. In Section 3.10 it was demonstrated that external mechanical damping reduces these resonances, having the drawback that a complete isolation is not possible anymore. There might be circumstances where external damping is unavailable or where it is not strong enough to limit the rotor displacements in the free rotor resonances. In these cases, the controller equations can be modified to also limit the rotor displacements in the free rotor resonances. Unfortunately, this modification impedes a complete force free rotor operation.

$$\dot{\mathbf{x}}_R = \underbrace{\begin{bmatrix} i\Omega & 0 & 0 \\ 0 & -i\Omega & 0 \\ 0 & 0 & -c_D k_D \end{bmatrix}}_{\mathbf{A}_R} \mathbf{x}_R - \underbrace{\begin{bmatrix} \delta & 0 & 0 \\ 0 & \delta & 0 \\ 0 & 0 & 0 \end{bmatrix}}_{\mathbf{A}_\delta} \mathbf{x}_R + \mathbf{B}_R F \tag{4.23}$$

In contrast to the previous controller, the modified version features a diagonal matrix $\mathbf{A}_\delta$ with two diagonal elements δ. During the controller derivation in Section 2.3.1, it was stated that the controller elements a_F^+ and a_B^- are integrators, defined in the their corresponding coordinate systems. In a free rotor resonance, the element a_F^+ is continuously integrating because there is no force equilibrium. One can imagine the δ-element as a return spring, preventing an infinite integration. The introduction of the δ-element leads to a combination of different control strategies. For $\delta \to \infty$, the integrating elements a_F and a_B are blocked, and the differential equation degenerates to an *Integral Force Feedback*-controller [12, 30]. For $\delta \to 0$, it returns to an ideal force free operation.

This additional parameter can either be determined through a simulation, or be chosen manually. In latter case, the control algorithm is initially adjusted with $\delta = 0$. When the actuator displacements become too large, the parameter δ is increased until the displacements remain within the limits.

5 Stability proof

The purpose of this chapter is to give a complete stability proof for the previously introduced controller on arbitrary, isotropic rotors. In contrast to the direct stability proof for the JEFFCOTT rotor demonstrated in Section 2.3.3, the corresponding proof for general rotors is considerably more sophisticated.

The stability proof is partitioned. To begin with, a new stability theorem based on LYAPUNOV's stability theory is developed. This theorem is not only useful for this particular problem, but also for general mechanical systems with attached collocated controllers. In a second step, the derived stability theorem is applied to the problem of general rotors controlled by active bearings.

Some parts of this chapter are based on the work of P. C. MÜLLER, an expert in the fields of rotordynamics [72], linear vibrations [75] and stability theory [73, 74]. The particular contributions are mentioned in the corresponding section. Furthermore, the stability proof has been already published in the joint publication "Unbalance and resonance elimination with active bearings on general rotors" authored by HEINDEL, MÜLLER and RINDERKNECHT [39].

5.1 Derivation of a stability theorem

This section deals with the derivation of a LYAPUNOV stability theorem for mechanical systems with collocated controllers. The evolution of stability theory is closely coupled to the understanding and analysis of dynamic systems. Modern stability theory originated in 1867, when THOMSON and TAIT published *Treatise on Natural Philosphy* [56]. Back then, the stability of mechanical systems was already well understood, including the effects of stiffness, damping and gyroscopy.

Some years later, STODOLA attempted to design a velocity governor for steam turbines, but initially failed because he could not determine the eigenvalues of problem's 7th-order characteristic polynomial [9]. HURWITZ then found a method to determine stability avoiding a direct eigenvalue calculation [61]. Despite its practicality, the proof gets tedious for systems of higher dimensions.

In 1892, LYAPUNOV published his work *The general problem of the stability of motion*, which connected the problem of stability to energy considerations rather than eigenvalues. Using only matrix properties, it elegantly proofs stability for whole classes of systems. Based on this idea, researches have obtained remarkable stability theorems within the last century, including ones for complicated mechanical arrangements [7, 48].

However, the special matrix structure of mechanical systems with collocated controllers inhibits a treatment of the problem using LYAPUNOV's stability theory [74]. Although INMAN proves stability for collocated controllers, his assumed matrix structure represents a standard mechanical system and is lacking in continuing progress over established solutions [49].

The absence of available solutions encouraged the development of a new theorem for mechanical systems with collocated controllers. After an introduction to the fundamentals of LYAPUNOV stability, the characteristic matrix structure of collocated systems is explained with a simple example. After the derivation of a stability theorem for this system, the approach is generalized to systems of arbitrary dimensions. Finally, the solution is extended to mechanical systems with damping and gyroscopy.

5.1.1 Fundamentals of Lyapunov stability

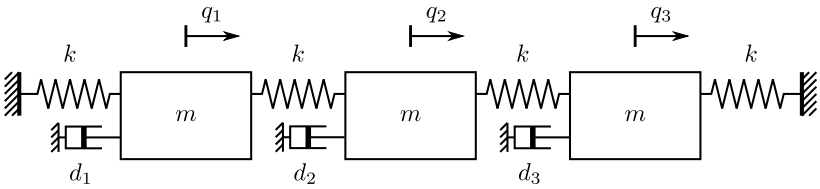

Figure 5.1: Three mass oscillator with damping.

An introductory example demonstrates how quickly a stability analysis based on HURWITZ-determinants leads to complicated calculations even for a simple systems. Figure 5.1 depicts an oscillatory, damped system with three masses and the corresponding equation of motion:

$$\mathbf{M}\ddot{\mathbf{q}} + \mathbf{D}\dot{\mathbf{q}} + \mathbf{K}\mathbf{q} = \mathbf{0} \tag{5.1}$$

Where the translational degrees of freedoms are defined as $\mathbf{q} = \begin{bmatrix} q_1 & q_2 & q_3 \end{bmatrix}^T$ with

$$\mathbf{M} = \begin{bmatrix} m & 0 & 0 \\ 0 & m & 0 \\ 0 & 0 & m \end{bmatrix}, \quad \mathbf{D} = \begin{bmatrix} d_1 & 0 & 0 \\ 0 & d_2 & 0 \\ 0 & 0 & d_3 \end{bmatrix}, \quad \mathbf{K} = \begin{bmatrix} 2k & -k & 0 \\ -k & 2k & -k \\ 0 & -k & 2k \end{bmatrix} \tag{5.2}$$

A stability analysis requires the system's transformation to a first order differential equation using the state vector $\mathbf{x}^T = \begin{bmatrix} \mathbf{q}^T & \dot{\mathbf{q}}^T \end{bmatrix}$.

$$\dot{\mathbf{x}} = \underbrace{\begin{bmatrix} \mathbf{0} & \mathbf{I} \\ -\mathbf{M}^{-1}\mathbf{K} & -\mathbf{M}^{-1}\mathbf{D} \end{bmatrix}}_{\mathbf{A}} \mathbf{x} \tag{5.3}$$

For asymptotic stability, all the real parts of all eigenvalues must be negative, $\lambda_i < 0$. The eigenvalue calculation leads to the characteristic polynomial

$$\begin{aligned} \det(\lambda\mathbf{I} - \mathbf{A}) &= 0 \\ \alpha_6\lambda^6 + \alpha_5\lambda^5 + \ldots + \alpha_1\lambda + \alpha_0 &= 0 \end{aligned} \tag{5.4}$$

A direct calculation of the eigenvalues is not possible for polynomials that exceed the degree of four. The theorem of Hurwitz [47] allows to determine whether the real parts of the individual eigenvalues λ_i are negative or positive, enabling a binary decision if the system is stable or unstable. Although the method is feasible for low-order polynomials, the calculation effort rises quickly for systems of higher order. Even for the presented, simple example, the calculation of six Hurwitz-determinants is lengthy. One positive aspect is that the derived conditions are both necessary and sufficient.

Even without lengthy calculations, structural engineers intuitively understand that the system from Figure 5.1 is stable. The physical background for this observation bases on energy considerations. An isolated system retains its energy. In case of a mechanical system, energy occurs in form of kinetic energy E_{kin}, potential energy E_{pot} and dissipated energy E_{dis} leading to heat.

$$E_{kin} + E_{pot} + E_{dis} = \text{const.} \tag{5.5}$$

The system's kinetic energy depends on the mass and their velocity: $E_{kin} = \frac{1}{2}m_1q_1^2 + \frac{1}{2}m_2q_2^2 + \ldots$. A more convenient representation uses quadratic forms:

$$E_{kin} = \tfrac{1}{2}\dot{\mathbf{q}}^T\mathbf{M}\dot{\mathbf{q}} \tag{5.6}$$

The oscillator's potential energy content can be expressed in a similar way:

$$E_{pot} = \tfrac{1}{2}\mathbf{q}^T\mathbf{K}\mathbf{q} \tag{5.7}$$

The idea of LYAPUNOV's second theorem, is that the dissipation of all kinetic and potential energy leads to vanishing movements, and thus a necessarily stable homogeneous solution. Decreasing kinetic and potential energy is guaranteed when the dissipation power $P_{dis} \geq 0$.

$$\tfrac{d}{dt}\left(E_{kin} + E_{pot}\right) = -\tfrac{d}{dt}\left(E_{dis}\right) = -P_{dis} \leq 0 \tag{5.8}$$

The expression $E_{kin} + E_{pot}$ can be further simplified using the state vector $\mathbf{x}$.

$$E_{kin} + E_{pot} = \underbrace{\begin{bmatrix}\mathbf{q}^T & \dot{\mathbf{q}}^T\end{bmatrix}}_{\mathbf{x}^T}\underbrace{\begin{bmatrix}\frac{1}{2}\mathbf{K} & \mathbf{0}\\ \mathbf{0} & \frac{1}{2}\mathbf{M}\end{bmatrix}}_{\mathbf{H}}\underbrace{\begin{bmatrix}\mathbf{q}\\ \dot{\mathbf{q}}\end{bmatrix}}_{\mathbf{x}} \tag{5.9}$$

Equation (5.9) connects the system's states with their mechanical energy. Based on the mathematical formalism for mechanical systems developed by HAMILTON, the expression $\mathbf{x}^T\mathbf{H}\mathbf{x}$ is named HAMILTON function while the matrix $\mathbf{H}$ is called HAMILTONian [33]. Similarly, the dissipation power $P_{dis} = \dot{\mathbf{q}}^T\mathbf{D}\dot{\mathbf{q}}$ is named RALEIGH dissipation function.

$$P_{dis} = \dot{\mathbf{q}}^T\mathbf{D}\dot{\mathbf{q}}^T = \mathbf{x}^T\underbrace{\begin{bmatrix}\mathbf{0} & \mathbf{0}\\ \mathbf{0} & \mathbf{D}\end{bmatrix}}_{\mathbf{Q}}\mathbf{x} \tag{5.10}$$

Combining Equation (5.8) with Equations (5.9) and (5.10) and the following derivation using the product rule yields

$$\tfrac{d}{dt}\left(\mathbf{x}^T\mathbf{H}\mathbf{x}\right) = \dot{\mathbf{x}}^T\mathbf{H}\mathbf{x} + \mathbf{x}^T\mathbf{H}\dot{\mathbf{x}} = -\mathbf{x}^T\mathbf{Q}\mathbf{x} \leq 0 \tag{5.11}$$

Inserting the state-space model from Equation (5.3) and the subsequent elimination of the variables $\mathbf{x}$ and $\mathbf{x}^T$ finally results in the LYAPUNOV equation:

$$\mathbf{x}^T\mathbf{A}^T\mathbf{H}\mathbf{x} + \mathbf{x}^T\mathbf{H}\mathbf{A}\mathbf{x} = -\mathbf{x}^T\mathbf{Q}\mathbf{x}$$

$$\mathbf{A}^T\mathbf{H} + \mathbf{H}\mathbf{A} = -\mathbf{Q} \tag{5.12}$$

A necessary condition for stability is that the RALEIGH dissipation function $P_{dis} \geq 0$ remains for all state vectors $\mathbf{x} \neq \mathbf{0}$. This is the case when the symmetric matrix $\mathbf{Q} = \mathbf{Q}^T$ is *positive semidefinite*. A sufficient condition for stability is the *positive definiteness* of the symmetric matrix $\mathbf{H}$, which is the case when the *quadratic form* $\mathbf{x}^T\mathbf{H}\mathbf{x} > 0$ for any nontrivial vector $\mathbf{x} \neq \mathbf{0}$.

For the presented mechanical system, both $\mathbf{M}$ and $\mathbf{K}$ are symmetric and positive definite, resulting in a positive definite HAMILTONian $\mathbf{H} > 0$. When the damping parameters $d_1, \ldots, d_3 > 0$, the system is completely damped, and $\mathbf{D}$ is positive definite. Since both necessary and sufficient conditions are satisfied and the system is stable.

The appeal of LYAPUNOV's theory is that stability can be evaluated using matrix properties, allowing to elegantly prove stability for systems of arbitrary dimensions. Based on LYAPUNOV's idea, researchers have found stability conditions for more complex mechanical systems, namely systems with gyroscopic or circulatory matrices [34]. Even though its origins base on energy considerations, the idea can be extended to arbitrary matrices $\mathbf{H}$ and $\mathbf{Q}$ satisfying the definiteness conditions.

LYAPUNOV *stability:* The system $\mathbf{A}$ is stable in sense of LYAPUNOV if there exists an arbitrary positive definite matrix $\mathbf{H} > 0$ that results in a positive semidefinite definite matrix $\mathbf{Q} \geq 0$.

5.1.2 Observability criteria

Even when the matrices $\mathbf{H}$ and $\mathbf{Q}$ satisfy the condition for LYAPUNOV stability, the system may still not be asymptotically stable, as the following example demonstrates. Figure 5.2 depicts an oscillatory system with three masses. In contrast to the previous example only one dissipative element is attached to the central mass, resulting in an updated damping matrix:

$$\mathbf{D} = \mathrm{diag}\,(0, d_2, 0) \tag{5.13}$$

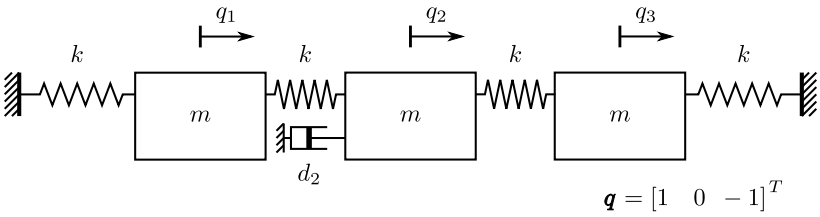

Figure 5.2: A marginally stable oscillatory system. For a particular eigenfrequency, the outer masses oscillate against each other while the central mass rests, nullifying the damper's effect.

For the frequency $\omega = \sqrt{2km^{-1}}$, the outer masses oscillate symmetrically against each other while the central mass remains still. Consequently, there is no dissipation, leading to continuous oscillations and a marginally stable system behavior [75]. In this case, the real part of at least one eigenvalue is zero ($\mathrm{Re}(\lambda_i) = 0$). In cases where only some degrees of freedom are damped and $\mathbf{D}$ is positive semidefinite only, asymptotic stability depends on the *observability* of the damped coordinates. A system is *asymptotically stable* when all eigenmodes are observable. In this case the real parts of all eigenvalues are negative ($\mathrm{Re}(\lambda_i) < 0$).

Criterion for asymptotic stability: The system matrix $\mathbf{A}$ is asymptotically stable if the conditions for LYAPUNOV stability are met and the matrix pair $(\mathbf{A}, \mathbf{Q})$ is observable, which can be checked by two criteria:

HAUTUS observability: $(\mathbf{A}, \mathbf{Q})$ is observable if and only if there is no vector $\mathbf{x}_i \neq \mathbf{0}$ that satisfies

$$\mathbf{A}\mathbf{x}_i = \lambda_i \mathbf{x}_i, \qquad \mathbf{Q}\mathbf{x}_i \neq \mathbf{0} \tag{5.14}$$

KALMAN observability: $(\mathbf{A}, \mathbf{Q})$ is observable if and only if the observability matrix is of full rank

$$\mathrm{rank}\begin{bmatrix}\mathbf{Q} & \mathbf{A}^T\mathbf{Q} & \mathbf{A}^{T\,2}\mathbf{Q} & \dots & \mathbf{A}^{T\,(p-1)}\mathbf{Q}\end{bmatrix} = p \tag{5.15}$$

Applying the KALMAN observability criterion from Equation (5.15) to the example system from Figure 5.13 reveals that the matrix pair $(\mathbf{A}, \mathbf{Q})$ is not fully observable, as the rank of the observability matrix is only four. Meanwhile, the matrices $\mathbf{A}$ and $\mathbf{Q}$ have the dimension six.

Even when systems are not completely damped, they can be asymptotically stable. The example considered is now modified in such a way that the damper is attached to the coordinate q_1, the damping matrix changes to $\mathbf{D} = \mathrm{diag}(d_1, 0, 0)$. In this case, the matrix pair $(\mathbf{A}, \mathbf{Q})$ is fully observable and therefore asymptotically stable. Systems where damping affects only some degrees of freedom ($\mathbf{D} \geq 0$), but which are still asymptotically stable are called *pervasively damped* [84, 99]. This case is of particular interest for rotating machinery, where in many cases significant damping is only provided through the bearings.

5.1.3 A simple system with semidefinite mass matrix

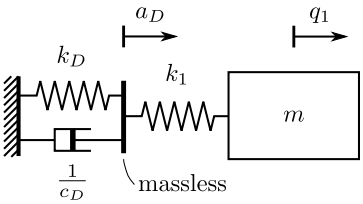

Figure 5.3: A damped mechanical system with a massless guide. The application of Lyapunov's theory is difficult for systems with semidefinite mass matrices.

Throughout the last century, stability theorems have been found even for complex mechanical systems. On the other hand, there are even simple systems where LYAPUNOV's theory cannot be applied. The mechanical system from Figure 5.3 represents such an example. The corresponding matrices are:

$$\mathbf{M} = \begin{bmatrix} m & 0 \\ 0 & 0 \end{bmatrix}, \quad \mathbf{D} = \begin{bmatrix} 0 & 0 \\ 0 & c_D^{-1} \end{bmatrix}, \quad \mathbf{K} = \begin{bmatrix} k_1 & -k_1 \\ -k_1 & k_1 + k_D \end{bmatrix}. \tag{5.16}$$

Since the mass matrix $\mathbf{M}$ is positive semidefinite and consequently noninvertible, the state-space representation from Equation (5.3) is invalid. With the modified state vector $\mathbf{x}^T = \begin{bmatrix} q_1 & \dot{q}_1 & a_D \end{bmatrix}^T$, the system matrix yields

$$\mathbf{A} = \begin{bmatrix} 0 & 1 & 0 \\ -m^{-1}k_1 & 0 & m^{-1}k_1 \\ c_D k_1 & 0 & -c_D(k_1 + k_D) \end{bmatrix} \tag{5.17}$$

Since the matrix structure of $\mathbf{A}$ has changed, the HAMILTONian found in Equation (5.9) does not satisfy the LYAPUNOV equation, partly because of a dimensional mismatch, but mainly because the state vector $\mathbf{x}$ lacks the state $\dot{a}_D$ which is needed for the dissipation function $\mathbf{x}^T\mathbf{Q}\mathbf{x}$. Finding a suitable HAMILTONian for mechanical systems with semidefinite mass matrices $\mathbf{M} \geq 0$ has been under investigation by various researchers [27, 74, 96]. Instead of finding a suitable HAMILTONian $\mathbf{H}$ for the modified system, the presented works rely on proofs by contradiction. On the downside, these approaches forfeit the elegance and clearness of the initial LYAPUNOV proof.

Although LYAPUNOV's theory originated from energy considerations, it can be further generalized. Any arbitrary matrix $\mathbf{H} > 0$ that results in a positive semidefinite matrix $\mathbf{Q} \geq 0$ implies a stable system matrix $\mathbf{A}$. Theoretically, these matrices could be chosen arbitrarily, but their definiteness properties must be known. Since the definiteness of a matrix depends on its eigenvalues, the problem shifts from the eigenvalue calculation of $\mathbf{A}$ to the eigenvalues of $\mathbf{H}$ and $\mathbf{Q}$. Consequently, this helps only when the matrices have a structure that allows for a simple determination of the definiteness properties. When the matrices are diagonal or block-diagonal, determining the definiteness is relatively easy, as it only depends on the diagonal elements. For instance, the matrices from Equations (5.9) and (5.10) have such a convenient form, that results in an elegant stability proof for $\mathbf{M}, \mathbf{D}, \mathbf{K}$-systems. Unfortunately, there is no general recipe how to choose the matrices $\mathbf{H}$ and $\mathbf{Q}$ so that they count with favorable properties. As starting point for good choices of the matrix $\mathbf{Q}$ is the inclusion of dissipation elements at their respective coordinates, as it was done in Equation (5.10). For the system of Figure 5.3, the dissipation function is $P_{dis} = \dot{a}_D c_D^{-1} \dot{a}_D$. Since only the position a_D is part of the state vector $\mathbf{x}$, a direct dissipation representation with respect to $\dot{a}_D$ is not possible and the quantity $a_D 2c_D^{-1} a_D$ is chosen instead.

$$\mathbf{Q} = \operatorname{diag}\left(0, 0, 2c_D^{-1}\right) \tag{5.18}$$

The expression is physically meaningless, but the symmetric and positive semidefinite matrix $\mathbf{Q}$ serves as valid starting point for the solution of Equation (5.12). With both $\mathbf{A}$ and $\mathbf{Q}$ defined, the solution $\mathbf{H}$ can be determined.

Historically, several methods for the analytical solution of LYAPUNOV equations emerged. One method bases on LEVERRIER-FADDEEV-matrices [73, 74], another method bases on the KRONECKER-product [8, 17]. Latter method defines a $(p \times p)$ matrix $\mathbf{H}$ with the unknowns $h_{11} \ldots h_{pp}$. Expanding the LYAPUNOV equation leads to a system of p^2 linear equations, which can be solved with standard methods.

The complexity is further reduced since $\mathbf{H} = \mathbf{H}^T$, so only the upper triangular matrix must be considered, reducing the number of unknowns to $p\,(p-1)\,/2$.

Due to the large number of equations, the manual calculation of analytical solutions is complicated and prone to errors. Using computer algebra systems such as *Mathematica* or *Matlab* solve even complicated analytical problems almost instantly and without errors. The following result was obtained using MATLAB's symbolic toolbox.

$$\mathbf{H} = \begin{bmatrix} m & 0 & 0 \\ 0 & m^2\tilde{k}^{-1} & mc_D^{-1}k_D^{-1} \\ 0 & mc_D^{-1}k_D^{-1} & c_D^{-2}k_D^{-1} \end{bmatrix} \quad \text{with} \quad \tilde{k}^{-1} = \frac{k_1 + k_D}{k_1 k_D} \tag{5.19}$$

The matrix is positive definite if the *leading principal minors* are positive [3].

$$\begin{aligned} a_1 &= m \\ a_2 &= \begin{vmatrix} m & 0 \\ 0 & m^2\tilde{k} \end{vmatrix} = m^3\tilde{k} \\ a_3 &= \begin{vmatrix} m & 0 & 0 \\ 0 & m^2\tilde{k}^{-1} & mc_D^{-1}k_D^{-1} \\ 0 & mc_D^{-1}k_D^{-1} & c_D^{-2}k_D^{-1} \end{vmatrix} = m^3 c_D^{-2}(k_1 k_D)^{-1} \end{aligned}$$

The matrix is positive definite when the mass m is positive, the series connection of the two stiffnesses is positive $\tilde{k} > 0$ and the product $k_1 k_D$ is positive. It is surprising that an arbitrary value for c_D leads to $\mathbf{H} > 0$, however $\mathbf{Q}$ is positive definite only for $c_D > 0$. To summarize, a sufficient condition for the stability of $\mathbf{A}$ is that the parameters m, k_1, k_D, c_D are positive. This result is consistent with the expectations of a mechanical engineer. Indeed, the same result can be obtained with less effort using the HURWITZ stability criterion [9, 47]. However, the advantages of LYAPUNOV's theory are better visible for large systems.

5.1.4 Complex mechanical systems

The previous section demonstrated how a suitable HAMILTONian for a simple mechanical system with a semidefinite mass matrix can be found. This basic stability proof is now extended to a more complex mechanical system. However it is modified in such a way that preserves various similarities with the previous result.

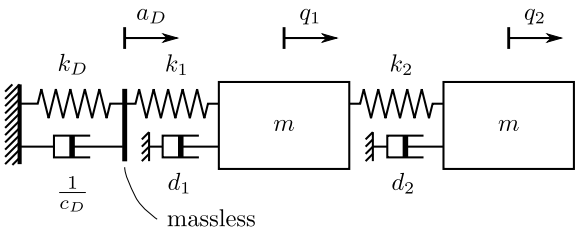

Figure 5.4: Extension of the previous system to more general mechanical systems.

Figure 5.4 represents a similar system to the one of Figure 5.3, with the only difference that an additional oscillatory system and a new coordinate q_2 are introduced. The problem is represented by the following system matrix:

$$\mathbf{A} = \begin{bmatrix} \mathbf{0} & \mathbf{I} & \mathbf{0} \\ -\mathbf{M}^{-1}\mathbf{K} & \mathbf{0} & -\mathbf{M}^{-1}\mathbf{A}_A \\ \mathbf{A}_S & \mathbf{0} & \mathbf{A}_C \end{bmatrix} \tag{5.20}$$

With the state vector $\mathbf{x}^T = \begin{bmatrix} q_1 & q_2 & \dot{q}_1 & \dot{q}_2 & a_D \end{bmatrix}^T$, the remaining matrices yield:

$$\mathbf{M} = \begin{bmatrix} m & 0 \\ 0 & m \end{bmatrix}, \quad \mathbf{K} = \begin{bmatrix} k_1 + k_D & -k_D \\ -k_D & k_D \end{bmatrix}$$

$$\mathbf{A}_A = \begin{bmatrix} -k_1 \\ 0 \end{bmatrix}, \quad \mathbf{A}_S = \begin{bmatrix} c_D k_1 & 0 \end{bmatrix}, \quad \mathbf{A}_C = -c_D\,(k_1 + k_D) \tag{5.21}$$

In analogy to the previous example, a suitable matrix $\mathbf{Q}$ must be chosen. As before, the only dissipative element is attached to the coordinate a_D. Consequently, the same 'dissipation' quantity $a_D 2c_D^{-1} a_D$ is chosen.

$$\mathbf{Q} = \operatorname{diag}\left(0, 0, 0, 0, 2c_D^{-1}\right)$$

With $\mathbf{A}$ and $\mathbf{Q}$ known, a *computer algebra system* can now find a HAMILTONian $\mathbf{H}$ which satisfies the LYAPUNOV equation (5.12). Although the solution of $\mathbf{H}$ is parametric, it is bound to the specific matrix structure that was defined in Equation (5.21). Consequently, the solution $\mathbf{H}$ is restricted to the specific, parametric problem of Figure 5.4. A useful stability theorem should be applicable

for more general systems such as the one from Equation (5.20) – with only few restrictions on the structure of $\mathbf{M}, \mathbf{K}, \mathbf{A}_A, \mathbf{A}_S, \mathbf{A}_C$.

It would appear that finding a general HAMILTONian for Equation (5.20) should be manageable, considering that it inherits the same matrix structure as the simple system of Equation (5.17) where a solution was easily found. Unfortunately, the block-matrix structure of Equation (5.20) inhibits the use of direct solution techniques that were introduced in Section 5.1.3. Contrary to scalar calculations, matrix algebra is not commutative, so $\mathbf{X}\cdot\mathbf{Y}$ is generally not the same as $\mathbf{Y}\cdot\mathbf{X}$. Even though some *computer algebra systems* support noncommutative matrix algebra, a different solution technique is preferred.

The presented approach has the advantage of not requiring noncommutative matrix algebra. It bases on the *hypothesis* that there is a solution $\mathbf{H}$ for the general state-space system $\mathbf{A}$ of Equation (5.20) which can be expressed somehow in terms of the matrices $\mathbf{M}, \mathbf{K}, \mathbf{A}_A, \mathbf{A}_S, \mathbf{A}_C$. If this hypothesis holds, the HAMILTONian of Equation (5.19) must be a specific solution for the still unknown, general matrix $\mathbf{H}$. Similarly, if there is a universal solution for $\mathbf{H}$, inserting the specific matrices of Equation (5.21) must result in the correct solution of the LYAPUNOV equation. *Any specific system must be a part of the general solution*. This property can be exploited to find a general solution:

- Create the simplest (scalar) system $\mathbf{A}$ that satisfies the problem's general matrix structure (In this case, Equation (5.17) is the simplest system that satisfies the general form of Equation (5.20)).
- Set-up a matrix $\mathbf{Q}$ and find a parametric solution $\mathbf{H}$ with a computer using the techniques presented in Section 5.1.3.
- Express the scalar solution matrix $\mathbf{H}$ in terms of the matrices $\mathbf{M}, \mathbf{K}, \mathbf{A}_A, \ldots$
- Create a new, more complex system matrix $\mathbf{A}$. (The matrices of Equation (5.1.4) are a good choice to proceed).
- Find a parametric solution $\mathbf{H}$ using the computer. Check if the *guessed* matrix operation still satisfies the more complex system. Modify if necessary.
- The process is finished when the guessed solution for $\mathbf{H}$ automatically satisfies any new system.
- The final solution is verified using the LYAPUNOV equation.

The presented process is highly iterative and certainly lacks the mathematical elegance of a direct calculation. On the other hand, it is unclear if there even are efficient methods to solve the LYAPUNOV equation when only the general block-matrix structure and their respective matrix properties are known. The presented method demonstrates a straightforward way to obtain a stability theorem for a collocated mechanical system, and should be seen only as a tool. In future works, this manual approach could be replaced by dedicated algorithms to find stability theorems for even more complex systems.

5.1.5 Damping, gyroscopy and complexity

To generalize the result of the previous section further, the system can be augmented with a damping matrix $\mathbf{D}$ and a gyroscopic matrix $\mathbf{G}$. Similar to the matrices $\mathbf{M}$ and $\mathbf{K}$, the damping matrix $\mathbf{D} = \mathbf{D}^T$ is symmetric, whereas the gyroscopic matrix $\mathbf{G} = -\mathbf{G}^T$ is *skew-symmetric*.

$$\mathbf{A} = \begin{bmatrix} \mathbf{0} & \mathbf{I} & \mathbf{0} \\ -\mathbf{M}^{-1}\mathbf{K} & -\mathbf{M}^{-1}(\mathbf{D}+\mathbf{G}) & -\mathbf{M}^{-1}\mathbf{A}_A \\ \mathbf{A}_S & \mathbf{0} & \mathbf{A}_C \end{bmatrix} \tag{5.22}$$

Equation (5.22) augments the previous system from Equation (5.4) with damping and gyroscopy. The introduction of a dissipative matrix $\mathbf{D}$ also requires an update of $\mathbf{Q}$. In Equation (5.10), the quadratic form $P_{dis} = \dot{\mathbf{q}}^T \mathbf{D} \dot{\mathbf{q}}$ represented the dissipation energy. With the state-space vector $\mathbf{x}^T = \begin{bmatrix} \mathbf{q} & \dot{\mathbf{q}} & \mathbf{x}_R \end{bmatrix}^T$, the natural choice for $\mathbf{Q} = \mathrm{diag}(\mathbf{0}, 2\mathbf{D}, ...)$, representing a dissipation energy. However, it turns out that solutions of $\mathbf{H}$ become large and cumbersome. The alternative choice $\mathbf{Q} = \mathrm{diag}(2\mathbf{D}, \mathbf{0}, ...)$ results in simpler solutions $\mathbf{H}$. Even though the quantity is physically meaningless, the definiteness properties of $\mathbf{Q}$ remain unaffected.

Gyroscopic forces are conservative and do not alter the system's energy [34]. For this reason, the gyroscopic matrix $\mathbf{G}$ does not contribute to the dissipation function, leaving the dissipation matrix $\mathbf{Q}$ unchanged. The augmented system with the previously presented techniques.

So far, it is supposed that the matrix $\mathbf{A}$ is real. The use of complex coordinates requires an extension of the stability theorem to complex numbers. The com-

plex version of the LYAPUNOV Equation (5.12) is similar to the real one [21], except that it requires the complex conjugate transpose $\mathbf{A}^H$:

$$\mathbf{A}^H\mathbf{H} + \mathbf{H}\mathbf{A} = -\mathbf{Q} \tag{5.23}$$

The introduction of complex coordinates leads to updated symmetry properties: the matrix $\mathbf{D} = \mathbf{D}^H$ must be *hermitian*, and the matrix $\mathbf{G} = -\mathbf{G}^H$ is now *skew-hermitian*. Permitting complex matrices $\mathbf{A}$ may lead to problems with some computer algebra systems. As a solution, each complex matrix can be decomposed into a real (subindex "r"), and an imaginary (subindex "i") part, leading to two individual problems with real coefficient matrices.

$$\underbrace{(\mathbf{A}_r + i\mathbf{A}_i)^H}_{\mathbf{A}^H}\underbrace{(\mathbf{H}_r + i\mathbf{H}_i)}_{\mathbf{H}} + \underbrace{(\mathbf{H}_r + i\mathbf{H}_i)}_{\mathbf{H}}\underbrace{(\mathbf{A}_r + i\mathbf{A}_i)}_{\mathbf{A}} = -\underbrace{(\mathbf{Q}_r + i\mathbf{Q}_i)}_{\mathbf{Q}} \tag{5.24}$$

$$\text{real:} \quad \mathbf{A}_r^T\mathbf{H}_r + \mathbf{H}_r\mathbf{A}_r + \mathbf{A}_i^T\mathbf{H}_i - \mathbf{H}_i\mathbf{A}_i = -\mathbf{Q}_r \tag{5.25}$$

$$\text{imag:} \quad \mathbf{A}_r^T\mathbf{H}_i + \mathbf{H}_i\mathbf{A}_r - \mathbf{A}_r^T\mathbf{H}_r + \mathbf{H}_r\mathbf{A}_i = -\mathbf{Q}_i \stackrel{!}{=} \mathbf{0} \tag{5.26}$$

5.1.6 Lyapunov stability theorem for controlled mechanical systems

The previous considerations result in a LYAPUNOV stability theorem for general mechanical systems with collocated controllers. This result has already been published in a publication written bei HEINDEL, MÜLLER and RINDERKNECHT [39]. Consider a matrix $\mathbf{A}$ of the structure

$$\mathbf{A} = \begin{bmatrix} \mathbf{0} & \mathbf{I} & \mathbf{0} \\ -\mathbf{M}^{-1}\mathbf{K} & -\mathbf{M}^{-1}(\mathbf{G}+\mathbf{D}) & -\mathbf{M}^{-1}\mathbf{A}_A \\ \mathbf{A}_S & \mathbf{0} & \mathbf{A}_C \end{bmatrix} \tag{5.27}$$

with hermitian matrices $\mathbf{M}, \mathbf{K}, \mathbf{D}$ and a skew-hermitian matrix $\mathbf{G}$. It is further assumed that an arbitrary chosen matrix $\mathbf{P}$ with the following properties can be found:

- $\mathbf{P}$ satisfies $\mathbf{A}_A^H = \mathbf{P}\mathbf{A}_S$ (generalized collocation),
- The matrix product $\mathbf{P}\mathbf{A}_C$ is hermitian, i.e. $\mathbf{P}\mathbf{A}_C = (\mathbf{P}\mathbf{A}_C)^H$.

With a regular matrix $\mathbf{A}_C$, a hermitian SCHUR complement $\mathbf{S} = \mathbf{S}^H$ can be introduced:

$$\mathbf{S} = \left(\mathbf{K} - \mathbf{A}_A \mathbf{A}_C^{-1} \mathbf{A}_S\right)^{-1} = \mathbf{S}^H \tag{5.28}$$

Afterwards, the HAMILTONian $\mathbf{H}$ and the dissipation matrix $\mathbf{Q}$ satisfy the LYAPUNOV matrix equation (5.23). For the sake of a better presentation, the abbreviation $\left(\mathbf{A}_C^{-1}\right)^H = \mathbf{A}_C^{-H}$ is introduced. The solution has been independently verified by P. C. MÜLLER in a private correspondence.

$$\mathbf{H} = \begin{bmatrix} \mathbf{M} + (\mathbf{G}+\mathbf{D})^H \mathbf{S}(\mathbf{G}+\mathbf{D}) & (\mathbf{G}+\mathbf{D})^H \mathbf{S}\mathbf{M} & (\mathbf{G}+\mathbf{D})^H \mathbf{S}\mathbf{A}_A \mathbf{A}_C^{-1} \\ \mathbf{M}\mathbf{S}(\mathbf{G}+\mathbf{D}) & \mathbf{M}\mathbf{S}\mathbf{M} & \mathbf{M}\mathbf{S}\mathbf{A}_A \mathbf{A}_C^{-1} \\ \mathbf{A}_C^{-H} \mathbf{A}_A^H \mathbf{S}(\mathbf{G}+\mathbf{D}) & \mathbf{A}_C^{-H} \mathbf{A}_A^H \mathbf{S}\mathbf{M} & \mathbf{A}_C^{-H} \mathbf{P} + \mathbf{A}_C^{-H} \mathbf{A}_A^H \mathbf{S}\mathbf{A}_A \mathbf{A}_C^{-1} \end{bmatrix} \tag{5.29}$$

$$\mathbf{Q} = \begin{bmatrix} 2\mathbf{D} & \mathbf{0} & \mathbf{0} \\ \mathbf{0} & \mathbf{0} & \mathbf{0} \\ \mathbf{0} & \mathbf{0} & -\mathbf{P} - \mathbf{P}^H \end{bmatrix} \tag{5.30}$$

A necessary condition for stability is the positiveness of $\mathbf{H}$. P. C. MÜLLER also suggested a clever decomposition of $\mathbf{H}$ using the hermitian form $\mathbf{H} = \mathbf{L}^H \mathbf{W} \mathbf{L}$ which facilitates the definiteness proof.

$$\mathbf{L} = \begin{bmatrix} \mathbf{I} & \mathbf{0} & \mathbf{0} \\ \mathbf{S}(\mathbf{D}+\mathbf{G}) & \mathbf{S}\mathbf{M} & \mathbf{0} \\ \mathbf{0} & \mathbf{0} & \mathbf{A}_C^{-1} \end{bmatrix}, \qquad \mathbf{W} = \begin{bmatrix} \mathbf{M} & \mathbf{0} & \mathbf{0} \\ \mathbf{0} & \mathbf{S}^{-1} & \mathbf{A}_A \\ \mathbf{0} & \mathbf{A}_A^H & \mathbf{P}\mathbf{A}_C + \mathbf{A}_A^H \mathbf{S}\mathbf{A}_A \end{bmatrix} \tag{5.31}$$

In accordance with the previous assumptions, $\mathbf{L}$ is a regular matrix. In this case, $\mathbf{H}$ is positive definite if and only if $\mathbf{W}$ is positive definite [3, 31]. Given those findings, the problem facilitates to a definiteness check of $\mathbf{W}$ only:

$$\mathbf{M} > 0, \qquad \mathbf{S}^{-1} = \mathbf{K} - \mathbf{A}_A \mathbf{A}_C^{-1} \mathbf{A}_S > 0, \qquad \mathbf{P}\mathbf{A}_C > 0 \tag{5.32}$$

A sufficient condition for stability in sense of LYAPUNOV is the semidefiniteness of $\mathbf{Q}$. Due to the block-diagonal structure, this case is satisfied when:

$$\mathbf{D} \geq 0, \qquad -\mathbf{P} - \mathbf{P}^H \geq 0 \tag{5.33}$$

As a concluding remark, it shall be noted that the conditions (5.32), (5.33) only guarantee *marginal stability*, that is $\mathrm{Re}(\lambda_i) \leq 0$, since $\mathbf{Q}$ is semidefinite. Asymptotic stability can be proven with the observability criterion from Section 5.1.2.

5.1.7 A note on circulatory matrices and inner damping

Most mechanical systems can be represented with mass, stiffness, damping and gyroscopic matrices. However, some systems count with forces whose definition depends on the displacement of the body on which they act, so called follower forces [44]. Due to their nonconservative nature, they differ from the conservative elastic forces and cannot be represented in a stiffness matrix. The position-dependent, but skew-symmetric *circulatory* matrix $\mathbf{N} = -\mathbf{N}^H$ represents these forces [49]. For example, an aeroelastic instability phenomenon called *flutter* is contributed to follower forces [41]. On aircraft, flutter causes vibrations of the wings or control surfaces and may lead to structural damage [95].

In rotordynamics, circulatory matrices are mainly attributed to *inner damping*. As already mentioned in Section 3.2.5, it describes damping that occurs on the rotor itself. This phenomenon is of particular interest as it may lead to violent vibrations [94]. This effect often occurs on built-up rotors which are assembled from several force- or form-fitted elements, such as discs or blades [63]. It is found that this instability mechanism is mathematically closely related to flutter, as the damping's coordinate transformation from rotating to inertial coordinates also leads to skew-symmetric matrices $\mathbf{N}$. It is worth mentioning that inner damping is ambivalent: for subcritical rotor operation, it stabilizes the rotor, whereas it destabilizes the system for supercritical operation [28].

Finding stability theorems for systems with circulatory forces is difficult, as the nonconservative nature of $\mathbf{N}$ makes it difficult to find suitable LYAPUNOV-functions [34]. MINGORI distinguished between systems with actual follower forces and those where circulatory matrices arise only in certain coordinate systems [69, 70]. For the latter ones, he demonstrates that an appropriate coordinate transformation eliminates the circulatory matrices, and that the resulting system can be processed using standard methods. The proposed transformation only worked for positive definite damping matrices $\mathbf{D} > 0$, a restriction which could be dropped in a consecutive work [74].

Attempts to widen the presented stability proof to systems with circulatory forces were unsuccessful. Using the method from Section 5.1.4 resulted in

overly complex solutions for the HAMILTONian **H** even for simple systems, being too complicated to be useful. When general stability statements are required, an adaption of MINGORI's transformation theorem to controlled mechanical systems is promising. For the investigation of a particular machine, a numeric eigenvalue calculation is the fastest way to check stability.

5.2 Stability of the controlled rotor

The stability theorem is now used to prove the stability of the controlled system with arbitrary rotors. To enhance readability, the proof is sectioned. Starting with the proof's applicability, the reasoning shifts to a check of the matrix definiteness properties. A subsequent proof of the system's observability ensures asymptotic stability. In conclusion, all necessary and sufficient conditions for stability are conveniently listed.

5.2.1 Proof applicability

A prerequisite for the stability proof is the checking of whether or not the proof for collocated mechanical systems from Equation (5.27) is applicable to the system matrix of the controlled rotor system from Equations (3.27) and (3.40). The presented proof was tailored to the problem and later generalized. Consequently it is no surprise that the system matrix of the controlled rotor indeed satisfies the conditions. A matrix comparison reveals that:

$$\mathbf{K} = \mathbf{K}_R + \mathbf{K}_L \tag{5.34}$$

And for the controller Equations:

$$\mathbf{A}_A = -\mathbf{K}_L \mathbf{n} \mathbf{C}_R, \qquad \mathbf{A}_S = \mathbf{B}_R \mathbf{n}^T \mathbf{K}_L, \qquad \mathbf{A}_C = \mathbf{A}_R - \mathbf{B}_R \mathbf{n}^T \mathbf{K}_L \mathbf{n} \mathbf{C}_R \tag{5.35}$$

According to the conditions of Section 5.1.6, the stability proof is only applicable if an arbitrary matrix **P** can be found which satisfies both the conditions for generalized collocation, and also the condition that the matrix product $\mathbf{P}\mathbf{A}_C$ must be hermitian. With **P** defined as:

$$\mathbf{P} = \operatorname{diag}\left(\mathbf{P}_A, \mathbf{P}_B, \cdots, \mathbf{P}_j, \cdots\right), \qquad \mathbf{P}_j = \begin{bmatrix} -i\tilde{c}_{Cj}^{-1} & 0 & 0 \\ 0 & i\tilde{c}_{Cj}^{-1} & 0 \\ 0 & 0 & -c_{Dj}^{-1} \end{bmatrix} \tag{5.36}$$

The condition for generalized collocation requires that $\mathbf{A}_A^H = \mathbf{P}\mathbf{A}_S$. Using the relations from Equation (5.35) and (5.36), the problem can be rewritten as $\mathbf{C}_R^H = -\mathbf{P}\mathbf{B}_R$. The block-diagonal, repetitive form of the matrices $\mathbf{B}_R$, $\mathbf{C}_R$ of Equation (3.25) reduces the problem to only one block, and results in the condition being satisfied. Furthermore, the condition $\mathbf{P}\mathbf{A}_C = (\mathbf{P}\mathbf{A}_C)^H$ must be satisfied and can be rewritten as $\mathbf{P}\mathbf{A}_C = \mathbf{P}\mathbf{A}_R + (\mathbf{n}\mathbf{C}_R)^T \mathbf{K}_L \mathbf{n}\mathbf{C}_R$. As it turns out, the second summand is a hermitian form, so only the first summand $\mathbf{P}\mathbf{A}_R$ must be checked. This is true since the resulting matrix is diagonal and real. With both conditions satisfied, it is clear that Equation (5.36) is valid and the proof is applicable.

5.2.2 Positive definiteness of H

A necessary condition for the stability of the matrix $\mathbf{A}$ is the positive definiteness of $\mathbf{H}$. According to Equation (5.32), the first condition is that $\mathbf{M} > 0$. A semidefinite mass matrix can be ruled out as Equation (5.27) requires its inverse. Thus, $\mathbf{M}$ must be regular. A second condition is that the inverse SCHUR complement $\mathbf{S}^{-1} = \mathbf{K} - \mathbf{A}_A \mathbf{A}_C^{-1} \mathbf{A}_S$ is positive definite:

$$\mathbf{S}^{-1} = \mathbf{K} - \mathbf{A}_A \mathbf{A}_C^{-1} \mathbf{A}_S = \mathbf{K}_R + \mathbf{K}_L + \mathbf{K}_L \mathbf{n}\mathbf{C}_R \left(\mathbf{A}_R - \mathbf{B}_R \mathbf{n}^T \mathbf{K}_L \mathbf{n}\mathbf{C}_R\right)^{-1} \mathbf{B}_R \mathbf{n}^T \mathbf{K}_L \tag{5.37}$$

The WOODBURY *Matrix Identity* [40, 97] could be applied to simplify the expression, but it requires the regularity of $\mathbf{K}_L$, which is generally not given. The problem is solved by expanding the expression $\mathbf{K}_L = \mathbf{K}_L \mathbf{n}\mathbf{n}^T = \mathbf{n}\mathbf{n}^T \mathbf{K}_L$, as the expression $\mathbf{n}\mathbf{n}^T$ acts like a neutral element for $\mathbf{K}_L$. Finally, the matrix $\mathbf{n}^T \mathbf{K}_L \mathbf{n}$ is per definition invertible, and Equation (5.37) can first be rewritten and subsequently simplified:

$$\begin{aligned} \mathbf{S}^{-1} &= \mathbf{K}_R + \mathbf{n}\left(\mathbf{n}^T \mathbf{K}_L \mathbf{n} + \mathbf{n}^T \mathbf{K}_L \mathbf{n}\mathbf{C}_R \left(\mathbf{A}_R - \mathbf{B}_R \mathbf{n}^T \mathbf{K}_L \mathbf{n}\mathbf{C}_R\right)^{-1} \mathbf{B}_R \mathbf{n}^T \mathbf{K}_L \mathbf{n}\right) \mathbf{n}^T \\ &= \mathbf{K}_R + \mathbf{n}\left(\left(\mathbf{n}^T \mathbf{K}_L \mathbf{n}\right)^{-1} - \mathbf{C}_R \mathbf{A}_R^{-1} \mathbf{B}_R\right)^{-1} \mathbf{n}^T \\ &= \mathbf{K}_R + \mathbf{n} \operatorname{diag}\left(\cdots, k_{Lj}^{-1} + k_{Dj}^{-1} + 2\tilde{c}_{Cj}\Omega^{-1}, \cdots\right)^{-1} \mathbf{n}^T \quad \text{for any } j \end{aligned} \tag{5.38}$$

Two conditions govern the definiteness of the inverse SCHUR complement $\mathbf{S}^{-1}$ from Equation (5.38). The first summand is the positive semidefinite rotor stiffness matrix $\mathbf{K}_R$. The second summand is at least positive semidefinite when its inner diagonal matrix is positive definite. A sufficient condition is that the summands k_{Lj}, k_{Dj}, and $2\tilde{c}_{Cj}\Omega^{-1}$ are all positive. It is remarkable that the parameter $2\tilde{c}_{Cj}\Omega^{-1}$ might lead to instability for negative values of Ω. This surprising result was already found during the stability analysis of the controlled JEFFCOTT rotor in Section 2.3.3. As a solution, a new parameter c_{Cj} from Equation (2.27) was introduced to circumvent the problem. Finally, the sum of both semidefinite summands $\mathbf{K}_R + \mathbf{n}\,\mathrm{diag}\,(\cdots)^{-1}\,\mathbf{n}^T$ must be positive definite, which is given when $\mathbf{K}_R + \mathbf{K}_L > 0$. This condition means that the rotor must be supported in a statically (in-)determined manner by the bearings.

The last condition for $\mathbf{H} > 0$ is the positive definiteness of $\mathbf{PA}_C$. In Section 5.2.1 the relation $\mathbf{PA}_C = \mathbf{PA}_R + (\mathbf{nC}_R)^T\,\mathbf{K}_L\mathbf{nC}_R$ was uncovered. The second summand is at least positive semidefinite, consequently the first one must be positive definite. The block-diagonal form of both $\mathbf{P}$ and $\mathbf{A}_R$ reduces the definiteness check to a check of the definiteness of $\mathbf{P}_j\mathbf{A}_{Rj}$.

$$\mathbf{P}_j\mathbf{A}_{Rj} = \mathrm{diag}\left(\tilde{c}_{Cj}^{-1}\Omega, \quad \tilde{c}_{Cj}^{-1}\Omega, \quad k_{Dj}\right) = \mathrm{diag}\left(c_{Cj}^{-1}, \quad c_{Cj}^{-1}, \quad k_{Dj}\right) \tag{5.39}$$

Equation (5.39) is positive definite when all parameters k_{Dj} and c_{Cj} are positive for each controller j. This condition is redundant to the ones found earlier. After all conditions have been satisfied, it is clear that $\mathbf{H} > 0$.

5.2.3 Positive semidefiniteness of Q

According to Equation (5.33), $\mathbf{Q}$ is positive semidefinite when either the mechanical damping matrix is positive semidefinite $\mathbf{D} \geq 0$ or when the matrix sum $-\mathbf{P}-\mathbf{P}^H$ is positive semidefinite. Using the definition of $\mathbf{P}$ from Equation (5.36) yields:

$$-\mathbf{P}-\mathbf{P}^H = \mathrm{diag}\left(\ldots, -\mathbf{P}_j - \mathbf{P}_j^H, \ldots\right), \quad -\mathbf{P}_j - \mathbf{P}_j^H = \mathrm{diag}\left(0, \quad 0, \quad 2c_{Dj}^{-1}\right) \tag{5.40}$$

The expression is positive semidefinite when the controller parameters c_{Dj} are positive. An external mechanical damping $\mathbf{D}$ is not required to ensure positive semidefiniteness of $\mathbf{Q}$.

5.2.4 Observability and asymptotic stability

The previous section proved that the system matrix $\mathbf{A}$ of the controlled rotor is at least stable in sense of LYAPUNOV, hence at least marginally stable. However, a successful control requires *asymptotic stability*. Section 5.1.2 stated that an additional stability criterion must be satisfied to guarantee asymptotic stability. In this case, the HAUTUS-criterion is used. The matrix pair $(\mathbf{A}, \mathbf{Q})$ is completely observable if and only if there does not exist an eigenvector $\mathbf{x}_i$ of $\mathbf{A}$ which is orthogonal to $\mathbf{Q}$:

$$(\mathbf{A} - \lambda_i \mathbf{I})\,\mathbf{x}_i = \mathbf{0}, \qquad \mathbf{Q}\mathbf{x}_i \neq \mathbf{0} \qquad \text{for all } i \tag{5.41}$$

Together with the definition of the matrix $\mathbf{A}$ from Equation (3.44) and $\mathbf{Q}$ from Equation (5.30), this observability definition leads to the following expressions:

$$\left(\mathbf{M}\lambda_i^2 + (\mathbf{D}+\mathbf{G})\lambda_i + \mathbf{K}\right)\mathbf{q}_{Si} + \mathbf{A}_A\mathbf{x}_{Ri} = \mathbf{0}, \qquad \mathbf{D}\mathbf{q}_{Si} \neq \mathbf{0} \tag{5.42}$$

$$\mathbf{A}_S\mathbf{q}_{Si} + (\mathbf{A}_C - \lambda_i\mathbf{I})\,\mathbf{x}_{Ri} = \mathbf{0}, \qquad \left(\mathbf{P} + \mathbf{P}^H\right)\mathbf{x}_{Ri} \neq \mathbf{0} \tag{5.43}$$

The stability criterion of Equations (5.42) and (5.43) can be divided into two different cases, which will be treated separately:

Case I: Pervasive damping. When assuming that the controller states are zero, hence $\mathbf{x}_{Ri} = \mathbf{0}$, the reduced equations are:

$$\left(\mathbf{M}\lambda_i^2 + \mathbf{G}\lambda_i + \mathbf{K}\right)\mathbf{q}_{Si} = \mathbf{0}, \qquad \mathbf{A}_S\mathbf{q}_{Si} = \mathbf{0}, \qquad \mathbf{D}\mathbf{q}_{Si} = \,? \tag{5.44}$$

This case can also be divided in two cases. The first case is that the passive mechanical system without controller is pervasively damped:

$$\operatorname{rank}\begin{bmatrix} \mathbf{M}\lambda_i^2 + (\mathbf{D}+\mathbf{G})\,\lambda_i + \mathbf{K} \\ \mathbf{D}\lambda_i \end{bmatrix} = p \qquad \text{for all } \lambda_i \tag{5.45}$$

Equation (5.45) is an observability criterion for the mechanical subsystem, where p reflects the number of shaft nodes. When this condition is satisfied, it is guaranteed that $\mathbf{D}\mathbf{q}_{Si} \neq \mathbf{0}$, and the system is pervasively damped and consequently asymptotically stable. In case that the mechanical damping is *not* pervasive, there is at least one i with λ_i, $\mathbf{q}_{Si} \neq \mathbf{0}$, so that

$$\left(\mathbf{M}\lambda_i^2 + (\mathbf{D}+\mathbf{G})\lambda_i + \mathbf{K}\right)\mathbf{q}_{Si} = \mathbf{0}, \qquad \mathbf{D}\mathbf{q}_{Si} = \mathbf{0} \tag{5.46}$$

Now asymptotic stability depends on the expression $\mathbf{A}_S\mathbf{q}_{Si}$:

$$\mathbf{A}_S\mathbf{q}_{Si} = \mathbf{B}_R\mathbf{n}^T\mathbf{K}_L\mathbf{q}_{Si} = \underbrace{\mathbf{B}_R\mathbf{n}^T\mathbf{K}_L\mathbf{n}}_{\text{rank}=z}\mathbf{n}^T\mathbf{q}_{Si}$$

$$\longrightarrow \qquad \mathbf{A}_S\mathbf{q}_{Si} = \mathbf{0} \qquad \Longleftrightarrow \qquad \mathbf{n}^T\mathbf{q}_{Si} = \mathbf{0} \tag{5.47}$$

The system is marginally stable when the natural vibrations of the passive mechanical systems have vibration nodes at *all* bearings. When for at least at one bearing $\mathbf{n}_j^T\mathbf{q}_{Si} \neq 0$, hence at least one bearing is not located in the vibration node, damping is introduced through this bearing and the controlled system is asymptotically stable.

Case II: Free rotor resonance. In this case, it is assumed that $\mathbf{x}_{Ri} \neq \mathbf{0}$, but $\left(\mathbf{P}+\mathbf{P}^H\right)\mathbf{x}_{Ri} = \mathbf{0}$. This is only possible when *all* controller damping elements are zero, hence $a_{Dji} = 0$ for all controllers. According to the controller Equation (3.24), this also leads to vanishing forces at *all* bearings, hence $F_j = 0$. The controller equation then simplifies to $\dot{\mathbf{x}}_{Rj} = \mathbf{A}_{Rj}\mathbf{x}_{Rj}$. For $\lambda_i = \pm i\Omega$, there are nontrivial eigenvectors $\mathbf{x}_{Rj+}$ and $\mathbf{x}_{Rj-}$ that solve the following equation:

$$\text{For } \lambda_i = +i\Omega: \quad \left(\mathbf{A}_{Rj} - i\Omega\mathbf{I}\right)\mathbf{x}_{Rj+} = \mathbf{0} \quad \text{with} \quad \mathbf{x}_{Rj+} = \begin{bmatrix}1 & 0 & 0\end{bmatrix}^T \tag{5.48}$$

$$\text{For } \lambda_i = -i\Omega: \quad \left(\mathbf{A}_{Rj} + i\Omega\mathbf{I}\right)\mathbf{x}_{Rj-} = \mathbf{0} \quad \text{with} \quad \mathbf{x}_{Rj-} = \begin{bmatrix}0 & 1 & 0\end{bmatrix}^T \tag{5.49}$$

With these particular eigenvalues $\lambda_i = \pm i\Omega$, the eigenvalue problem from Equation (5.43) with the matrix definitions from Equation (5.35) leads to:

$$\begin{aligned} \mathbf{A}_S\mathbf{q}_{Si} + (\mathbf{A}_C - \lambda_i\mathbf{I})\,\mathbf{x}_{Ri} &= \mathbf{0} \qquad \text{for } \lambda_i = \pm i\Omega \\ \mathbf{B}_R\mathbf{n}^T\mathbf{K}_L\mathbf{q}_{Si} + \underbrace{\big(\mathbf{A}_R \pm i\Omega\mathbf{I}\big)\mathbf{x}_{Ri}}_{=\mathbf{0}} - \mathbf{B}_R\mathbf{n}^T\mathbf{K}_L\mathbf{n}\mathbf{C}_R\mathbf{x}_{Ri} &= \mathbf{0} \end{aligned} \tag{5.50}$$

Using the definition that relates the controller states $\mathbf{x}_{Ri}$ with the actuator displacements $\mathbf{a}_i$ from Equations (3.21) and (3.25) gives:

$$\begin{aligned} \mathbf{B}_R\mathbf{n}^T\mathbf{K}_L\mathbf{q}_{Si} - \mathbf{B}_R\mathbf{n}^T\mathbf{K}_L\underbrace{\mathbf{n}\mathbf{C}_R\mathbf{x}_{Ri}}_{a_i} &= \mathbf{0} \\ \underbrace{\mathbf{B}_R\mathbf{n}^T\mathbf{K}_L}_{\text{reg.}}(\mathbf{q}_{Si} - \mathbf{a}_i) &= \mathbf{0} \\ \mathbf{q}_{Si} &= \mathbf{a}_i \end{aligned} \tag{5.51}$$

With this result, the mechanical subsystem from Equation (5.42) is considered:

$$\big(\mathbf{M}\lambda_i^2 + (\mathbf{D}+\mathbf{G})\lambda_i + \mathbf{K}\big)\,\mathbf{q}_{Si} + \mathbf{A}_A\mathbf{x}_{Ri} = \mathbf{0} \tag{5.52}$$

With the matrix definitions from Equations (5.34), (5.35) and the result from Equation (5.51) finally leads to:

$$\begin{aligned} \big(-\mathbf{M}\Omega^2 \pm i\Omega\,(\mathbf{D}+\mathbf{G}) + \mathbf{K}_R + \mathbf{K}_L\big)\,\mathbf{q}_{Si} - \mathbf{K}_L\underbrace{\mathbf{n}\mathbf{C}_R\mathbf{x}_{Ri}}_{=\mathbf{a}_i=\mathbf{q}_{Si}} &= \mathbf{0} \\ \big(-\mathbf{M}\Omega^2 \pm i\Omega\,(\mathbf{D}+\mathbf{G}) + \mathbf{K}_R\big)\,\mathbf{q}_{Si} &= \mathbf{0} \end{aligned} \tag{5.53}$$

The problem now reduces to an investigation of the mechanical system: If there is a nontrivial eigenvector $\mathbf{q}_{Si} \neq \mathbf{0}$ that solves Equation (5.53), the system is marginally stable only. On the contrary, if $\mathbf{q}_{Si} = \mathbf{0}$ is the only solution, the system is asymptotically stable. The mechanical interpretation of Equation (5.53) is the following: The equation represents the free, unconstrained rotor. A nontrivial eigenvector $\mathbf{q}_{Si}$ exists when the rotational speed Ω matches a free rotor resonance ($\lambda_i = +i\Omega$ is the forward whirl; whereas $\lambda_i = -i\Omega$ is the backward whirl). When no external mechanical damping is present $\mathbf{D}\mathbf{q}_{Si} = \mathbf{0}$, the system is only marginally stable in the free rotor resonance.

5.2.5 Proof results

The diversity of different conditions complicate the stability proof. Removing the redundant conditions and categorizing them leads to a few comprehensible results:

- *Mechanical system*:
  The mass matrix must be positive definite. ($\mathbf{M} > 0$)
  The stiffness matrix of the free rotor is positive semidefinite. ($\mathbf{K}_R \geq 0$)
  The rotor is entirely supported by the active bearings. ($\mathbf{K}_R + \mathbf{K}_L > 0$)
  Mechanical damping may or may not be present. ($\mathbf{D} \geq 0$)
  The system is stable in presence of gyroscopy. ($\mathbf{G} = -\mathbf{G}^H$)
  The proof gives no statements for circulatory matrices ($\mathbf{N} = \mathbf{0}$)

- *Controller*:
  All controller stiffness parameters are positive. ($k_{Lj}, k_{Dj} > 0$)
  The controller damping parameters are positive. ($c_{Dj} > 0$)
  The controllers adaption parameters are positive. ($c_{Cj} > 0$)

- *Asymptotic stability*:
  Is given when the external mechanical damping is pervasive. ($\mathbf{D}\mathbf{q}_{Si} \neq 0$)
  Without external mechanical damping ($\mathbf{D} = 0$):

  - Is given when the rotational speed Ω does not match the rotor's free eigenfrequency ($\Omega^2 + \lambda_i^2 \neq 0$)
  - At least one bearing must be outside the rotor's passive vibration nodes ($\mathbf{n}^T \mathbf{q}_{Si} \neq \mathbf{0}$)

6 Experiments

A series of experiments is performed to evaluate whether the previous assumptions hold under real-world conditions. Two test rigs with different rotor configurations are used to compare the theoretic considerations with the experimental results. Both test rigs are equipped with piezoelectric actuators as active elements.

6.1 Rotor with one disc and piezoelectric actuators

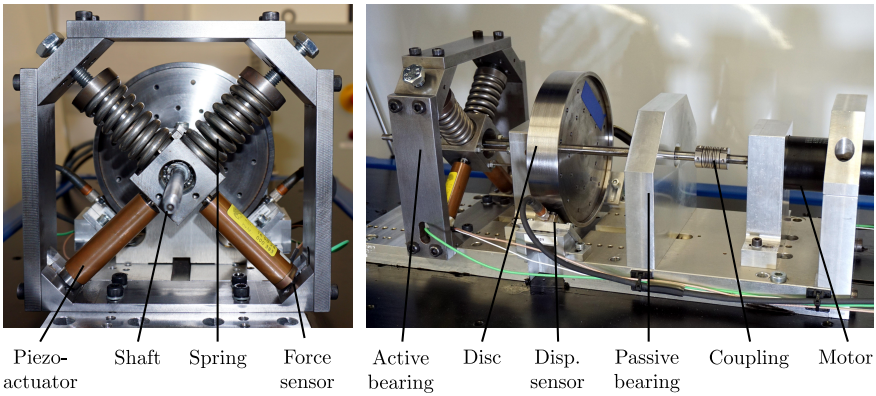

Figure 6.1: Jeffcott rotor test rig with one disc and one active bearing. Left: the active bearing assembly with piezoactuators and collocated force sensors displaces the shaft, while the coil springs ensure the mechanical integrity. Right: Displacement sensors measure the disc's position, but are not used for control.

Figure 6.1 depicts a test rig with one disc and an active bearing plane using piezoelectric actuators. The central disc has a mass of 2.5 kg. It is attached to a steel shaft with a diameter of 9 mm and spans a length of 190 mm between both a passive bearing plane on the right side and an active one on the left

side. Both bearing planes are equipped with industrial-grade self-aligning ball bearings. An electric motor drives the shaft through a flexible coupling with a maximum speed of $9000\,\mathrm{min}^{-1} = 150\,\mathrm{s}^{-1}$. The active bearing consists of two perpendicularly arranged piezoelectric actuators with a maximum stroke of $\Delta a = 60\,\mu\mathrm{m}$. The piezoelectric actuators are equipped with strain gauges to measure the actuator deflections. Two coil springs exert a force on the bearing assembly to ensure the mechanical integrity. Two piezoelectric force sensors are arranged directly below the actuators. This arrangement ensures collocation in the considered frequency range. Two eddy-current sensors monitor the disc displacements, but remain unused for control. The controller is implemented using *Simulink Real-Time* with a sampling frequency of $t_S^{-1} = 15\,\mathrm{kHz}$.

The test rig description allows its *classification* whether a bearing force elimination can be achieved. The free rotor is connected to the environment on three points: the coupling, the passive bearing and the active bearing. Both coupling and passive bearing can be considered as parasitic stiffnesses $\mathbf{K}_S$. The pre-tension coil springs of the active bearing plane also qualifies as parasitic stiffness. The actuator stiffness resides in the actuator stiffness matrix $\mathbf{K}_L$. With three entries in the bearing stiffness matrix $\mathbf{K}_S$ and only two degrees of freedom for the rotor, it is clear that the system is statically indeterminate. However, since the effect of the parasitic coupling stiffness is negligible and the coil spring stiffness can be compensated, the setup allows for the elimination of one passive resonance. It is assumed that the actuator is connected to an ideal voltage source with negligible series resistance. To allow a linear problem treatment, the actuator's hysteresis is neglected. In standard literature [30, 50], the governing actuator equation is given as:

$$\underbrace{f}_{F} = \underbrace{K_A}_{k_L} \left(\underbrace{\Delta}_{q_W} - \underbrace{n d_{33} U}_{a} \right) \tag{6.1}$$

In this equation f denotes the actuator force, n the number of active piezoelectric elements, d_{33} the piezoelectric constant, K_A the actuator stiffness, Δ the actuator displacement and U the applied actuator voltage. With the given substitutions, they match the previous assumptions from Equation (2.11).

Although the voltage is directly proportional to the actuator displacement $a = n d_{33} U$ and a voltage control is feasible, a different control approach is chosen. A subsidiary Proportional-Integral (PI) controller minimizes the deviation between the measured actuator displacement and the commanded setpoint to remove the actuator hysteresis, especially for larger actuator strokes. The setup

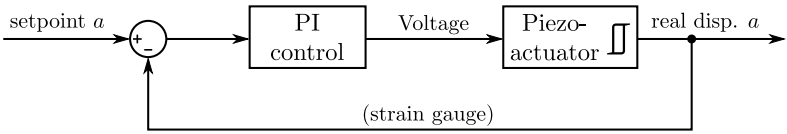

Figure 6.2: Subsidiary PI control. This additional control loop removes the actuator hysteresis, resulting in better linearity. It is optional and has only little effect on the overall performance.

is depicted in Figure 6.2. This additional control algorithm is not generally necessary, but removes the higher harmonics induced by hysteresis.

The parasitic bearing stiffness causes a difference between bearing and actuator forces. The estimated bearing forces $\bar{F}$ were calculated according to Equation (4.9) and subsequently used as control input. The actuator displacements a are then passed to the subsidiary PI-controller.

The algorithm's simplicity allowed a manual parameter tuning. The standstill rotor was excited with a small hammer and the parameters c_D and k_D were adjusted until the excitation response quickly vanished. The unbalance compensation parameter c_C was adjusted during rotor operation close to the passive resonance and changed until the controller converged quickly.

Although the control algorithm is unconditionally stable in theory, the controlled system became unstable for certain rotational frequencies. Surprisingly, these problems occurred at rotational speeds that did *not* match the resonance frequency of the passive system. It is reckoned that deviations between the parasitic bearing stiffness k_S and the estimated bearing stiffness $\bar{k}_S$ might have a negative impact on the rotor's unbalance response. This effect is assumed to be particularly significant outside the resonance where the ratio between bearing force and actuator displacement is small. To ensure stability, a small δ-summand prevents an integrator windup, as explained in Section 4.4. Small values for δ prevent instability and degrade the controller's performance merely insignificantly.

The practical application of the theory is demonstrated with a rotor run-up from standstill to $9000\,\mathrm{min}^{-1}$ in both passive and active configuration. Since the theoretical consideration neglected rotational accelerations, a rather low run-up acceleration of $25\,\mathrm{min}^{-1}\mathrm{s}^{-1}$ was chosen to minimize transient behavior. The presented bearing forces and disc displacements were recorded in both

passive and active case. During the passive run-up, the piezoactuators were disconnected from the amplifiers.

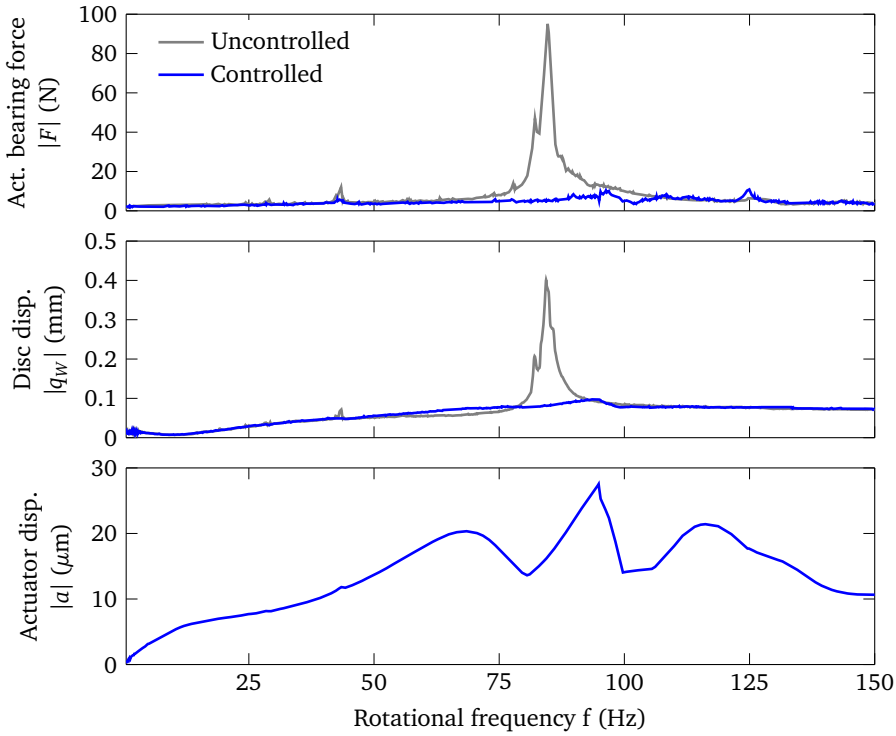

Figure 6.3: Experimental run-up of a rotor test rig with one disc and an active bearing using piezoactuators. The uncontrolled resonance peak leads to a force magnitude of 95 N, whereas the forces are below 6 N in controlled case at the same frequency. The controlled case shows no visible resonance.

Figure 6.3 shows the envelopes for bearing forces and disc displacements. The magnitude of the actuator displacement $|a|$ is estimated through the actuator voltages. The passive rotor has a distinct resonance at 85 Hz, where the disc displacements exceed 0.4 mm and the bearing forces reach 95 N. Whereas in the controlled case, no clear resonance peak is visible neither in the disc displacements nor in the forces. However, the previously mentioned instability is still visible in the actuator displacements $|a|$ at a frequency of 95 Hz. In-

creasing the damping value δ lowers this peak, but also degrades the controller performance.

With one disc and one distinct resonance, the test rig resembles the conditions of a JEFFCOTT rotor. According to theory, the shaft displacements q_W from Chapter 2 match the disc displacements, and in steady state-operation, the actuator displacements a should match the eccentricity ε. However, the theoretic considerations are idealized, neglecting real-world conditions such as a slightly different kinematic setup, a continuous mass distribution, a statically indeterminate system, bearing clearances, and so on. Even though these real-world effects are not covered by the basic theory, it is remarkable how well the theoretic predictions from Figure 2.5 match the experimental unbalance response in Figure 6.3, particularly for the disc displacements q_W and the bearing forces F. In contrast to theory, the actuator displacements a are not constant. The probable origin for this deviation lies in the simplified assumption of the non-ideal real-world conditions. However, the resonant rotor behavior completely vanished. This can be considered as strong evidence that resonances cannot only be eliminated theoretically, but also practically.

6.2 Rotor with two discs and piezoelectric actuators

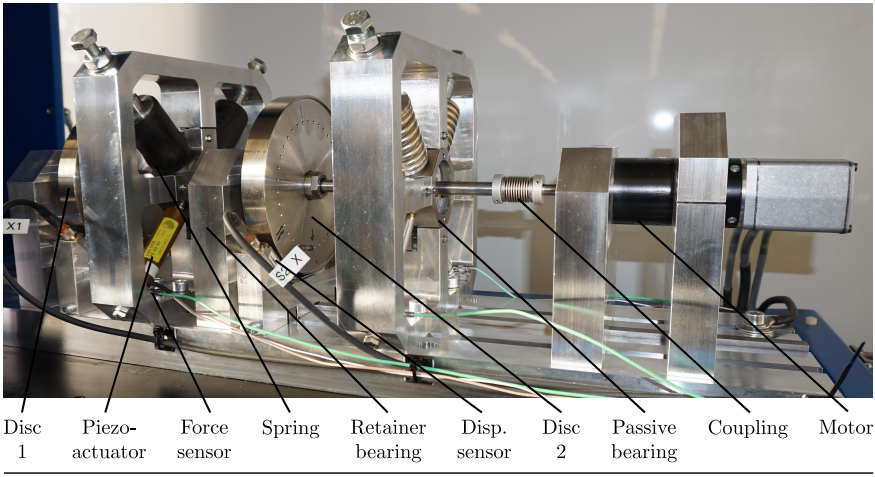

Figure 6.4: Rotor test rig with two discs and one active bearing. The cantilevered disc on the left causes a significant gyroscopic effect.

A different test rig demonstrates the controllers' ability to control more complex rotor systems. Figure 6.4 depicts a rotor test rig with two discs and one active bearing. The first cantilevered disc with the coordinate q_{W1} causes a gyroscopic effect; whereas the remaining setup resembles the properties of the test rig from Section 6.1. Similarly to the previous setup, the second disc with the coordinate q_{W2} resides between the active and passive bearing planes. The setup of the active bearing plane is similar to the previous one, except that the coil spring is replaced by an elastomeric spring. This test rig allows for a measurement of both disc positions as well as the forces in both bearing planes. A system classification reveals that the active bearing is only able to eliminate one out of two resonances.

The same control strategy from Section 6.1 was also applied here. Similar to the previous example, the controller was tuned manually. According to theory, only the bearing forces in the active plane were used as control inputs.

The experiment required a rotor run-up from standstill to $9000\,\mathrm{min}^{-1}$ with a rotational acceleration of $25\,\mathrm{min}^{-1}\mathrm{s}^{-1}$. Figure 6.5 shows the results of the experiment. In uncontrolled case, two distinct resonances develop at 61 Hz and 131 Hz. The first resonance could be reduced from 258 N in passive to 7 N in active case, whereas the second resonance allowed a reduction from 655 N in uncontrolled to 7 N in the controlled case. Although the active bearing force F was used as control input, both shaft deflections and passive bearing forces remain small, showing no resonant behavior. In contrast to the previous experiment, the actuator displacements were directly measured using the actuator strain gauges.

According to theory, there should be at least one free rotor resonance with large rotor displacements. However, no clear resonant behavior is visible. It is assumed that the actuator displacement peak at 87 Hz origins in the predicted free rotor resonance, as in this particular frequency range the controller showed poor convergence behavior. There are two plausible explanations why the free resonance is not clearly visible. First, the modal unbalance excitation of the free resonance is smaller. And second, there is always some amount of damping through the rotor environment and the controller factor δ. The origin of the first actuator displacement peak at 56 Hz remains unknown. However, a mismatch of the parasitic bearing stiffness seems the most probable cause.

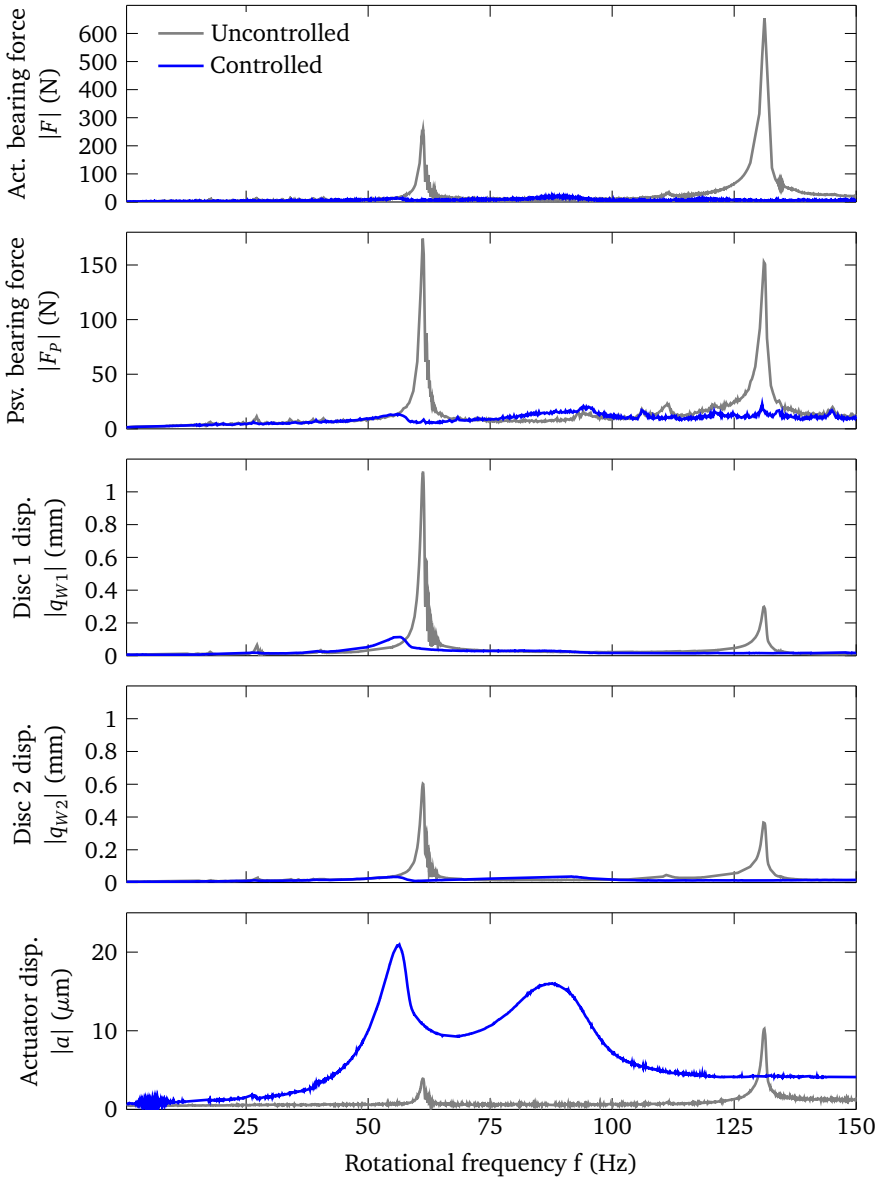

Figure 6.5: Experimental run-up of a rotor test rig with two discs and an active bearing using piezoactuators.

7 Conclusion

This work deals with the elimination of unbalance-induced forces on general isotropic rotors with active bearings. Starting with the JEFFCOTT rotor as the simplest and most representative rotordynamic model, it was reasoned that active bearings can statically displace the rotor without bearing forces. A new adaptive controller is introduced which uses the bearing forces as input and controls the actuator displacements. A subsequent analysis of the controlled system reveals that the bearing forces can be completely eliminated for any rotational speed, also leading to an elimination of the rotor's resonance. A stability analysis proves that the controller is always stable, a property which can be attributed to the electronic coupling of the rotor's perpendicular axes.

The same controller is used to extend the approach to general, isotropic rotors. The analytical closed-loop unbalance response indicates that the controller can even eliminate the forces of arbitrary rotors, while additionally canceling out two critical speeds. Advanced rotordynamic effects such as the influence of outer and inner damping, gyroscopy and parasitic stiffnesses are thoroughly investigated, solved and discussed.

A physical realization requires a distinction between displacement and force actuators. The ones aforementioned are inherently stiff and able to support the rotor without additional control, while the latter ones require an electronic stabilization. The consistent derivation of control laws for both actuator types requires the generalized theory from the previous Chapters. Suitable coordinate transformations simplify the controller implementation and allow a direct observation of the rotor's eccentricity in magnitude and phase. The correct actuator selection is simplified through dimensioning formulas based on the analytical solutions. Additionally, guidelines how to treat free rotor resonances are also given.

A universal stability proof for controlled general rotors requires the application of LYAPUNOV's second theorem. The theory's main advantage is that stability can be guaranteed for systems of arbitrary dimensions, knowing solely their matrix properties. However, the problem's particular matrix inhibited an application of known stability theorems. Consequently, a new stability theorem for mechanical systems with collocated controller has been derived. Using this theorem, it

could be proven that the presented model-free controller is stable for arbitrary, gyroscopic rotors.

The theoretic assumptions are validated in two experiments. The first experiment is performed on a test rig with one active piezoelectric bearing plane and a disc attached to a flexible shaft, resembling a JEFFCOTT rotor. The comparison between passive and active rotor run-up revealed that not only the bearing forces lowered from 95 N to 7 N, but also led to an elimination of the resonance, confirming the previous assumptions. The following experiment with a more complex rotor system demonstrated even better force and displacement reductions.

7.1 Scientific contribution

In the introductory Section 1.1 it was indicated that the current problem understanding is inconsistent and fragmented. This work strives to eliminate these problems, giving a clear, consistent problem solution which is compatible with structural mechanics, control engineering and different active bearing technologies. In particular, the scientific contributions of this work are:

General solution for flexible rotors. This approach gives a general solution for the unbalance elimination with active bearings on general, flexible rotors. Naturally, rigid rotors are also covered by the same theoretical considerations.

Clear principle of operation. The introduced actuator displacements resolve the ongoing confusion between filtering and adaptive feedforward compensation. According to Chapter 4, active bearings with force actuators require a controller that both supports the rotor and eliminates the unbalance forces, resulting in a notch filter characteristic. For statically stabilized rotors, adaptive feedforward compensation can be applied. In this case, the injected harmonic signals are actuator displacements, changing the rotor's axis of rotation.

No rotor model required. The presented collocated controller removes the unbalance-induced bearing forces even in the absence of a mathematical model. To do so, actuator and sensor must be collocated. Even with a flexible casing, no modeling effort is necessary. Regardless, the controller still requires the rotor's rotational speed.

Elimination of two rotor resonances. This work gave mathematical evidence for why two resonances can be eliminated. The root cause can be found in the rank deficiency of the rotor's stiffness matrix, reflecting the fact that the rotor can be

translated and tilted. Moreover, the analytical solution proves that a force free rotor operation at the speed of the free rotor resonance is generally impossible.

Accurate rotordynamics. Many approaches originate from a signal-theoretic viewpoint, often leading to an oversimplification of the underlying rotordynamics. The presented approach is compatible with control engineering, structural mechanics and rotordynamics, resulting in a complete treatment of the problem including more complicated rotordynamic effects such as gyroscopy and inner damping.

Generalized solution. The abstract, technology-independent solution leads to a generalized understanding how active bearings of all types can be used to eliminate unbalance-induced bearing forces. Chapter 4 demonstrated how different actuator technologies and arrangements can be linked consistently to the same system representation, bridging the gap between active magnetic bearings, piezoelectric bearings and balancing actuators.

Proven stability. In contrast to all existing approaches, the stability of the controlled rotor system was proven analytically. The analysis revealed that the controlled system is generally asymptotically stable, except when either the rotor's passive eigenmodes are unobservable or when the rotor is operated at its free resonance frequency. This remarkable solution is based on the discovered *hyperstable* controller and the developed stability proof. Naturally, this proof is not only limited to the investigated system, but can be applied to any mechanical system with collocated controllers.

7.2 Outlook

The elimination of unbalance-induced bearing forces not only reduces stresses, but also allows for quieter machine operation. The experiments demonstrated an impressive reduction of both forces and displacements, still, there is theoretical and practical evidence that both performance and stability are poor in the vicinity of a free rotor resonance. Without external forces, the rotor bends indefinitely – a clearly unwanted behavior. Further analytical approaches could not only consider the active bearing forces, but also the rotor's bending energy. This leads to the question of how the actuator displacements should be controlled in order to minimize this energy expression. It is assumed that this problem has a general, analytical solution based on specific eigenmodes or other matrix properties. Given these findings, the insight gained will contribute valuable assets for the development of new, even more powerful control algorithms.

Bibliography

[1] Abraham, D. *Aktive Beeinflussung von Rotoren: Dissertation, Universität der Bundeswehr Hamburg*. 1992.

[2] Alizadeh Roshdi, A. *Robuste Regelung zur aktiven Schwingungsdämpfung elastischer Rotoren mit Piezo-Stapelaktoren: Dissertation, Technische Universität Darmstadt*. 2005.

[3] Ayres, F. *Schaum's outline of theory and problems of matrices*. Schaum's outline series. New York: McGraw-Hill, 1962.

[4] Balas, M. J. "Modal Control of Certain Flexible Dynamic Systems". In: *SIAM Journal on Control and Optimization* 16.3 (1978), pp. 450–462. ISSN: 0363-0129. DOI: 10.1137/0316030.

[5] Beards, C. F. and Williams, J. L. "The damping of structural vibration by rotational slip in joints". In: *Journal of Sound and Vibration* 53.3 (1977), pp. 333–340. ISSN: 0022460X. DOI: 10.1016/0022-460X(77)90418-7.

[6] Becker, F., Heindel, S., and Rinderknecht, S. "Active Vibration Isolation of a Flexible Rotor Being Subject to Unbalance Excitation and Gyroscopic Effect Using H∞-Optimal Control". In: *Proceedings of the 9th IFToMM*. Vol. 21. 2015, pp. 1727–1739. DOI: 10.1007/978-3-319-06590-8_142.

[7] Bernstein, D. S. and Bhat, S. P. "Lyapunov Stability, Semistability, and Asymptotic Stability of Matrix Second-Order Systems". In: *Journal of Vibration and Acoustics* 117.B (1995), p. 145. ISSN: 07393717. DOI: 10.1115/1.2838656.

[8] Bingulac, S. "An alternate approach to expanding PA+A'P=-Q". In: *IEEE Transactions on Automatic Control* 15.1 (1970), pp. 135–137. ISSN: 0018-9286. DOI: 10.1109/TAC.1970.1099386.

[9] Bissell, C. C. "Stodola, Hurwitz and the genesis of the stability criterion". In: *International Journal of Control* 50.6 (1989), pp. 2313–2332. ISSN: 0020-7179. DOI: 10.1080/00207178908953500.

[10] Bleuler, H. et al. “Application of digital signal processors for industrial magnetic bearings”. In: *IEEE Transactions on Control Systems Technology* 2.4 (1994), pp. 280–289. doi: 10.1109/87.338647.

[11] Blutke, R. et al. “Nichtlineares rotordynamisches Verhalten eines Niederdruckrotors bei nicht zentrierten Quetschöldämpfern”. In: *8. Internationale Tagung Schwingungen in rotierenden Maschinen*. Vienna, 2009.

[12] Borsdorf, M. *Aktive Schwingungsminderung elastischer Flugtriebwerksrotoren mit Piezostapelaktoren unter Berücksichtigung der Dynamik des Triebwerkgehäuses: Dissertation, Technische Universität Darmstadt*. Aachen: Shaker, 2014. isbn: 3-8440-3007-7.

[13] Brogliato, B. *Dissipative systems analysis and control: Theory and applications*. 2nd ed. London: Springer, 2007. isbn: 978-1-84628-517-2.

[14] Burrows, C. R. “An evaluation of some strategies for vibration control of flexible rotors”. In: *International Symposium on Magnetic Suspension*. Washington, DC, 1992.

[15] Burrows, C. R., Sahinkaya, M., and S. Clements. “Active Vibration Control of Flexible Rotors: An Experimental and Theoretical Study”. In: *Proceedings of the Royal Society of London. Series A, Mathematical and Physical Sciences* 422.1862 (1989), pp. 123–146. issn: 00804630.

[16] Campos, R. O. and Nicoletti, R. “Vibration reduction in vertical washing machine using a rotating dynamic absorber”. In: *Journal of the Brazilian Society of Mechanical Sciences and Engineering* 37.1 (2015), pp. 339–348. issn: 1678-5878. doi: 10.1007/s40430-014-0151-1.

[17] Chen, C. and Shieh, L. “A note on expanding PA + A'P= -Q”. In: *IEEE Transactions on Automatic Control* 13.1 (1968), pp. 122–123. issn: 0018-9286. doi: 10.1109/TAC.1968.1098819.

[18] Childs, D. W. *Turbomachinery rotordynamics: Phenomena, modeling, and analysis*. New York: Wiley, 1993. isbn: 9780471538400.

[19] Deaux, R. and Eves, H. *Introduction to the Geometry of Complex Numbers*. Newburyport: Dover Publications, 2013. isbn: 978-0-486-15804-4.

[20] Ehrich, F. F. *Handbook of rotordynamics*. Malabar: Krieger Pub., 2004. isbn: 1575242567.

[21] Fairman, F. W. *Linear control theory: The state space approach*. Chichester: Wiley, 1998. isbn: 0471974897.

[22] Fertig, F. “Untersuchung begrenzender Faktoren für die Anwendung aktiver piezoelektrischer Lager in Rotorsystemen”. MA thesis. TU Darmstadt, 2016.

[23] Fomi Wamba, F. *Automatische Auswuchtstrategie für einen magnetgelagerten elastischen Rotor mit Auswuchtaktoren: Dissertation, Technische Universität Darmstadt*. 2009.

[24] Gasch, R. “Vibration of large turbo-rotors in fluid-film bearings on an elastic foundation”. In: *Journal of Sound and Vibration* 47.1 (1976), pp. 53–73. issn: 0022460X. doi: 10.1016/0022-460X(76)90407-7.

[25] Gasch, R. and Knothe, K. *Strukturdynamik: Band 1: Diskrete Systeme*. Berlin: Springer, 1987. isbn: 3540168494.

[26] Gasch, R., Nordmann, R., and Pfützner, H. *Rotordynamik*. Berlin: Springer, 2006. isbn: 3-540-41240-9.

[27] Genin, J. and Maybee, J. S. “Nonconservative linear systems with constant coefficients”. In: *Journal of the Institute of Mathematics and its Applications* 8 (1971), pp. 358–370.

[28] Genta, G. “On a Persistent Misunderstanding of the Role of Hysteretic Damping in Rotordynamics”. In: *Journal of Vibration and Acoustics* 126.3 (2004), p. 459. issn: 07393717. doi: 10.1115/1.1759694.

[29] Genta, G. and Ling, F. F. *Dynamics of Rotating Systems*. New York: Springer, 2005. isbn: 978-0-387-28687-7. doi: 10.1007/0-387-28687-X.

[30] Gladwell, G. and Preumont, A. *Vibration Control of Active Structures*. Vol. 179. Dordrecht: Springer, 2011. isbn: 978-94-007-2032-9. doi: 10.1007/978-94-007-2033-6.

[31] Golub, G. H. and Van Loan, C. *Matrix computations*. 3rd ed. Johns Hopkins studies in the mathematical sciences. Baltimore: Johns Hopkins University Press, 1996. isbn: 0801854148.

[32] Gomis-Bellmunt, O. and Campanile, L. F. *Design Rules for Actuators in Active Mechanical Systems*. London: Springer, 2010. isbn: 978-1-84882-613-7. doi: 10.1007/978-1-84882-614-4.

[33] Greiner, W. *Classical mechanics: Systems of particles and Hamiltonian dynamics*. Heidelberg: Springer, 2010. isbn: 978-3-642-03434-3.

[34] Hagedorn, P. and Hochlenert, D. *Technische Schwingungslehre: Schwingungen linearer diskreter mechanischer Systeme*. Frankfurt: H. Deutsch, 2012. isbn: 9783817118908.

[35] Han, F., Wu, Q., and Gao, Z. “Initial levitation of an electrostatic bearing system without bias”. In: *Sensors and Actuators A: Physical* 130-131 (2006), pp. 513–522. ISSN: 09244247. DOI: 10.1016/j.sna.2005.12.007.

[36] Han, F. et al. “Nonlinear compensation of active electrostatic bearings supporting a spherical rotor”. In: *Sensors and Actuators A: Physical* 119.1 (2005), pp. 177–186. ISSN: 09244247. DOI: 10.1016/j.sna.2004.08.030.

[37] Hasch, B. et al. “Model-Based Fault Detection on a Rotor in an Actively Supported Bearing Using Piezoelectric Actuators and the FXLMS-Algorithm”. In: *Motion and Vibration Control*. Dordrecht: Springer, 2009, pp. 123–132. ISBN: 978-1-4020-9437-8. DOI: 10.1007/978-1-4020-9438-5.

[38] Heindel, S., Becker, F., and Rinderknecht, S. “Unbalance and resonance elimination with active bearings on a Jeffcott Rotor”. In: *Mechanical Systems and Signal Processing* 85 (2017), pp. 339–353. DOI: 10.1016/j.ymssp.2016.08.016.

[39] Heindel, S., Müller, P. C., and Rinderknecht, S. “Unbalance and resonance elimination with active bearings on general rotors”. In: *Journal of Sound and Vibration* (2018). ISSN: 0022-460X. DOI: 10.1016/j.jsv.2017.07.048.

[40] Henderson, H. and Searle, S. “On Deriving the Inverse of a Sum of Matrices”. In: *SIAM Review* 23.1 (1981), pp. 53–60. ISSN: 00361445.

[41] Herrmann, G. *Dynamics and stability of mechanical systems with follower forces*. Vol. CR-1782. NASA contractor report. Washington, DC: National Aeronautics and Space Administration, 1971.

[42] Herzog, R. et al. “Unbalance compensation using generalized notch filters in the multivariable feedback of magnetic bearings”. In: *IEEE Transactions on Control Systems Technology* 4.5 (1996), pp. 580–586. DOI: 10.1109/87.531924.

[43] Heyman, J. *Structural analysis: A historical approach*. Cambridge: Cambridge University Press, 1998. ISBN: 0521622492.

[44] Hibbit, H. D. “Some follower forces and load stiffness”. In: *International Journal for Numerical Methods in Engineering* 14.6 (1979), pp. 937–941. ISSN: 0029-5981. DOI: 10.1002/nme.1620140613.

[45] Higuchi, T., Otsuka, M., and Mizuno, T. “Identification of Rotor Unbalane and Reduction of Housing Vibration by Periodic Learning Control in Magnetic Bearings”. In: *Proceedings of the 3rd International Symposium on Magnetic Bearings*. Alexandria, USA, 1992.

[46] Horst, H. G. *Aktive Schwingungsminderung an elastischen Rotoren mittels piezokeramischer Aktoren: Dissertation, Technische Universität Darmstadt*. Aachen: Shaker, 2005. isbn: 3-8322-4150-7.

[47] Hurwitz, A. “Ueber die Bedingungen, unter welchen eine Gleichung nur Wurzeln mit negativen reellen Theilen besitzt”. In: *Mathematische Annalen* 46.2 (1895), pp. 273–284. issn: 0025-5831. doi: 10.1007/BF01446812.

[48] Huseyin, K., Hagedorn, P., and Teschner, W. “On the stability of linear conservative gyroscopic systems”. In: *ZAMP Zeitschrift für angewandte Mathematik und Physik* 34.6 (1983), pp. 807–815. doi: 10.1007/BF00949057.

[49] Inman, D. J. *Vibration with Control*. Chichester: Wiley, 2006. isbn: 9780470010532. doi: 10.1002/0470010533.

[50] Institute of Electrical and Electronics Engineers (IEEE). *Standard on piezoelectricity*. New York, N.Y.: Institute of Electrical and Electronics Engineers, 1988.

[51] International Organization for Standardization (ISO). *Mechanical vibration: Vibration of rotating machinery equipped with active magnetic bearings*. First edition. Vol. ISO 14839-4. Geneva, 2012.

[52] Janocha, H., Bonertz, T., and Pappert, G. *Unkonventionelle Aktoren: Eine Einführung*. Zweite ergänzte und aktualisierte Auflage. München: Oldenbourg Verlag, 2013. isbn: 978-3-486-75692-0.

[53] Jeffcott, H. H. “The lateral vibration of loaded shafts in the neighbourhood of a whirling speed - The effect of want of balance”. In: *Philosophical Magazine Series 6* 37.219 (1919), pp. 304–314. issn: 1941-5982. doi: 10.1080/14786440308635889.

[54] Kai, Y. L., Coppola, V. T., and Bernstein, D. S. “Adaptive autocentering control for an active magnetic bearing supporting a rotor with unknown mass imbalance”. In: *IEEE Transactions on Automatic Control* 4.5 (1996), pp. 587–597. doi: 10.1109/87.531925.

[55] Kai, Y. L. et al. “Adaptive virtual autobalancing for a magnetic rotor with unknown dynamic imbalance”. In: *Proceedings of the 34th IEEE Conference on Decision and Control*. Vol. 3. 1995, pp. 2159–2164. ISBN: 0-7803-2685-7. DOI: 10.1109/CDC.1995.480522.

[56] Kelvin, W. T. and Tait, P. G. *Treatise on natural philosophy*. Oxford: Clarendon Press, 1867.

[57] Knospe, C., Tamir, S., and Fedigan, S. “Design of robust adaptive unbalance response controllers for rotors with magnetic bearings”. In: *Proceedings of the 3rd International Symposium on Magnetic Suspension Technology*. Tallahassee, USA, 1995.

[58] Lindenborn, O., Hasch, B., and Nordmann, R. “Vibration Reduction and Isolation of a Rotor in an Actively Supported Bearing Using Piezoelectric Actuators and the FXLMS Algorithm”. In: *9th International Conference on Vibrations in Rotating Machinery*. 2008.

[59] Löwis, J. and Rudolph, J. “Adaptive inertial autocentering of a rigid rotor with unknown imbalance supported by active magnetic bearings”. In: *Proceedings of the 7th International Symposium on Magnetic Bearings*. Switzerland, 2000.

[60] Lum, K. Y., Coppola, V. T., and Bernstein, D. S. “Adaptive Virtual Autobalancing for a Rigid Rotor With Unknown Mass Imbalance Supported by Magnetic Bearings”. In: *Journal of Vibration and Acoustics* 120.2 (1998), p. 557. ISSN: 07393717. DOI: 10.1115/1.2893865.

[61] Lunze, J. *Regelungstechnik 1: Systemtheoretische Grundlagen, Analyse und Entwurf einschleifiger Regelungen*. 9th ed. Berlin: Springer, 2013. ISBN: 978-3-642-29533-1.

[62] Lunze, J. *Regelungstechnik 2: Mehrgrößensysteme, Digitale Regelung*. 7th ed. Berlin: Springer, 2013. ISBN: 978-3-642-29561-4.

[63] Mahrenholtz, O. *Dynamics of rotors: Stability and system identificaton*. Vol. no. 273. Courses and lectures. Wien: Springer, 1984. ISBN: 9783211818466.

[64] Markert, R. *Strukturdynamik*. Darmstadt: Technische Universität Darmstadt, 2011. ISBN: 978-3-9814163-1-2.

[65] Markert, R., Stricka, N., and Zhang, X. “Unbalance compensation on flexible rotors by magnetic bearings using transfer functions”. In: *8th International Symposium on Magnetic Bearings*. Mito, Japan, 2002.

[66] Maslen, E. H. and Schweitzer, G. *Magnetic Bearings*. Berlin: Springer, 2009. ISBN: 978-3-642-00496-4. DOI: 10.1007/978-3-642-00497-1.

[67] Meek, J. L. *Matrix structural analysis*. New York: McGraw-Hill, 1971. ISBN: 9780070413160.

[68] Meschede, D. and Gerthsen, C. *Gerthsen Physik*. Berlin: Springer-Spektrum, 2015. ISBN: 3-662-45976-0.

[69] Mingori, D. L. "A Stability Theorem for Mechanical Systems With Constraint Damping". In: *Journal of Applied Mechanics* 37.2 (1970), p. 253. ISSN: 00218936. DOI: 10.1115/1.3408497.

[70] Mingori, D. L. "Stability of whirling shafts with internal and external damping". In: *International Journal of Non-Linear Mechanics* 8.2 (1973), pp. 155–160. ISSN: 00207462. DOI: 10.1016/0020-7462(73)90032-2.

[71] Mitschke, M. and Wallentowitz, H. *Dynamik der Kraftfahrzeuge*. 5th ed. Wiesbaden: Springer Vieweg, 2014. ISBN: 978-3-658-05068-9.

[72] Müller, P. C. "Allgemeine lineare Theorie für Rotorsysteme ohne oder mit kleinen Unsymmetrien". In: *Ingenieur-Archiv* 51.1-2 (1981), pp. 61–74. DOI: 10.1007/BF00535955.

[73] Müller, P. C. "Solution of the Matrix Equations $AX + XB = -Q$ and $S^TX+XS = -Q$". In: *SIAM Journal on Applied Mathematics* 18.3 (1970), pp. 682–687. ISSN: 0036-1399. DOI: 10.1137/0118061.

[74] Müller, P. C. *Stabilität und Matrizen: Matrizenverfahren in der Stabilitätstheorie linearer dynamischer Systeme*. Berlin: Springer, 1977. ISBN: 0387079815.

[75] Müller, P. C. and Schiehlen, W. O. *Forced linear vibrations*. Wien: Springer, 1977. ISBN: 978-3-7091-4356-8.

[76] Mushi, S. E., Lin, Z., and Allaire, P. E. "Design, Construction, and Modeling of a Flexible Rotor Active Magnetic Bearing Test Rig". In: *IEEE/ASME Transactions on Mechatronics* 17.6 (2012), pp. 1170–1182. ISSN: 1083-4435. DOI: 10.1109/TMECH.2011.2160456.

[77] Palazzolo, A. B. et al. "Active Vibration Control of Rotating Machinery With a Hybrid Piezohydraulic Actuator System". In: *Journal of Engineering for Gas Turbines and Power* 117.4 (1995), p. 767. ISSN: 07424795. DOI: 10.1115/1.2815463.

[78] Palazzolo, A. B. et al. “Piezoelectric Pushers for Active Vibration Control of Rotating Machinery”. In: *Journal of Vibration Acoustics Stress and Reliability in Design* 111.3 (1989), p. 298. ISSN: 07393717. DOI: 10.1115/1.3269856.

[79] Palazzolo, A. B. et al. “Test and Theory for Piezoelectric Actuator-Active Vibration Control of Rotating Machinery”. In: *Journal of Vibration and Acoustics* 113.2 (1991), p. 167. ISSN: 07393717. DOI: 10.1115/1.2930165.

[80] Peters, D. *Schwingungsdämpfung elastischer Flugtriebwerksrotoren in Quetschöldämpfern: Dissertation, TU Darmstadt*. 2011.

[81] Pian, T. *A study of the structural damping of a simple built-up beam with riveted joints in bending*. Cambridge, USA: M.I.T. Aeroelastic and Structures Research Laboratory, 1954.

[82] Pinte, G. et al. “A piezo-based bearing for the active structural acoustic control of rotating machinery”. In: *Journal of Sound and Vibration* 329.9 (2010), pp. 1235–1253. ISSN: 0022460X. DOI: 10.1016/j.jsv.2009.10.036.

[83] Popper, K. *Logik der Forschung*. Vienna: Springer, 1935. ISBN: 978-3-7091-2021-7. DOI: 10.1007/978-3-7091-4177-9.

[84] Pringle, R. “Stability of damped mechanical systems”. In: *AIAA Journal* 3.2 (1965), p. 363. ISSN: 0001-1452. DOI: 10.2514/3.2861.

[85] Schneider, H. *Auswuchttechnik*. Berlin: Springer, 2003. ISBN: 3-540-00596-X.

[86] Shafai, B. et al. “Magnetic bearing control systems and adaptive forced balancing”. In: *IEEE Control Systems* 14.2 (1994), pp. 4–13. DOI: 10.1109/37.272775.

[87] Shi, J., Zmood, R., and Qin, L. “The indirect adaptive feed-forward control in magnetic bearing systems for minimizing the selected vibration performance measures”. In: *8th International Symposium on Magnetic Bearings*. Mito, Japan, 2002.

[88] Stallaert, B., Devos, S., and Pinte, G. “Active Structural Acoustic Source Control of Rotating Machinery Using Piezo Bearings”. In: *26th IMAC*. Bethel: Society for Experimental Mechanics, 2008. ISBN: 9781605600666.

[89] Stodola, A. *Die Dampfturbinen, mit einem Anhang über die Aussichten der Wärmekraftmaschinen und über die Gasturbine*. Berlin: Springer, 1905.

[90] Strikwerda, J. C. *Finite difference schemes and partial differential equations*. 2nd ed. Philadelphia: Society for Industrial and Applied Mathematics, 2004. isbn: 0898715679.

[91] Tammi, K. *Active control of radial rotor vibrations: Identification, feedback, feedforward, and repetitive control methods*. Espoo, Finland: VTT Technical Research Centre, 2007. isbn: 9513870073.

[92] Thomson, W. T. *Theory of vibration with applications*. Englewood Cliffs, USA: Prentice-Hall, 1972. isbn: 0139145494.

[93] Unbehauen, H. *Regelungstechnik I: Klassische Verfahren zur Analyse und Synthese linearer kontinuierlicher Regelsysteme, Fuzzy-Regelsysteme*. Wiesbaden: Vieweg+Teubner, 2008. isbn: 978-3-8348-9491-5.

[94] Vance, J. M., Murphy, B., and Zeidan, F. *Machinery vibration and rotordynamics*. Hoboken, USA: Wiley, 2010. isbn: 978-0-471-46213-2.

[95] Vedeneev, V. V. "Panel flutter at low supersonic speeds". In: *Journal of Fluids and Structures* 29 (2012), pp. 79–96. issn: 08899746. doi: 10.1016/j.jfluidstructs.2011.12.011.

[96] Weidner, P. "Zur Stabilität linearer Systeme unter dem Einfluß von Dämpfungs- und Kreiselkräften". In: *ZAMM Zeitschrift für Angewandte Mathematik und Mechanik* 50.1-4 (1970), pp. 249–250. doi: 10.1002/zamm.19700500120.

[97] Woodbury, M. A. *Inverting modified matrices: Statistical Research Group, Memo. 42*. Princeton University, 1950.

[98] Yoo, S. et al. "Optimal Notch filter for active magnetic bearing controllers". In: *2011 IEEE/ASME International Conference on Advanced Intelligent Mechatronics (AIM)*, pp. 707–711. doi: 10.1109/AIM.2011.6027087.

[99] Zajac, E. E. "Comments on: Stability of Damped Mechanical Systems and a Further Extension". In: *AIAA Journal* 3.9 (1965), pp. 1749–1750. issn: 0001-1452. doi: 10.2514/3.55187.

[100] Zhang, X. *Aktive Regel- und Kompensationsstrategien für magnetgelagerte Mehrfreiheitsgrad-Rotoren: Dissertation, Technische Universität Darmstadt*. Herdecke: GCA-Verlag, Jan. 2003. isbn: 3-89863-118-4.

[101] Zhao, X. *Transmission of Vibration Caused by Unbalance in an Aircraft Engine with Active Control Strategies: Dissertation, Technische Universität Darmstadt*. Aachen: Shaker, 2016. isbn: 978-3-8440-4271-9.

[102] Ziegler, F. *Mechanics of Solids and Fluids*. New York: Springer, 1995. ISBN: 978-1-4612-6907-6. DOI: 10.1007/978-1-4612-0805-1.

[103] Zienkiewicz, O. C. and Cheung, Y. K. *The finite element method in structural and continuum mechanics*. European civil engineering series. London: McGraw-Hill, 1967.

[104] Zurmühl, R. and Falk, S. *Matrizen 1: Grundlagen*. 6th ed. Berlin: Springer, 1992. ISBN: 3540539441.

Index

Appendix A: Unbalance response calculation

A.1 Steady-state solution of the controlled rotor

The solution of a linear differential equation with constant coefficients of the form is particularly comprehensive when its perturbation function is harmonic. The unbalance causes such an excitation with $\boldsymbol{\varepsilon} = \boldsymbol{\varepsilon}^{+}\,\mathrm{e}^{i\Omega t}$. From the theory of linear equations, it is known that the systems responds with the excitation frequency. Using $\mathbf{x} = \mathbf{x}^{+}\,\mathrm{e}^{i\Omega t}$ and its derivative $\dot{\mathbf{x}} = \mathbf{x}^{+} i\Omega\,\mathrm{e}^{i\Omega t}$ leads to the unbalance response:

$$\begin{aligned} \dot{\mathbf{x}} &= \mathbf{A}\mathbf{x} + \mathbf{B}\boldsymbol{\varepsilon} \\ \mathbf{x}^{+} &= (i\Omega\mathbf{I} - \mathbf{A})^{-1}\,\mathbf{B}\boldsymbol{\varepsilon}^{+} \end{aligned} \tag{A.1}$$

The matrices $\mathbf{A}$ and $\mathbf{B}$ are partitioned into several submatrices $\mathbf{A}_1 \ldots \mathbf{A}_4$ and $\mathbf{B}_1, \mathbf{B}_2$.

$$\mathbf{x}^{+} = \begin{bmatrix} \mathbf{A}_1 & \mathbf{A}_2 \\ \mathbf{A}_3 & \mathbf{A}_4 \end{bmatrix}^{-1} \begin{bmatrix} \mathbf{B}_1 \\ \mathbf{B}_2 \end{bmatrix} \boldsymbol{\varepsilon}^{+} \tag{A.2}$$

The partitioned matrices are defined as:

$$\begin{bmatrix} \mathbf{A}_1 & \mathbf{A}_2 \\ \mathbf{A}_3 & \mathbf{A}_4 \end{bmatrix} = \left[\begin{array}{cc|c} i\Omega\mathbf{I} & -\mathbf{I} & \mathbf{0} \\ \mathbf{M}^{-1}(\mathbf{K}_R + \mathbf{K}_L) & i\Omega\mathbf{I} + \mathbf{M}^{-1}(\mathbf{D} + \mathbf{G}) & -\mathbf{M}^{-1}\mathbf{K}_L\mathbf{n}\mathbf{C}_R \\ \hline -\mathbf{B}_R\mathbf{n}^{T}\mathbf{K}_L & \mathbf{0} & i\Omega\mathbf{I} - \mathbf{A}_R + \mathbf{B}_R\mathbf{n}^{T}\mathbf{K}_L\mathbf{n}\mathbf{C}_R \end{array}\right]$$

$$\begin{bmatrix} \mathbf{B}_1 \\ \mathbf{B}_2 \end{bmatrix} = \left[\begin{array}{c} \mathbf{0} \\ \mathbf{M}^{-1}(\mathbf{K}_R + \mathbf{K}_L) \\ \hline -\mathbf{B}_R\mathbf{n}^{T}\mathbf{K}_L \end{array}\right] \tag{A.3}$$

The matrix inversion lemma [40] allows the inversion of partitioned matrices:

$$\mathbf{x}^{+} = \begin{bmatrix} \mathbf{S}_A^{-1} & -\mathbf{S}_A^{-1}\mathbf{A}_2\mathbf{A}_4^{-1} \\ -\mathbf{A}_4^{-1}\mathbf{A}_3\mathbf{S}_A^{-1} & \mathbf{A}_4^{-1} + \mathbf{A}_4^{-1}\mathbf{A}_3\mathbf{S}_A^{-1}\mathbf{A}_2\mathbf{A}_4^{-1} \end{bmatrix} \begin{bmatrix} \mathbf{B}_1 \\ \mathbf{B}_2 \end{bmatrix} \boldsymbol{\varepsilon}^{+} \tag{A.4}$$

It extensively uses the SCHUR complement $\mathbf{S}_A$, which is defined as:

$$\mathbf{S}_A = \left(\mathbf{A}_1 - \mathbf{A}_2\mathbf{A}_4^{-1}\mathbf{A}_1\right) \tag{A.5}$$

The inverse of $\mathbf{A}$ only exists if the controller submatrix $\mathbf{A}_4$ is regular:

$$\det\left(\mathbf{A}_4\right) = \prod_{j=A}^{z} 2c_{Cj}k_{Lj}\Omega\left(i\Omega + c_{Dj}k_{Dj}\right) \tag{A.6}$$

This is the case when all control parameters c_{Cj}, c_{Dj}, and the bearing stiffnesses k_{Lj} are non-zero and real and the rotational speed Ω is non-zero. Additionally, solving the SCHUR complement $\mathbf{S}_A$ requires the calculation of $\mathbf{A}_4^{-1}\mathbf{B}_2$ and $\mathbf{A}_4^{-1}\mathbf{A}_3$. Both products require the solution of:

$$\left(i\Omega\mathbf{I} - \mathbf{A}_R + \mathbf{B}_R\mathbf{n}^T\mathbf{K}_L\mathbf{n}\mathbf{C}_R\right)^{-1}\left(-\mathbf{B}_R\mathbf{n}^T\mathbf{K}_L\right) = -\mathbf{R}\mathbf{n}^T \tag{A.7}$$

with the definition of the right-hand side matrix:

$$\mathbf{R} = \operatorname{diag}\left(\mathbf{r}, \mathbf{r}, \cdots\right) \qquad \text{with} \quad \mathbf{r} = \begin{bmatrix} 1 & 0 & 0 \end{bmatrix}^T \tag{A.8}$$

The further considerations require the matrix product $\mathbf{C}_R\mathbf{R}$. Due their block-diagonal definition from Equations (3.24) and (A.8), each of their diagonal elements can be treated separately so that $\mathbf{C}_{Rj}\mathbf{r} = \begin{bmatrix} 1 & 1 & 1 \end{bmatrix} \cdot \begin{bmatrix} 1 & 0 & 0 \end{bmatrix}^T = 1$. This leads to the matrix identity:

$$\mathbf{C}_R\mathbf{R} = \mathbf{I} \qquad (z \times z) \tag{A.9}$$

The solution of Equation (A.7) is the key equation for the force free unbalance response. As an additional check, it is verified by bringing the inverse to the right-hand side:

$$\underbrace{-\left(i\Omega\mathbf{I} - \mathbf{A}_R\right)\mathbf{R}\mathbf{n}^T}_{=\mathbf{0}} - \mathbf{B}_R\mathbf{n}^T\underbrace{\mathbf{K}_L\mathbf{n}\mathbf{C}_R\mathbf{R}\mathbf{n}^T}_{=\mathbf{K}_L} = -\mathbf{B}_R\mathbf{n}^T\mathbf{K}_L \tag{A.10}$$

Equation (A.10) reveals that $-\mathbf{R}\mathbf{n}^T$ is indeed the solution of Equation (A.7). This simple solution relies on the special structure of the controller matrix $\mathbf{A}_R$ and the definitions for $\mathbf{R}, \mathbf{n}, \mathbf{B}_R, \mathbf{K}_L$ and $\mathbf{C}_R$. The obtained result can be used to calculate $\mathbf{A}_4^{-1}\mathbf{B}_2$ and $\mathbf{A}_4^{-1}\mathbf{A}_3$.

$$\mathbf{A}_4^{-1}\mathbf{B}_2 = -\mathbf{R}\mathbf{n}^T \tag{A.11}$$

$$\mathbf{A}_4^{-1}\mathbf{A}_3 = \begin{bmatrix} -\mathbf{R}\mathbf{n}^T & \mathbf{0} \end{bmatrix} \tag{A.12}$$

The identity $\mathbf{K}_L\mathbf{n}\mathbf{C}_R\mathbf{R}\mathbf{n}^T = \mathbf{K}_L$ leads to more intermediate results:

$$\mathbf{A}_2\mathbf{A}_4^{-1}\mathbf{A}_3 = \begin{bmatrix} \mathbf{0} & \mathbf{0} \\ \mathbf{M}^{-1}\mathbf{K}_L & \mathbf{0} \end{bmatrix} \qquad \mathbf{A}_2\mathbf{A}_4^{-1}\mathbf{B}_2 = \begin{bmatrix} \mathbf{0} \\ \mathbf{M}^{-1}\mathbf{K}_L \end{bmatrix} \tag{A.13}$$

Finally, the SCHUR complement $\mathbf{S}_A$ from Equation (A.5) can be calculated. With the result from Equation (A.13) it finally yields

$$\begin{aligned} \mathbf{S}_A &= \begin{bmatrix} i\Omega\mathbf{I} & -\mathbf{I} \\ \mathbf{M}^{-1}(\mathbf{K}_R + \mathbf{K}_L) & i\Omega\mathbf{I} + \mathbf{M}^{-1}(\mathbf{D} + \mathbf{G}) \end{bmatrix} - \begin{bmatrix} \mathbf{0} & \mathbf{0} \\ \mathbf{M}^{-1}\mathbf{K}_L & \mathbf{0} \end{bmatrix} \\ &= \begin{bmatrix} i\Omega\mathbf{I} & -\mathbf{I} \\ \mathbf{M}^{-1}\mathbf{K}_R & i\Omega\mathbf{I} + \mathbf{M}^{-1}(\mathbf{D} + \mathbf{G}) \end{bmatrix} \end{aligned} \tag{A.14}$$

The inverse of $\mathbf{S}_A$ only exists if the determinant is non-zero.

$$\det(\mathbf{S}_A) = \left(-\Omega^2\mathbf{M} + i\Omega(\mathbf{D} + \mathbf{G}) + \mathbf{K}_R\right) \tag{A.15}$$

The inverse is then

$$\mathbf{S}_A^{-1} = \begin{bmatrix} -\frac{i}{\Omega}\mathbf{I} + \frac{i}{\Omega}\det(\mathbf{S}_A)^{-1}\mathbf{K}_R & \det(\mathbf{S}_A)^{-1}\mathbf{M} \\ -\det(\mathbf{S}_A)^{-1}\mathbf{K}_R & i\Omega\det(\mathbf{S}_A)^{-1}\mathbf{M} \end{bmatrix} \tag{A.16}$$

Other products for the final solution are calculated here:

$$\mathbf{S}_A^{-1}\mathbf{B}_1 = \begin{bmatrix} \det(\mathbf{S}_A)^{-1}(\mathbf{K}_R + \mathbf{K}_L) \\ i\Omega\det(\mathbf{S}_A)^{-1}(\mathbf{K}_R + \mathbf{K}_L) \end{bmatrix} \tag{A.17}$$

$$\mathbf{S}_A^{-1}\mathbf{A}_2\mathbf{A}_4^{-1}\mathbf{B}_2 = \begin{bmatrix} \det(\mathbf{S}_A)^{-1}\mathbf{K}_L \\ i\Omega\det(\mathbf{S}_A)^{-1}\mathbf{K}_L \end{bmatrix} \tag{A.18}$$

$$\mathbf{A}_4^{-1}\mathbf{A}_3\mathbf{S}_A^{-1}\mathbf{A}_2\mathbf{A}_4^{-1}\mathbf{B}_2 = -\mathbf{R}\mathbf{n}^T \det(\mathbf{S}_A)^{-1}\,\mathbf{K}_L \tag{A.19}$$

$$\mathbf{A}_4^{-1}\mathbf{A}_3\mathbf{S}_A^{-1} = \left[-\mathbf{R}\mathbf{n}^T\left(\tfrac{i}{\Omega}\det(\mathbf{S}_A)^{-1}\,\mathbf{K}_R - \tfrac{i}{\Omega}\mathbf{I}\right) \quad -\mathbf{R}\mathbf{n}^T\left(\det(\mathbf{S}_A)^{-1}\,\mathbf{M}\right)\right] \tag{A.20}$$

$$\mathbf{A}_4^{-1}\mathbf{A}_3\mathbf{S}_A^{-1}\mathbf{B}_1 = -\mathbf{R}\mathbf{n}^T \det(\mathbf{S}_A)^{-1}\,(\mathbf{K}_R + \mathbf{K}_L) \tag{A.21}$$

The final unbalance response can be calculated using Equation (A.4).

$$\mathbf{x}^+ = \begin{bmatrix} \mathbf{S}_A^{-1}\mathbf{B}_1 - \mathbf{S}_A^{-1}\mathbf{A}_2\mathbf{A}_4^{-1}\mathbf{B}_2 \\ -\mathbf{A}_4^{-1}\mathbf{A}_3\mathbf{S}_A^{-1}\mathbf{B}_1 + \mathbf{A}_4^{-1}\mathbf{B}_2 + \mathbf{A}_4^{-1}\mathbf{A}_3\mathbf{S}_A^{-1}\mathbf{A}_2\mathbf{A}_4^{-1}\mathbf{B}_2 \end{bmatrix} \boldsymbol{\varepsilon}^+ \tag{A.22}$$

and finally

$$\mathbf{x}^+ = \begin{bmatrix} \left(-\Omega^2\mathbf{M} + i\Omega\,(\mathbf{D}+\mathbf{G}) + \mathbf{K}_R\right)^{-1}\mathbf{K}_R \\ i\Omega\left(-\Omega^2\mathbf{M} + i\Omega\,(\mathbf{D}+\mathbf{G}) + \mathbf{K}_R\right)^{-1}\mathbf{K}_R \\ \mathbf{R}\mathbf{n}^T\left(-\Omega^2\mathbf{M} + i\Omega\,(\mathbf{D}+\mathbf{G}) + \mathbf{K}_R\right)^{-1}\mathbf{K}_R - \mathbf{R}\mathbf{n}^T \end{bmatrix} \boldsymbol{\varepsilon}^+ \tag{A.23}$$

A.2 Unbalance response with rotating damping

In this section, the unbalance response with rotating damping is calculated. Therefore, two damping matrices are introduced: the one with nonrotating damping $\mathbf{D}$ and the one with rotating damping $\mathbf{D}_I$. The special feature of latter matrix is that it appears as a summand with the stiffness matrices $\mathbf{K}_R$ and $\mathbf{K}_L$. Although the damping matrix $\mathbf{D}_I$ is symmetric, the coordinate transformation to inertial coordinates made it skew-symmetric. The solution of the state-space system

$$\dot{\mathbf{x}} = \mathbf{A}\mathbf{x} + \mathbf{B}\boldsymbol{\varepsilon}$$

with the matrices

$$\mathbf{A} = \begin{bmatrix} \mathbf{0} & \mathbf{I} & \mathbf{0} \\ -\mathbf{M}^{-1}\,(\mathbf{K}_R + \mathbf{K}_L - i\Omega\mathbf{D}_I) & -\mathbf{M}^{-1}\,(\mathbf{D} + \mathbf{D}_I + \mathbf{G}) & \mathbf{M}^{-1}\mathbf{K}_L\mathbf{n}\mathbf{C}_R \\ \mathbf{B}_R\mathbf{n}^T\mathbf{K}_L & \mathbf{0} & \mathbf{A}_R - \mathbf{B}_R\mathbf{n}^T\mathbf{K}_L\mathbf{n}\mathbf{C}_R \end{bmatrix}$$

$$\mathbf{B} = \begin{bmatrix} \mathbf{0} \\ \mathbf{M}^{-1}(\mathbf{K}_R + \mathbf{K}_L) \\ -\mathbf{B}_R \mathbf{n}^T \mathbf{K}_L \end{bmatrix} \tag{A.24}$$

can be calculated in the same fashion as it was done in Appendix A.1. For brevity, only the differences in the calulation are reported here. Most notably, the SCHUR complement of Equation (A.14) has changed:

$$\mathbf{S}_A = \begin{bmatrix} i\Omega\mathbf{I} & -\mathbf{I} \\ \mathbf{M}^{-1}(\mathbf{K}_R - i\Omega\mathbf{D}_I) & i\Omega\mathbf{I} + \mathbf{M}^{-1}(\mathbf{D} + \mathbf{D}_I + \mathbf{G}) \end{bmatrix} \tag{A.25}$$

A short calculation reveals that the determinant of $\mathbf{S}_A$ does not contain the rotating damping matrix $\mathbf{D}_I$:

$$\det(\mathbf{S}_A) = \left(-\Omega^2\mathbf{M} + i\Omega(\mathbf{D} + \mathbf{G}) + \mathbf{K}_R\right) \tag{A.26}$$

The matrix inverse $\mathbf{S}_A^{-1}$ then yields:

$$\mathbf{S}_A^{-1} = \begin{bmatrix} -\frac{i}{\Omega}\mathbf{I} + \frac{i}{\Omega}\det(\mathbf{S}_A)^{-1}(\mathbf{K}_R - i\Omega\mathbf{D}_I) & \det(\mathbf{S}_A)^{-1}\mathbf{M} \\ -\det(\mathbf{S}_A)^{-1}(\mathbf{K}_R - i\Omega\mathbf{D}_I) & i\Omega\det(\mathbf{S}_A)^{-1}\mathbf{M} \end{bmatrix} \tag{A.27}$$

Despite the fact that the matrix inverse has changed compared to Equation (A.16), the Equations (A.17)-(A.21) show that the only products formed with the SCHUR complements are $\mathbf{S}_A^{-1}\mathbf{A}_2$ and $\mathbf{S}_A^{-1}\mathbf{B}_1$. It turns out that the products are left unchanged, because both $\mathbf{A}_2$ and $\mathbf{B}_1$ contain null matrices. The unbalance response for the system with inner and outer damping is then:

$$\mathbf{x}^+ = \begin{bmatrix} \left(-\Omega^2\mathbf{M} + i\Omega(\mathbf{D} + \mathbf{G}) + \mathbf{K}_R\right)^{-1}\mathbf{K}_R \\ i\Omega\left(-\Omega^2\mathbf{M} + i\Omega(\mathbf{D} + \mathbf{G}) + \mathbf{K}_R\right)^{-1}\mathbf{K}_R \\ \mathbf{R}\mathbf{n}^T\left(-\Omega^2\mathbf{M} + i\Omega(\mathbf{D} + \mathbf{G}) + \mathbf{K}_R\right)^{-1}\mathbf{K}_R - \mathbf{R}\mathbf{n}^T \end{bmatrix} \boldsymbol{\varepsilon}^+ \tag{A.28}$$

As a conclusion, the rotating damping $\mathbf{D}_I$ has no influence on the steady-state solution.

A.3 Parasitic stiffness compensation

The compensation of parasitic stiffnesses with the controller leads to the state-space system $\dot{\mathbf{x}} = \mathbf{A}\mathbf{x} + \mathbf{B}\boldsymbol{\varepsilon}$ with the matrices $\mathbf{A}$, $\mathbf{B}$:

$$\mathbf{A} = \begin{bmatrix} \mathbf{0} & \mathbf{I} & \mathbf{0} \\ -\mathbf{M}^{-1}\left(\mathbf{K}_R + \mathbf{K}_L + \mathbf{K}_S\right) & -\mathbf{M}^{-1}\left(\mathbf{D} + \mathbf{G}\right) & \mathbf{M}^{-1}\mathbf{K}_L\mathbf{n}\mathbf{C}_R \\ \mathbf{B}_R\mathbf{n}^T\left(\mathbf{K}_L + \bar{\mathbf{K}}_S\right) & \mathbf{0} & \mathbf{A}_R - \mathbf{B}_R\mathbf{n}^T\mathbf{K}_L\mathbf{n}\mathbf{C}_R \end{bmatrix}$$
$$\mathbf{B} = \begin{bmatrix} \mathbf{0} \\ \mathbf{M}^{-1}\left(\mathbf{K}_R + \mathbf{K}_L + \mathbf{K}_S\right) \\ -\mathbf{B}_R\mathbf{n}^T\left(\mathbf{K}_L + \bar{\mathbf{K}}_S\right) \end{bmatrix} \tag{A.29}$$

The matrix $\mathbf{K}_S$ represents the parasitic stiffnesses, whereas $\bar{\mathbf{K}}_S$ is the matrix of the estimated parasitic bearing stiffnesses and is defined similarly to Eqn. (3.11).

$$\bar{\mathbf{K}}_S = \mathbf{n}\,\mathrm{diag}\left(\bar{k}_{SA}, ..., \bar{k}_{Sj}, ..., \bar{k}_{Sz}\right)\mathbf{n}^T \tag{A.30}$$

The solution process is similar to the one given in Appendix A.1, so only the main difference is given here. Similar to Equation (A.7), the solution requires the calculation of:

$$\left(i\Omega\mathbf{I} - \mathbf{A}_R + \mathbf{B}_R\mathbf{n}^T\mathbf{K}_L\mathbf{n}\mathbf{C}_R\right)^{-1}\left(-\mathbf{B}_R\mathbf{n}^T\left(\mathbf{K}_L + \bar{\mathbf{K}}_S\right)\right) = -\mathbf{R}\tilde{\mathbf{K}}_L^{-1}\mathbf{n}^T\left(\mathbf{K}_L + \bar{\mathbf{K}}_S\right) \tag{A.31}$$

The solution requires the condensed bearing stiffness matrix $\tilde{\mathbf{K}}_L$ defined in Equation (3.10). The unbalance response is then:

$$\mathbf{x}^+ = \begin{bmatrix} \left(-\Omega^2\mathbf{M} + i\Omega\left(\mathbf{D} + \mathbf{G}\right) + \mathbf{K}_R + \mathbf{K}_S - \bar{\mathbf{K}}_S\right)^{-1}\left(\mathbf{K}_R + \mathbf{K}_S - \bar{\mathbf{K}}_S\right) \\ i\Omega\left(-\Omega^2\mathbf{M} + i\Omega\left(\mathbf{D} + \mathbf{G}\right) + \mathbf{K}_R + \mathbf{K}_S - \bar{\mathbf{K}}_S\right)^{-1}\left(\mathbf{K}_R + \mathbf{K}_S - \bar{\mathbf{K}}_S\right) \\ \mathbf{R}\mathbf{n}^T\mathbf{Z}\left(-\Omega^2\mathbf{M} + i\Omega\left(\mathbf{D} + \mathbf{G}\right) + \mathbf{K}_R + \mathbf{K}_S - \bar{\mathbf{K}}_S\right)^{-1}\left(\mathbf{K}_R + \mathbf{K}_S - \bar{\mathbf{K}}_S\right) - \mathbf{R}\mathbf{n}^T\mathbf{Z} \end{bmatrix}\boldsymbol{\varepsilon}^+ \tag{A.32}$$

The matrix $\mathbf{Z}$ describes dimensionless factors defined as:

$$\mathbf{Z} = \mathbf{n}\tilde{\mathbf{K}}_L^{-1}\mathbf{n}^T\left(\mathbf{K}_L + \bar{\mathbf{K}}_S\right) = \mathbf{n}\left(\mathbf{n}^T\mathbf{K}_L\mathbf{n}\right)^{-1}\mathbf{n}^T\left(\mathbf{K}_L + \bar{\mathbf{K}}_S\right) \tag{A.33}$$

A.4 Unbalance response with casing

The approach starts with the equations of motion for rotor and casing. To differentiate between both, additional subindices are introduced. The subindex r (rotor) is appended to all vectors and matrices of the rotating parts, while the support structure is augmented with the subindex c (casing).

$$\begin{aligned} \text{Rotor:} \quad & \mathbf{M}_r \ddot{\mathbf{q}}_{Sr} + (\mathbf{D}_r + \mathbf{G}_r)\,\dot{\mathbf{q}}_{Sr} + \mathbf{K}_{Rr}\mathbf{q}_{Wr} = -\mathbf{F}_r \\ \text{Casing:} \quad & \mathbf{M}_c \ddot{\mathbf{q}}_{Sc} + (\mathbf{D}_c + \mathbf{G}_c)\,\dot{\mathbf{q}}_{Sc} + \mathbf{K}_{Rc}\mathbf{q}_{Sc} = -\mathbf{F}_c \end{aligned} \tag{A.34}$$

The matrices $\mathbf{M}_c, \mathbf{D}_c, \mathbf{G}_c, \mathbf{K}_{Rc}$ are arbitrary mass, damping, gyroscopic and stiffness matrices of the casing. Furthermore, the unbalance acts only on the rotating part with the eccentricity $\boldsymbol{\varepsilon}_r$, whereas the eccentricity $\boldsymbol{\varepsilon}_c = \mathbf{0}$ for the casing. The force on the individual active bearings are then:

$$\tilde{\mathbf{F}} = \tilde{\mathbf{K}}_L\,(\tilde{\mathbf{q}}_{Wr} - \tilde{\mathbf{q}}_{Sc} - \tilde{\mathbf{a}}) \tag{A.35}$$

In accordance with the previous definitions, the vector $\tilde{\mathbf{F}}$ contains the bearing forces $F_A, ..., F_z$ and $\tilde{\mathbf{a}}$ represents the condensed actuator forces. The condensed bearing stiffness matrix $\tilde{\mathbf{K}}_L$ was defined in Equation (3.10), the condensed vectors $\tilde{\mathbf{q}}_{Wc}$, $\tilde{\mathbf{q}}_{Sc}$ that only contain the j coordinates for the attached bearings. The transformation matrix $\mathbf{n}_r$ uses the definition from Equation (3.8) and converts the rotor's nodes $\mathbf{q}_{Wr}$ to their condensed counterparts $\tilde{\mathbf{q}}_{Wr}$.

$$\tilde{\mathbf{q}}_{Wr} = \mathbf{n}_r^T \mathbf{q}_{Wr}, \qquad \tilde{\mathbf{q}}_{Sc} = \mathbf{n}_c^T \mathbf{q}_{Sc} \tag{A.36}$$

The same principle applies for the transformation of bearing forces, but with the peculiarity that the forces which act on the rotor are opposing the ones of the fixed part:

$$\mathbf{F}_r = \mathbf{n}_r \tilde{\mathbf{F}}, \qquad \mathbf{F}_c = -\mathbf{n}_c \tilde{\mathbf{F}} \tag{A.37}$$

With the kinematic relations from Equation (3.6) , the active bearing forces that act on both systems can be expressed as:

$$\underbrace{\begin{bmatrix}\mathbf{F}_r\\ \mathbf{F}_c\end{bmatrix}}_{\mathbf{F}_g}=\underbrace{\begin{bmatrix}\mathbf{n}_r\tilde{\mathbf{K}}_L\mathbf{n}_r^T & -\mathbf{n}_r\tilde{\mathbf{K}}_L\mathbf{n}_c^T\\ -\mathbf{n}_c\tilde{\mathbf{K}}_L\mathbf{n}_r^T & \mathbf{n}_c\tilde{\mathbf{K}}_L\mathbf{n}_c^T\end{bmatrix}}_{\mathbf{K}_{Lg}}\left(\underbrace{\begin{bmatrix}\mathbf{q}_{Sc}\\ \mathbf{q}_{Sc}\end{bmatrix}}_{\mathbf{q}_{Sg}}-\underbrace{\begin{bmatrix}\boldsymbol{\varepsilon}_c\\ \mathbf{0}\end{bmatrix}}_{\boldsymbol{\varepsilon}_g}-\begin{bmatrix}\mathbf{n}_r\\ \mathbf{0}\end{bmatrix}\tilde{\mathbf{a}}\right) \tag{A.38}$$

The actuator displacements and controller's states are connected with $\tilde{\mathbf{a}}=\mathbf{C}_R\mathbf{x}_R$ and can be rewritten in matrix form:

$$\begin{bmatrix}\mathbf{n}_r\\ \mathbf{0}\end{bmatrix}\tilde{\mathbf{a}}=\underbrace{\begin{bmatrix}\mathbf{n}_r & \mathbf{0}\\ \mathbf{0} & \mathbf{n}_c\end{bmatrix}}_{\mathbf{n}_g}\underbrace{\begin{bmatrix}\mathbf{C}_R\\ \mathbf{0}\end{bmatrix}}_{\mathbf{C}_{Rg}}\mathbf{x}_R \tag{A.39}$$

Both rotor and stator equations can be joined to a single system when the following definitions are used:

$$\mathbf{M}_g=\begin{bmatrix}\mathbf{M}_r & \mathbf{0}\\ \mathbf{0} & \mathbf{M}_c\end{bmatrix},\ \mathbf{D}_g=\begin{bmatrix}\mathbf{D}_r & \mathbf{0}\\ \mathbf{0} & \mathbf{D}_c\end{bmatrix},\ \mathbf{G}_g=\begin{bmatrix}\mathbf{G}_r & \mathbf{0}\\ \mathbf{0} & \mathbf{G}_c\end{bmatrix},\ \mathbf{K}_{Rg}=\begin{bmatrix}\mathbf{K}_{Rr} & \mathbf{0}\\ \mathbf{0} & \mathbf{K}_{Rc}\end{bmatrix} \tag{A.40}$$

Although the use of the abbreviation $\mathbf{n}_g^T\mathbf{F}_g$ leads to the required force, it is dimensionally incompatible with the controller equation. To circumvent this problem, the matrix $\mathbf{B}_R$ is replaced by one with matching dimensions, hence

$$\mathbf{B}_{Rg}=\begin{bmatrix}\mathbf{B}_R & \mathbf{0}\end{bmatrix} \tag{A.41}$$

Although the controller matrix $\mathbf{A}_R$ has not changed, it will be renamed in $\mathbf{A}_{Rg}$ for consistency. Both the mechanical Equation (3.49) and the one of the controller from Equation (3.24) can be combined to a single state-space system.

$$\begin{aligned}\dot{\mathbf{x}}_g=&\begin{bmatrix}\mathbf{0} & \mathbf{I} & \mathbf{0}\\ -\mathbf{M}_g^{-1}\left(\mathbf{K}_{Rg}+\mathbf{K}_{Lg}\right) & -\mathbf{M}_g^{-1}\left(\mathbf{D}_g+\mathbf{G}_g\right) & \mathbf{M}_g^{-1}\mathbf{K}_{Lg}\mathbf{n}_g\mathbf{C}_{Rg}\\ \mathbf{B}_{Rg}\mathbf{n}_g^T\mathbf{K}_{Lg} & \mathbf{0} & \mathbf{A}_{Rg}-\mathbf{B}_{Rg}\mathbf{n}_g^T\mathbf{K}_{Lg}\mathbf{n}_g\mathbf{C}_{Rg}\end{bmatrix}\mathbf{x}_g\\ &+\begin{bmatrix}\mathbf{0}\\ \mathbf{M}_g^{-1}\left(\mathbf{K}_{Rg}+\mathbf{K}_{Lg}\right)\\ -\mathbf{B}_{Rg}\mathbf{n}_g^T\mathbf{K}_{Lg}\end{bmatrix}\boldsymbol{\varepsilon}_g\end{aligned} \tag{A.42}$$

It is no coincidence that the matrix structure of (A.42) is the same as for the reduced problem with totally rigid supports. Good choices for the combined

matrices allow the exploitation of the already derived solution, generalizing it further. However, the unbalance response calculation from A.1 relies on simplifications and identities for some matrix operations. Before accepting the final solution, it has to be checked if each simplification also holds for this system with modified matrices. A central role takes the SCHUR complement $\mathbf{S}_A$, which was calculated in Equations (A.5)-(A.10). A dimensional analysis reveals that the matrix $\mathbf{R}$ from Equation (A.8) cannot be part of the solution. A new matrix $\mathbf{R}_g$ is defined as:

$$\mathbf{R}_G = \begin{bmatrix} \mathbf{R} & \mathbf{R} \end{bmatrix} \tag{A.43}$$

A central role in the verification of Equation (A.10) is the matrix identity $\mathbf{K}_L = \mathbf{K}_L \mathbf{n} \mathbf{C}_R \mathbf{R} \mathbf{n}^T$. However, it is still unclear if the matrix identity is also satisfied for:

$$\mathbf{K}_{Lg} = \mathbf{K}_{Lg} \mathbf{n}_g \mathbf{C}_{Rg} \mathbf{R}_g \mathbf{n}_g^T \tag{A.44}$$

Despite being immediately obvious, the choice of $\mathbf{R}_g$ indeed satisfies this matrix identity. With this result, it is easy to show that Equations (A.7) and (A.10) also hold. Since there are no further obstacles to overcome, the unbalance response of Appendix A.1 not only solves the problem of the rotor with fixed supports, but is also valid for the general case.

$$\mathbf{q}_{Sg} = \left(-\Omega^2 \mathbf{M}_g + i\Omega \left(\mathbf{D}_g + \mathbf{G}_g\right) + \mathbf{K}_{Rg}\right)^{-1} \mathbf{K}_{Rg} \boldsymbol{\varepsilon}_g^+ \, \mathrm{e}^{i\Omega t} \tag{A.45}$$